The mechanism of activation of the TRPV1 ion channel by the double-knot spider toxin

A thesis

submitted in partial fulfillment of the requirements

of the degree of

Doctor of Philosophy

By

Debayan Sarkar

Roll No. 20143323

INDIAN INSTITUTE OF SCIENCE EDUCATION AND RESEARCH PUNE

2019

Dedicated to

"Kosenrufu"

CERTIFICATE

Certified that the work incorporated in the thesis entitled "**The mechanism of activation of the TRPV1 ion channel by the double-knot spider toxin**" submitted by **Debayan Sarkar** was carried out by the candidate under my supervision. The work presented here or any part of it has not been included in any other thesis submitted previously for the award of any degree or diploma from any other University or institution.

Dr. Jeet Kalia

Date: 30.09.2019 (Supervisor)

DECLARATION

I declare that this written submission represents my ideas in my own words and where others' ideas have been included, I have adequately cited and referenced the original sources. I also declare that I have adhered to all principles of academic honesty and integrity and have not misrepresented or fabricated or falsified any idea/data/fact/source in my submission. I understand that violation of the above will be cause for disciplinary action by the Institute and can also evoke penal action from the sources which have thus not been properly cited or from whom proper permission has not been taken when needed.

Debayan Sarkar

(Name of the student)

Roll No. 20143323

Date: 30.09.2019

ACKOWLEDGEMENTS

"Defeat lies not in failing or making mistakes; rather, it lies in giving up on ourselves when we do so." - *Dr. Daisaku Ikaeda*

Getting a Ph.D. is mostly never an easy journey. We stumble upon different kinds of hurdles and then overcome them. Those who unconditionally hold our hands when we are down or teach us how to get up and get going, deserves a word of appreciation whether they want it or not.

I would like to start by thanking my parents for their immense support and patience throughout the span of my Ph.D. At times they had to confront me not in my best mood. By encouraging me and calming me down at those times they have contributed immensely to my well-being. My father being a retired engineer, a wholesome family person have taught me to be a balanced person. My mom being a retired government officer, who in spite of her several physical ailments yet inspire me by being one of the most hard-working individuals I know of her age. I have learned patience and perseverance from her, which has helped in all spheres of my life.

I need to dedicate a whole para for my elder brother, Dr. Devdeep Sarkar, who has been my idol of sorts in my early life, till I did not encounter greater people who are idols for the world. The aura of his personality is something I yet aspire to achieve. His academic and professional standards can only be compared to the bests I have known personally. I have learned a trick or two from him about scientific thinking as well as mentoring, yet much more is left for me to learn. His inspiration has been an asset in my career.

Up next I would like to thank my friends from my early career, who still remain not only in touch but people whom I can rely on. I thank Pavan, Samarth, Vandana, Prashant, Deepti, Aditya, Deepika and Bhavya from my Mysore days for persistently being there in spite of very little time afforded on my side in my busy schedules. You guys are keepers for sure. I would like to mention Vikram, Ashish, Kasthuri, Prerona, Blesson, Stephen and Sony for being in touch no matter what! I would like to mention Joydeep, Sulagna, Barenya and Vineeta from college days who have been great friends for wonderful conversations and support.

An acknowledgement would be incomplete without the mention of Srijoni and Payal. Srijoni, a great friend of mine from college days, seem to understand the pulse of my feelings whenever I have required her support. With 12 years gone by, I still feel strongly connected to her when it comes to have a hearty conversation in difficult times. Knowing Payal for past 6 years has been a pleasure. Throughout my Ph.D., she had taken it as a mission to try to keep me in happy mood no matter what goes on in her life. Her contributions to my well-being is massive.

I would also like to thank my previous mentors, Prof. Hussain Munavar, Prof. Sripathi Kandula, Dr. Been Pillai, Dr. Kasturi Sarkar and Dr. Arup Kumar Mitra for their great teachings, lessons for life and leadership qualities.

I would like to convey special thanks to my BSG family at Pune as well as Bhopal to keep me going and infusing me with the spirit of a roaring lion whenever I felt low. I thank Dr. Daisaku Ikaeda for his endless efforts and encouragements for keeping our lives always brimming with hope.

To talk about my teammates in crime and fun, Shweta and Simran, words fall short as I just believe they would know what I would want to say about them. Simran is always polite in giving a really check, whereas Shweta is blunt and to the point. Though I have never followed their advice on health, I respect their honest efforts of trying to bend me into a fitter version of me. I am thankful to Madhu, Anindya, Soumen and Siddhi likewise for giving me joyful company.

At IISERB, I found a great friend Ankit who made me feel like home. He is hard-working, inspirational and practical. I found several good friends in the forms of Abhishek, Chitra, Debjyoti, Sanjana, Ajith, Pranab and Surya. I am thankful to all students at IISERB who have made me feel welcome and comfortable during this 1.5 years of stay.

I would like to express my genuine gratitude to the labs and lab members and IISER Pune and IISER Bhopal who have helped me at all hours. I cannot but help taking the names of Manasi, Mahesh, Ishtiyaq, Neha, Jyoti and Shrikant (from Sai-G3 lab), Sachin, Manish, Shristi, Sukrut, Soumya and Krish (from TP lab), Priyanka and Tanusree (from AG lab), Chaitanya and Niraja (from COOL lab), Indu, Ashwin, Satyajit and Manu (from SG lab), Kriti, Bhagyashree,

Amar, Senthil and Prajna (from GR lab), Sameer, Bipasha, Sayali, Dnyanesh, Bhavin (from RR lab), Subham (from SK lab) and mostly Yamini, Rupali and Yashwant (from ABH lab).

I would like to express sincere gratitude to the following faculties at IISER Pune for their direct and indirect contributions towards my Ph.D.—Dr. Thomas Pucadyil, Dr. M. S. Madhusudhan, Dr. Amrita B. Hazra, Dr. Saikrishnan Kayarat, Dr. Gayathri Pananghat, Dr. Sudha Rajamani, Dr. Girish Ratnaparkhi, Dr. Kundan Sengupta, Dr. Richa Rikhi, Dr. Raghav Rajan, Dr. Nishad Matange, Prof. Nishikant Subhedar, Dr. Aurnab Ghose, Dr. S.G. Srivatsan, Dr. Partha Hazra, Dr. Shabana Khan, Prof. H. N. Gopi, Prof. Milind Watve, Prof. Sanjeev Galande, Prof. L.S. Shashidhara and honorable Director, Prof. Jayant B. Udgaonkar. I would take this opportunity to thank Dr. Amrita Hazra separately for helping us immensely during our shifting time to IISER Bhopal as faculty-in-charge and as mentor. I would also like to convey my deepest gratitude to Dr. Sourav Datta, Dr. Sunando Datta, Dr. Chandan Sahi, Dr. Sanjeev Shukla, Dr. Raghuvir Singh Tomar, Dr. Ram Kumar Mishra, Dr. Vimlesh Kumar, Dr. Varun Chowdhury, Dr. Ishu Sarogi, Dr. Atul Kumar, and Dr. Dimpy Kalia and their lab members at IISER Bhopal for extending a helping hand whenever sought. I convey my express gratitude to my Research advisory committee members, Dr. Thomas Pucadyil, Dr. M.S. Madhusudhan and Dr. Janesh Kumar.

I convey a heart-filled gratitude to Tushar sir and Anjali mam at academic office, Smita mam and Prabhas sir at finance, Varsha mam, Shabana mam, Yogesh sir at purchase, Mahesh sir. Mrinalini mam, Shabnam mam, Sandeep, Piyush and Kalpesh at bio-office, Mayuresh sir, Ganesh sir, Mahesh sir, Yatish, Ravi and Dnyaneshwar at chemistry and Nilesh sir from Physics for making our lives easier.

A special vote of thanks goes to my family at Dr. Jeet Kalia's laboratory. Thanks to Yashu, Aditi, Pawas, Avni, Avinil, Sumita, Subhadeep and Hrishikesh, I feel alive every day at work. Past members, Gregor, Rahul, Yamini, Susovan, Subham, Vani, Nevin, Lokesh, Anusree, Dheerendra, Charu, Carola, Shaila, Nitin, Sushma and Chitra have contributed a lot growth as a human being and in the field of science. Their tenacities and dedication inspire me consistently.

Lastly, I would like to thank my supervisor, Dr. Jeet Kalia. Few points about his scientific temperament is astoundingly impressive which has influenced my thought process from 1st month in the laboratory. His lab notebook maintenance style is so impeccable that it

would sound like a story to the reader with the details of each steps and their observations mentioned. In science this is crucial, and I hope that I have learnt this as a life's lesson from this lab. His scientific writing and speaking styles are some real treasure, which thankfully made my writing and speaking skills much better than before, although much more still remained for me to learn from him. Additionally, he has been a great support and active in troubleshooting when things did not work in experiments. This thesis would not have been in its current form without his persistent efforts spent on improving its quality. I truly am grateful for his consistent efforts in developing me as a scientist.

SYNOPSIS

The mechanism of activation of the TRPV1 ion channel by the double-knot spider toxin

Submitted by: Debayan Sarkar

Roll no. 20143323

Thesis Advisor: Dr. Jeet Kalia

Indian Institute of Science Education and Research, Pune

Dr. Homi Bhabha Road, Pashan, Pune-411008

September 2019

Venomous animals such as spiders, snakes and scorpions produce a remarkably diverse library of peptide toxins that specifically target their victims' neuronal ion channel proteins causing pain, paralysis, and even death. Over the past five decades, these toxins have been exquisitely utilized by biophysicists as powerful mechanistic tools for studying ion channels. Moreover, toxins have emerged as potent channel imaging agents, drugs candidates, and tools for controlling channel function *in vivo*.

In **Chapter 1** of this thesis, I introduce a class of peptide toxins known as the inhibitory cystine knot (ICK) toxins and describe how they have facilitated the study of tetrameric ion channels. I review some of the pioneering biophysical studies performed on these channels that employed ICK toxins as tools for elucidating fundamental aspects of channel structure and function including the identification of their pore-forming residues. Fascinatingly, my examination of the findings of these classical papers in light of the recently solved high-resolution structures of their target ion channels and channel-toxin complexes reveals that the structures support most of the key conclusions of the biophysical work performed decades earlier. Additionally, I discuss studies on membrane partitioning toxins that provide insights into the role of the membrane in ion channel function which is an aspect of ion channel biology that is at the forefront of the field. Lastly, I discuss efforts on developing toxins as therapeutic agents, as channel imaging agents, and as modulators of the cell-autonomous function of ion channels.

In **Chapter 2**, I describe my studies that employed the recently reported structure of the TRPV1 ion channel bound to its potent ICK toxin agonist, the double-knot toxin (DkTx), as a model system to investigate the roles of toxin-lipid interfaces in channel activation. This study involved the generation of a series of site-directed variants of DkTx followed by the

characterization of their TRPV1-activation properties by employing two-electrode voltage clamp electrophysiology. Together with membrane partitioning experiments, these studies reveal that toxin-lipid interfaces play a dominant role in channel activation. Additionally, I find that whereas the membrane interfaces formed by one of the knots of the toxin endow it with its low channel-dissociation rates, those formed by other knot contribute primarily to its potency. These studies establish that protein-lipid interfaces play nuanced yet profound roles in the function of protein-protein complexes within membranes.

Our discovery that the membrane plays an important role in endowing DkTx with its slow wash-off rates challenges the popular perception that it is the bivalency of the toxin that is responsible for its slow wash-off. In **Chapter 3**, I describe my experiments aimed at teasing apart the contributions of membrane partitioning and bivalency of DkTx in its channel activation properties. Achieving this goal entailed designing monovalent DkTx variants that partition well into membranes. To generate such toxin variants, I focused on the linker region of DkTx that connects the two cystine knots of the toxin and produced a series of DkTx variants containing alterations in linker length or rigidity. TRPV1 activation and the membrane partitioning studies revealed that two of my linker truncation variants were monovalent while retaining favorable membrane partitioning. Wash-off studies on these variants and comparisons with the wash-off kinetics of the single knots of the toxin enabled me to dissect the contributions of membrane partitioning and bivalency in endowing DkTx with its slow wash-off property. An unanticipated yet insightful discovery that I made while pursuing this study was that the length of the linker is evolutionarily optimized to endow the toxin with optimal membrane partitioning propensity.

Over the course of performing these studies, the necessity of a fluorescence-based quantitative assay for the precise characterization of the binding of the toxin to cellular membranes was perceived. In **Chapter 4**, I discuss my efforts in this direction that resulted in the development of a strategy for fluorescently labeling the C-terminus of DkTx without disruption of toxin activity by utilizing the sortase enzyme-based bioconjugation technology.

Taken together, my studies on the DkTx-TRPV1 system reveal that the membrane can play a dominant role in the function of membrane-embedded protein-protein complexes and set the stage for utilizing DkTx as a powerful tool for studying protein-lipid interactions.

CONTENTS:

LIST OF FIGURES

LIST OF TABLES

Chapter 1:

Peptide Toxin Modulation of Ion Channel Function

1.1. Introduction and historical perspective.

Many members of the phyla Arthropoda, Mollusca and Chordata produce venom and utilize it to protect themselves against their predators or to catch prey. Ion channel-targeting toxins are one of the principal active components of these venoms. These toxins target various types of ion channels including voltage-gated channels, ligand-gated ion channels, temperature-sensitive ion channels and acid-sensitive ion channels (Bosmans and Tytgat, 2007; Hanck and Sheets, 2007; Hille, 2001; Kalia et al., 2015; Swartz, 2007).

One of the earliest reports on the use of animal toxins as a tool for studying ion channel biology was in 1973 when E. A. Bernard's group used tritiated (^{3}H) α-bungarotoxin to generate electron microscope (EM) autoradiographic images of acetylcholine receptors (AChRs) on mice diaphragm muscle cells and frog sartorius muscles (Porter et al., 1973). This toxin was originally isolated by Chang and Lee in 1963 from *Bungarus multicinctus* (Chang and Lee, 1963). In 1974, ^{125}I labeled α-bungarotoxin (^{125}I- α-bungarotoxin) was used to elucidate the distribution of AChRs located at the motor end plate connected to the strenomastoid muscles in mice (Fertuck and Salpeter, 1974).

In the 1980s, Christopher Miller's laboratory started their pioneering work on employing potassium channel-targeting toxins for understanding the molecular basis of potassium ion conduction through these channels. In 1985, they published the discovery of charybdotoxin (CTX), a Ca^{2+} activated K^{+} (BK) channel pore-blocker isolated from the venom of an Israeli scorpion (Miller et al., 1985). They then used CTX as a powerful molecular tool to identify the pore-lining residues of the channel (MacKinnon and Miller, 1989). These insights constituted a huge leap forward in our understanding of the structural and functional details of ion channels especially as structures of ion channels had not been solved at this time. Over the course of the next 30 years, hundreds of toxins have been discovered that target voltage-gated and ligand-gated ion channels (Ahern et al., 2016; Bosmans and Swartz, 2010; Swartz, 2007). One of the major classes of these toxins is the family of the inhibitory cystine knot (ICK) toxins that possess a characteristic pattern of arrangement of cysteine residues that typically form three disulfide bonds.

In this introductory chapter of my thesis, I discuss the application of toxins in ion channel and receptor discovery, their profound contributions towards understanding the mechanisms

underlying ion channel gating, and studies that have demonstrated that several of these toxins interact intimately with membrane lipids with emphasis on how such interactions influence toxin-mediated channel modulation. I infuse these discussions with discourse on the insights provided by recent breakthroughs in structural biology that have yielded several structures of toxin-channel complexes. In the context of these new structures, I revisit some of the most pioneering work on ion channel biophysics performed decades before these structures were solved that utilized toxins as a guiding light to inform on key aspects of ion channel structure and function. In addition to these biophysical applications of toxins, I describe recent reports on employing toxins as highly specific channel-imaging agents and also discuss their emerging potential as therapeutic agents. I end the chapter with a brief discussion on how recent technological innovations in mass spectrometry and chemical biology have opened doors to pursue studies that can contribute to enhancing our relatively limited knowledge on the roles of lipids in ion channel and toxin function.

Although ICK toxins that target trimeric ion channels such as ASIC1a have been discovered (Chassagnon et al., 2017; Escoubas et al., 2000; Mazzuca et al., 2007), I restrict my discussions to exclusively those ICK toxins that target tetrameric cation channels. Another topic pertaining to cysteine-rich toxins that this chapter largely ignores for the sake of brevity is the family of cone snail toxins known as conotoxins that contain several different patterns of disulfide bonds and target a variety of channels and receptors. This family of toxins has been reviewed extensively elsewhere (Gao et al., 2017; Holmes, 2014; Morales Duque et al., 2019; Robinson and Norton, 2014).

1.2. ICK toxins

The ICK family of toxins target a variety of ion channels including voltage-gated potassium (K_v), voltage-gated sodium (Na_v), voltage-gated calcium (Ca_v), voltage-gated proton (H_v), transient receptor potential (TRP) and acid-sensing ion channels (ASICs) as well as receptors such as the acetylcholine and ryanodine receptors inducing either inhibitory (Miller et al., 1985; Schmalhofer et al., 2008; Swartz and MacKinnon, 1995) or excitatory (Bohlen et al., 2010; Siemens et al., 2006) responses. These toxins typically have six cysteine residues in their primary sequence although some of them such as Lqh2 and AaH2 (Possani et al., 1999) contain

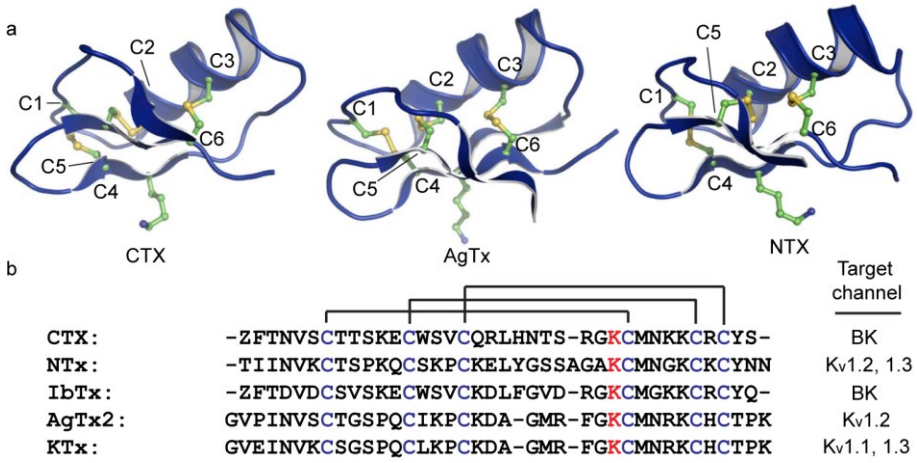

Figure 1.1. Pore-blocking ICK toxins. a) NMR structure of charybdotoxin (CTX, PDB: 2crd) (Bontems et al., 1992), Agitoxin2 (AgTx2, PDB: 1agt) (Krezel et al., 1995), noxiustoxin (NTX, PDB: 1sxm) (Dauplais et al., 1995) . b) Sequence alignment of pore-binding ICK toxins along with the names of channels they target. The cysteine residues forming disulfide linkages are depicted in blue and the pore-blocking lysine (K) residues are colored in red. The disulfide bonding pattern is depicted by connecting the residues with line segments. Figure adapted from Banerjee et al., 2013.

eight cysteine residues whereas others such as RhTx (Yang et al., 2015) contain only four cysteines. All of the six cysteine residues of ICK toxins are engaged in forming disulfide bonds that line up into a characteristic C1-C4, C2-C5, C3-C6 pattern as depicted in Figure 1.1 and Figure 1.5 (Bosmans and Swartz, 2010; Escoubas and Rash, 2004; Swartz, 2007). This rigid structural framework is believed to have evolved under critical selection pressure to withstand harsh temperatures, pH and protease assault (Herzig and King, 2015).

ICK toxins modulate the function of ion channels via two main types of mechanisms. While some of these toxins bind at the channel's pore region and either inhibit ion conduction by occluding the pore or activate the channel by stabilizing its open state, others bind peripheral domains of their target channels and modulate channel function by stabilizing one channel conformation over another.

1.2.1. Toxins that target the pore domain of ion channels

1.2.1.1. Voltage-gated ion channels. Tetrameric voltage-gated ion channels are made up of four subunits each composed of six transmembrane helices. Four of these helices (S1-S4) form the voltage sensor of the channel whereas the S5-S6 helices form the channel pore (Figure 1.2a) (Ahern et al., 2016; Hille, 2001; Kalia et al., 2015; Swartz, 2007). Miller and coworkers discovered that CTX (Figure 1.1) binds to BK channels in 1:1 ratio (Anderson et al., 1988; MacKinnon and Miller, 1988). In single channel experiments performed on channels embedded in uncharged planar lipid bilayers, they determined the dissociation constants of the CTX-channel complex under physiological ionic strengths. By clamping the open probability of the channel using stringent intracellular Ca^{2+} concentrations and varying the voltage, they deduced that the toxin can sense voltage and preferentially binds to the open state of the channel. They also concluded that higher extracellular concentration of cationic species such as K^+, Na^+ and arginine reduces the association rate of CTX to the BK channel (Anderson et al., 1988). In a subsequent article, MacKinnon and Miller reported that the increase in the internal solution's K^+ concentration facilitates toxin dissociation from the channel and that furthermore, membrane depolarization accelerates this process (MacKinnon and Miller, 1988). When the membrane is hyperpolarized, the toxin dissociation rate reduces regardless of the intracellular K^+ concentration. From this information, they inferred the presence of a toxin-binding site in the channel's ion-conduction pathway that can be competitively inhibited by the K^+ ions from the

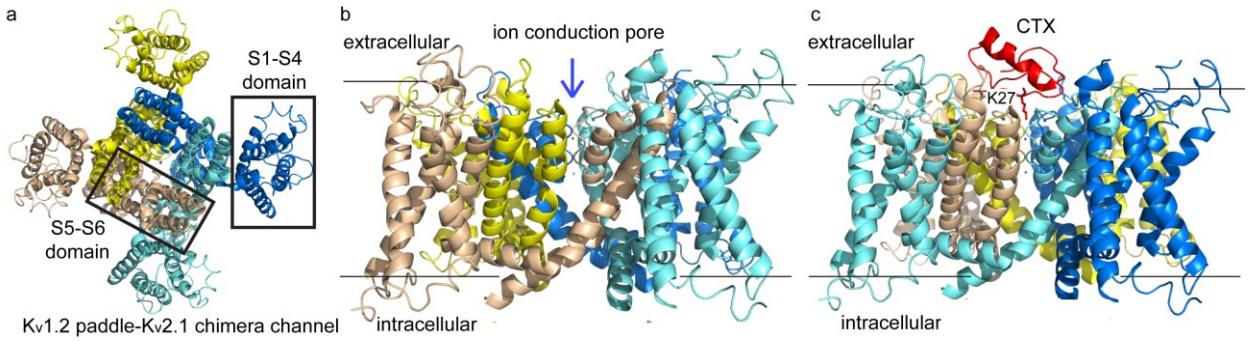

Figure 1.2. K_v channel architecture and charybdotoxin (CTX) binding. a) Cartoon diagram of K_v channel viewed from the top. Each subunit is depicted in different color. b) K_v channel side-view (PDB ID: 4jta, Banerjee et al., 2013). c) CTX (in red) bound on to the K_v1.2-2.1 paddle chimera channel (PDB ID: 4jta, Banerjee et al., 2013).

internal solution. Studies focused on deducing the binding site of CTX on the Shaker K_v channel resulted in the finding that neutral and cationic variants of the E422 residue of the channel cannot bind the toxin with high affinity. This result suggested that CTX binds to the pore loop of the channel and that this binding involves electrostatic interactions between the pore glutamate and the CTX lysine residues. This model also explained why intracellular K^+ ions can "kick-off" CTX by competing for this site (MacKinnon and Miller, 1989).

More than a couple of decades after the above studies were published, the crystal structure of CTX bound to a K_v channel was solved (Figure 1.2c) (Banerjee et al., 2013). Remarkably, this structure completely supports the conclusions of the previous work performed by the Miller research group. Indeed, the structure revealed that the amino side chain of the K27 residue of CTX inserts into the pore and is perfectly placed to hydrogen bond with the backbone carbonyls of the channel, thereby preventing the K^+ ion from binding to the top of the selectivity filter (Figure 1.2b, c). Furthermore, they discovered that when this K27 residue of the toxin was substituted to a methionine residue, the structure of the channel in complex with this toxin variant contained significant K^+ ion density at this position of the selectivity filter.

In 1994, the MacKinnon group reported the discovery of a 38 residues-long peptide, agitoxin-2 (AgTx-2) which was isolated from the venom of the scorpion, *Leiurus quinquestriatus* that binds to the Shaker K_v channel (Garcia et al., 1994). The similarities in the secondary structures and the disulfide binding patterns between AgTx and CTX in addition to the presence of a conserved lysine residue (Figure 1.1) that in CTX inserts into the channel to orchestrate inhibition motivated Mackinnon and coworkers to explore whether AgTx2 employs a similar mechanism of action. To test this hypothesis, they systematically mutated the pore region residues of the Shaker K_v channel to lysine residues to introduce positively charged centers in the channel that would hinder the toxin's lysine side chain from gaining access to negatively charged residues of the channel due to electrostatic repulsion. Eleven of these twenty-five variants gave non-functional channels but out of the other fourteen variants, five demonstrated a dramatic reduction in toxin affinity. Most of these residues, lie in the peripheral pore region of the Shaker channel (Gross and MacKinnon, 1996). In addition to this work on CTX and AgTx, the mechanism of action of a K_v channel-targeting sea anemone toxin named stichodactyla toxin

(ShK) has been studied and has been demonstrated to employ a mode of inhibition that is very similar to that of CTX (Bajaj and Han, 2019; Chang et al., 2018).

Very recently, a cone snail toxin, Conkunitzin-S1 (Cs1), has been discovered that blocks the $K_v1.2$ channel by binding to its pore turret (Karbat et al., 2019). Cs1 is believed to employ an arsenal of Tyr and Arg residues on the channel-facing surface of the toxin that form electrostatic, π–π, cation–π and aromatic–aliphatic stacking interactions with the hydrophobic and acidic residues of the channel's pore turret. The resultant channel inhibition is hypothesized to be more

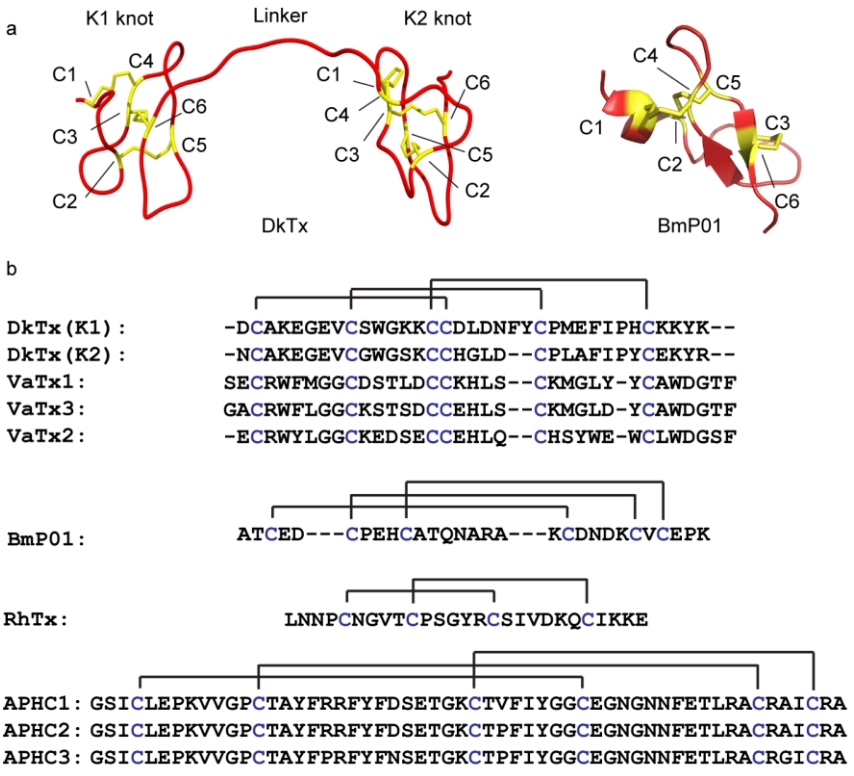

Figure 1.3. ICK toxins that target TRPV1. a) Structures of DkTx (PDB ID: 5irx), BmP01 (PDB ID: 1wm7) where the ICK backbones are shown in red with the disulfide bridge forming cysteines are shown in yellow (Gao et al., 2016; Wu et al., 2000). b) Peptide sequence alignment and disulfide bonding pattern of DkTx individual knots and vanillotoxins (all these toxins share similar cystine knot folds comparable to HaTx). The sequence of structurally unrelated toxins, BmP01, RhTx and APHC1-3 are depicted separately.

complicated than a simplistic model involving electrostatic pore block. Instead, the mechanism is proposed to involve the disruption of a mesh of hydrogen bonds that controls water entry to the peripheral cavities surrounding the central pore resulting in an abnormal flow of water triggering an asymmetric collapse of the pore.

1.2.1.2. TRP channels. Transient receptor potential (TRP) ion channels are non-selective cation channels expressed in diverse animal cell types that are characterized by their ability to be modulated by a variety of stimuli (Moran, 2018; Zheng, 2013). Despite the discovery of the *trp* gene back in 1969 (Cosens and Manning, 1969) and the cloning of the first TRP channel in 1989 (Montell and Rubin, 1989), molecular-level understanding of the mechanism of activation of these channels by various stimuli has remained limited. Perhaps a major contributing factor to this scenario was the lack of powerful and specific molecular tools such as selective toxins targeting these channels. Indeed, whereas ion channel biophysicists were making major progress in understanding K_v channel structure and function in the 1980s and 90s by employing both pore-target toxins such as CTX and AgTx as well as voltage sensor-targeting toxins discussed in detail in section 1.2.2 below, it was only after the functional annotation of the TRPV1 ion channel as a capsaicin and heat sensor by David Julius' laboratory (Caterina et al., 1997), that mechanistic studies on TRP channel function started being aggressively pursued.

In 2006, the first report on the discovery of TRP channel-activating ICK toxins called vanillotoxins (VaTx) was published by the Julius laboratory (Figure 1.3) (Siemens et al., 2006). Another important paper was published in 2010 by the Julius laboratory wherein the discovery of a potent TRPV1-activating toxin containing two ICK motifs referred to as the double-knot toxin or DkTx was reported (Figure 1.3). This toxin was isolated from the Chinese bird spider (*O. huwena*) and fascinatingly, was observed to activate the channel almost irreversibly (Bohlen et al., 2010). Whereas most of the other known toxins belonging to the ICK toxin family contain only one ICK motif, DkTx has two ICK motifs (lobes K1 and K2 joined by a linker, Figure 1.3a). Interestingly, the two lobes can independently activate the channel (as single ICK toxins), albeit with much poorer potency and faster wash-off rates as compared to DkTx (Bae et al., 2012; Bohlen et al., 2010). Even though the two lobes possess a high sequence similarity (65.7 %), the K2 lobe activates the channel with a much higher potency as compared to the K1 lobe

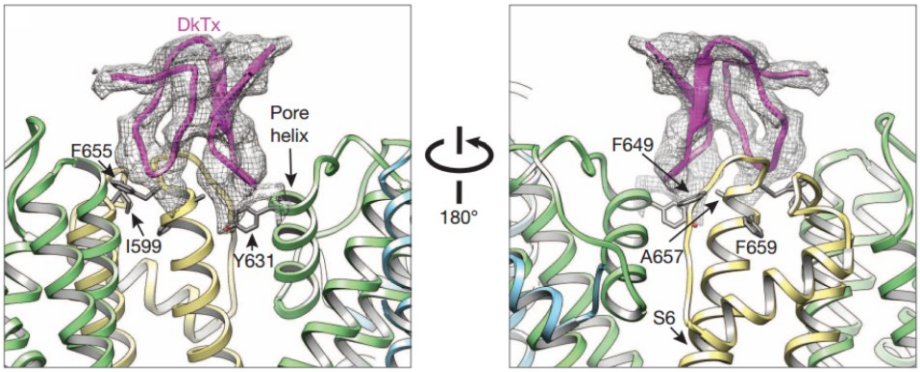

Figure 1.4. The cryo-EM structure of the DkTx-TRPV1 complex (Cao et al., 2013). The toxin binds in close proximity to the TRPV1 ion channel residues identified by the functional studies performed by Bohlen et al. (Bohlen et al., 2010). Figure adapted from Cao et al., 2013.

(Bae et al., 2012; Bohlen et al., 2010). To determine the binding site of the toxin on the channel, Julius and coworkers performed an alanine scan of the outer pore region of TRPV1 that suggested that the toxin binds to the residues I599, F649, A657 and F659 of the channel (Bohlen et al., 2010). In support of this prediction, the first cryo-electron microscopy (cryo-EM) structure of TRPV1 ion channel in an agonist bound activated state that was elucidated in 2013 revealed that the electron densities for the DkTx toxin were in close proximity to those of these residues of TRPV1 (Figure 1.4) (Cao et al., 2013).

A study published by the Kenton Swartz laboratory in 2016 provided some vital insights into the mechanism of activation of TRPV1 by DkTx (Bae et al., 2016). In this paper, the authors solved the NMR structure of DkTx and observed that the surface of DkTx is amphipathic potentially endowing it with the ability to partition into membranes akin to the properties of toxins such as hanatoxin (HaTx) that target the voltage sensors of voltage-gated ion channels by partitioning into the cell membrane (discussed in detail below in section 1.2.2). Swartz and coworkers went on to test this hypothesis by performing membrane partitioning studies that demonstrated that DkTx partitions very well into membranes (Bae et al., 2016). Furthermore, Swartz and coworkers performed a molecular dynamics simulation to predict the atomic level interactions between the channel and the toxin by docking their NMR structure of DkTx into the TRPV1-DkTx complex structure (Cao et al., 2013). These studies led them to infer that two

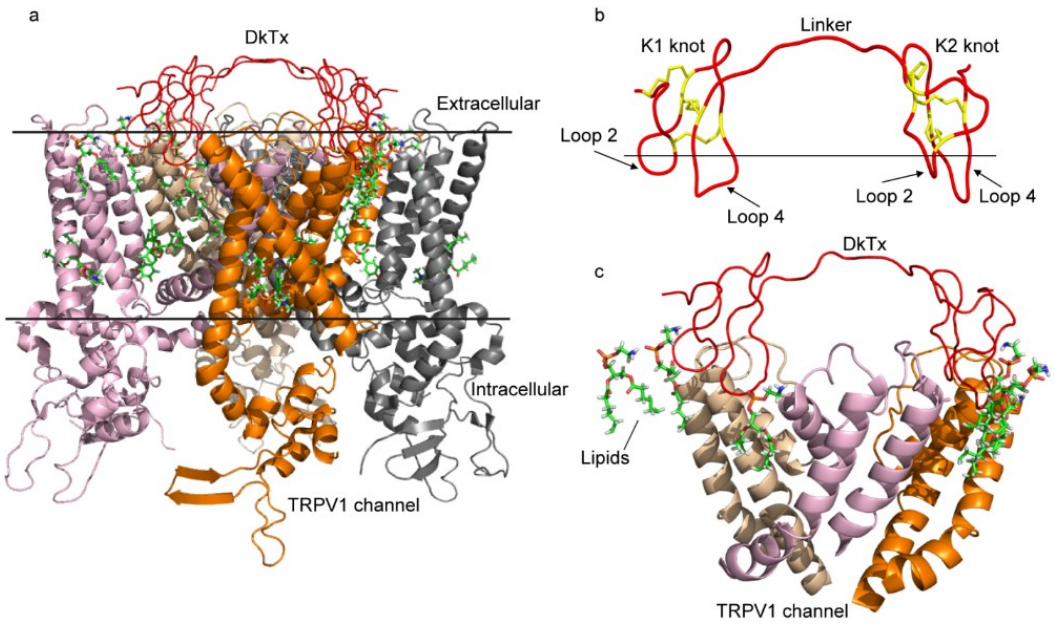

Figure 1.5. Structure of DkTx-TRPV1 complex obtained in lipid nanodiscs. a) Side-view of the DkTx-bound TRPV1 channel complex (PDB: 5irx) (Gao et al., 2016) with the four subunits of the TRPV1 channel depicted in different colors. Stick representations in the structure depict either lipid molecules or vanilloid agonists of the TRPV1 ion channel. Two DkTx molecules bound at the pore region of the channel are shown in red. b) DkTx structure (in red) depicting the K1 and K2 knots of the toxin and the linker that joins these knots with the disulfide bridges of the two knots in yellow. Membrane-interacting loops (loops 2 and 4) of the toxin are annotated and the outer membrane boundary is shown as a horizontal line. c) Magnified view of the toxin-lipid-chanel tripartite complex.

DkTx molecules bind onto the pore region of the channel in an anticlockwise manner and that the loop 2 and loop 4 of both the knots dip down into the membrane to form a channel-lipid-toxin tripartite complex. Additionally, Swartz and coworkers performed *in silico* docking experiments in artificial membranes composed of phosphatidylcholine lipids (POPC) to predict which residues of the toxin are likely to interact with membrane lipids. These studies predicted that the toxin, the channel and membrane lipids form a tripartite complex that plays an important role in the toxin-activation of the channel.

A structure of the DkTx-TRPV1 complex (Figure 1.5) in lipid nanodiscs was solved in 2016 (Gao et al., 2016) that validated several key predictions of the model proposed by the Swartz laboratory discussed above as well as the binding site information obtained from the mutagenesis experiments performed by David Julius's group back in 2010 (Bohlen et al., 2010). Solved at a resolution of 2.95 Å that was higher than that of the structure reported in 2013, this structure provided fascinating insights into the interactions of the toxin with membrane lipids in line with the predictions made by Swartz and coworkers discussed above (Bae et al., 2016). The structural framework that both these studies put forth provided a template on which my work reported in Chapter 2 of this thesis is based.

In addition to the aforementioned TRPV1 activating toxins, the scorpion toxin, BmP01 was discovered in the year 2000 (Wu et al., 2000), but was only found to target the TRPV1 channel in 2015 (Hakim et al., 2015). In contrast to other members of the α-KTX family of toxins that are channel inhibitors, BmP01 (Figure 1.3) activates the TRPV1 channel. Mutagenesis and thermodynamic double-mutant cycle experiments have suggested that the interaction between the K23 of BmP01 and E649 of the TRPV1 S6 helix are the primary functional determinants of this complex, however, alanine variants of the residues T651 and E652 also affects the toxin's TRPV1 activating potency (Yang et al., 2017). Another ICK toxin, RhTx, was discovered from the venom of the Chinese Red-headed centipede that induces pain by targeting the TRPV1 ion channel (Figure 1.3b). RhTx contains only two disulfide linkages and its mechanism of TRPV1 activation involves a charged residue cluster comprising of residues D20, Q22 and E27 of the toxin. Alanine mutagenesis profiling indicated that the residues D602 (pore turret), Y632 and T634 belonging to the pore helix of the TRPV1 channel are crucial for channel activation by toxin (Yang et al., 2015).

In addition to the TRPV1-activating toxins described above, Kunitz type ICK toxins from sea anemone (APHC1-3, Figure 1.3b) with TRPV1-inhibitory functions have been isolated and shown to act via a pore-binding mechanism (Andreev et al., 2013; Geron et al., 2017).

1.2.2. Toxins that target auxiliary motifs of ion channels

The ICK family of toxins that target tetrameric ion channels also consist of toxins that target motifs of channels that lie outside of the pore domain. Among these toxins, there are "paddle toxins" that bind to the voltage sensor domains (VSDs) of voltage-gated ion channels resulting in

channel inhibition (Clairfeuille et al., 2019; Shen et al., 2018; Shen et al., 2019; Xu et al., 2019). The voltage sensors of these channel are formed by their S1-S4 helices (Figure 1.2a) and the voltage-sensing arginine residues are found in the S4 helices of these channels (Kuang et al., 2015; Long et al., 2007; Xu et al., 2019). These paddle toxins have been demonstrated to partition into the membrane and target the S3b-S4 helix-turn-helix motif of the voltage sensors (Alabi et al., 2007; Bosmans et al., 2008; Milescu et al., 2007; Phillips et al., 2005; Swartz, 2008). The S3b-S4 motif is referred to as the "paddle" motif and it is believed to play a key role in voltage sensing by undergoing a conformational change upon voltage stimulation resulting in opening or closure of the channel pore.

Hanatoxin (HaTx, Figure 1.6a) was the first paddle toxin to be discovered (Swartz and MacKinnon, 1995). It was isolated from the venom of *Grammostola spatulata* and was found to target the mammalian potassium channel, $K_V2.1$. Contrary to the pore-binding toxins CTX and

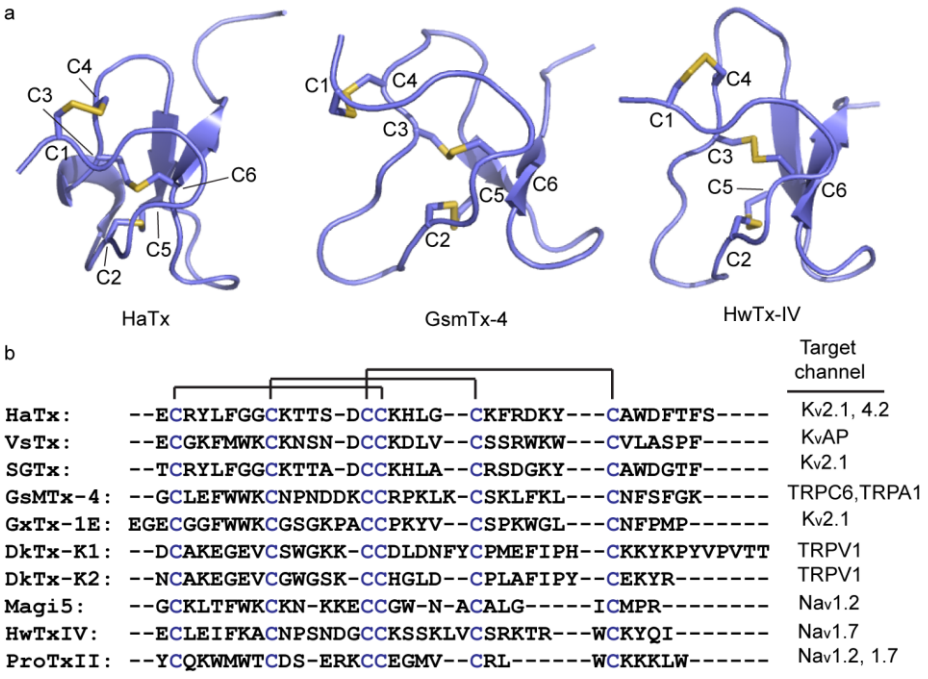

Figure 1.6. ICK toxins targeting the voltage sensors of voltage-gated ion channels. a) Structures of HaTx (PDB: 1d1h) (Takahashi et al., 2000), GsMTx4 (PDB: 1tyk) (Oswald et al., 2002) and HwTx-IV (PDB: 1mb6) (Peng et al., 2002). Disulfide bridges are shown in yellow sticks. b) The sequence alignments of a few selected ICK toxins with the cysteine residues marked in blue.

AgTx, HaTx did not inhibit a Shaker K_v channel variant containing the pore domain of $K_v2.1$ consistent with the observation that it does not target the pore of $K_v2.1$ (Swartz and MacKinnon, 1995). When the paddle motif of $K_v2.1$ was transplanted into the Shaker K_v channel, the resulting chimeric channel was rendered sensitive to HaTx (Alabi et al., 2007) demonstrating conclusively that HaTx is indeed a $K_v2.1$ paddle-targeting ICK toxin. Alanine scanning of the paddle motif of $K_v2.1$ revealed that the alanine variants of several residues located at the *C*-terminal region of the S3 helix demonstrated a considerable drop in potency. In a cohabitation assay where both AgTx2 and HaTx were allowed to bind the channel simultaneously, it was observed that at higher depolarizing voltages where HaTx is not able to inhibit the channel currents completely, AgTx2 can still bind to its channel binding site resulting in channel inhibition, thereby provided further support for the hypothesis that the channel binding sites of HaTx and AgTx2 do not overlap (Swartz and MacKinnon, 1997).

The nature of interactions between HaTx and the $K_v2.1$ channel were investigated by the Swartz group by performing mutagenesis-based functional studies (Li-Smerin and Swartz, 2000). The results of these studies when considered along with the insights obtained from the NMR structure of HaTx (Takahashi et al., 2000) resulted in the identification of hydrophobic and salt bridging interactions between the residues of the toxin and those of the S3 helix of the channel. In another important paper on the mechanism of action of HaTx (Lee et al., 2003), the effects of the toxin on the gating currents of $K_v2.1$ were studied which revealed that HaTx hinders the motion of the voltage sensor at low depolarization voltages. At higher depolarization voltages, however, the toxin binding affinity was observed to be reduced, suggesting that HaTx binds and stabilizes the resting state of the voltage sensors (Phillips et al., 2005). Within 20 years of the discovery of HaTx, several other ICK paddle-toxins targeting K_v, Na_v and Ca_v channels have been discovered, the sequences of some of which are provided in Figure 1.6b. Studies on the toxins SGTx1, ScTx1 and GxTx1E that target $K_v2.1$, and PaTx1-2, HpTx1-3 and TLTx1 that target K_v4 channels have been demonstrated to employ channel modulatory mechanisms similar to that described above for HaTx (Swartz, 2007).

Na_v channels are targeted by more than a hundred spider and scorpion toxins (Bosmans and Swartz, 2010; Possani et al., 1999). Biophysical and biochemical studies on these toxins and their target Na_v channels have elucidated three major modes by which these toxins modulate

channel function (Ahern et al., 2016). One of these mechanisms that is employed by the α-scorpion toxins Lqh2 that contains 8 cysteine residues (as opposed to the classical ICK toxins that contain 6 cysteines) involves the binding of these toxins to the VSD of domain IV of $Na_v1.2$ in the resting state thereby limiting the movement of the VSD under depolarizing voltages ultimately resulting in inhibition of fast inactivation of the channel (Benzinger et al., 1998; Gur et al., 2011). The classical ICK toxin, JZTx-IV, also inhibits the $Na_v1.5$ channel via a similar mechanism (Wang et al., 2008). On the contrary, the β-scorpion toxins Ts1 and Magi5 interact with the domain II S3b-S4 motif of $Na_v1.4$ and $Na_v1.2$ respectively and promote opening of the channel at hyperpolarizing voltages (Campos et al., 2007; Cestele et al., 1998; Cestele et al., 2006; Corzo et al., 2007; Leipold et al., 2012; Marcotte et al., 1997). Several other ICK toxins such as ProTx-II inhibit channel opening at depolarizing voltages by binding to the domain II VSD of $Na_v1.2$ channels (Ahern et al., 2016; Bosmans et al., 2008; Edgerton et al., 2008; Sokolov et al., 2008). In addition to structure-function studies, antibody and photocrosslinking assays have demonstrated that the sodium channel gating-modifier α-scorpion toxins LqTx and

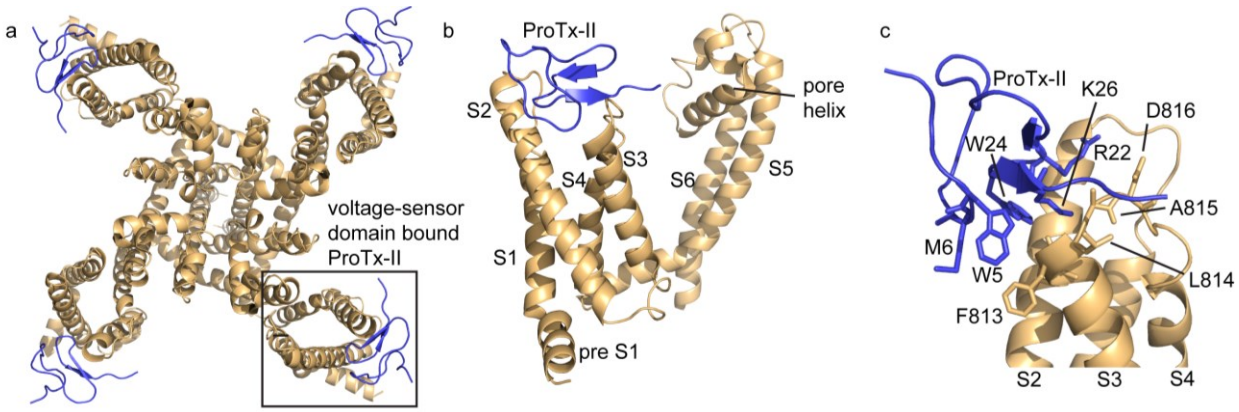

Figure 1.7. Structure of the ProTx-II bound $Na_v1.7$-VSD-Na_vAb chimeric channel (PDB: 6n4i) (Xu et al., 2019). a) Top-view depicting all the four voltage sensor domains of the homotetrameric chimeric channel bound to the toxin. b) Magnified view of a single subunit of the chimeric channel bound to ProTx-II depicting its binding site at the VSD. c) Residues of the toxin and the channel VSD that participate in non-covalent interactions. Residues of the 'LFLAD' motif of the channel denoted in the structure.

Lqh2 also interact with the S5-S6 loop of domain I and the S1-S2 loop of domain IV besides interacting with domain IV S3b-S4 motif of Na_v 1.2 (Tejedor and Catterall, 1988; Thomsen and Catterall, 1989; Wang et al., 2011). Recently, four different structures of ICK paddle toxins bound to Na_v channels at their VSDs have been solved (Clairfeuille et al., 2019; Shen et al., 2018; Shen et al., 2019; Xu et al., 2019). In the α-scorpion toxin AaH2-bound structure of the VSD4 of the Na_vPas channel, the toxin is seen to interact with not only the S3b-S4 motif of the VSD4 but also with the channel's S2 helix as determined by mutagenesis and biochemical studies on other α-scorpion toxins such as Lqh2 and LqTx discussed above (Clairfeuille et al., 2019). In a crystal structure of the ProTx-II bound $Na_v1.7$-VSD-Na_vAb chimeric channel wherein the VSD2 of $Na_v1.7$ was transferred into the Na_vAb channel, interactions between W5, M6 and W24 of the ProTx-II and the LFLAD motif of the $Na_v1.7$ paddle region (comprising of the L812, F813, L814, A815 and D816 of the S3b-S4helix) are clearly visible (Figure 1.7). The authors also report electrophysiology-based structure-function studies involving the generation of variants of the channel at its toxin-binding site (Xu et al., 2019).

Besides K_v and Na_v channels, TRP channel-targeting gating modifier ICK toxins have also been reported. Hill and Schaefer had demonstrated that GsMTx-4 (Figure 1.6) isolated from the venom of *G. spatulata*, activates the TRPA1 mechanosensitive ion channel (Hill and Schaefer, 2007). The same toxin was also found to inhibit TRPC1, TRPC6 and Piezo1 channels (Alessandri-Haber et al., 2009; Bae et al., 2011; Ostrow et al., 2003; Spassova et al., 2006). A report from Wanke and coworkers demonstrated that GsMTx4 is indeed a promiscuous toxin that can inhibit seven subtypes of Na_v and two subtypes of K_v channels (Redaelli et al., 2010).

1.2.3. Insights from structures of ICK toxins alone (without the channel)

Although success in solving the structures of ICK toxins in complex with the channels they target has been obtained only very recently, several structures of ICK toxins alone have been solved over the years (Cardoso and Lewis, 2019). The structures of the paddle toxins, HaTx (Figure 1.6a) and VSTx1 were one of the first ICK toxin structures to be solved apart from the CTX family of toxins. These structures revealed that both HaTx and VsTx1 are made up of three strands of antiparallel β-sheets devoid of any α-helical folds (as seen with the CTX family of toxins) (Jung et al., 2005; Takahashi et al., 2000). However, other structures of paddle toxins have shown variation in number of β-strands present in their structures (Lee et al., 2004; Oswald

et al., 2002). Many voltage sensor ICK toxins such as HaTx and SGTx1 are amphipathic and are comprised of a cluster of hydrophobic residues that is surrounded by basic, acidic or polar residues that allow a high degree of solvent exposure (Lee et al., 2003; Takahashi et al., 2000) as shown in Figure 1.8, where I have employed the Eisenberg scale of hydrophobicity (Eisenberg et al., 1984) to depict the surface properties of these ICK toxins. Whereas the pore-binding toxins CTX and AgTx have charged or polar residues on their channel-binding surfaces, the membrane-

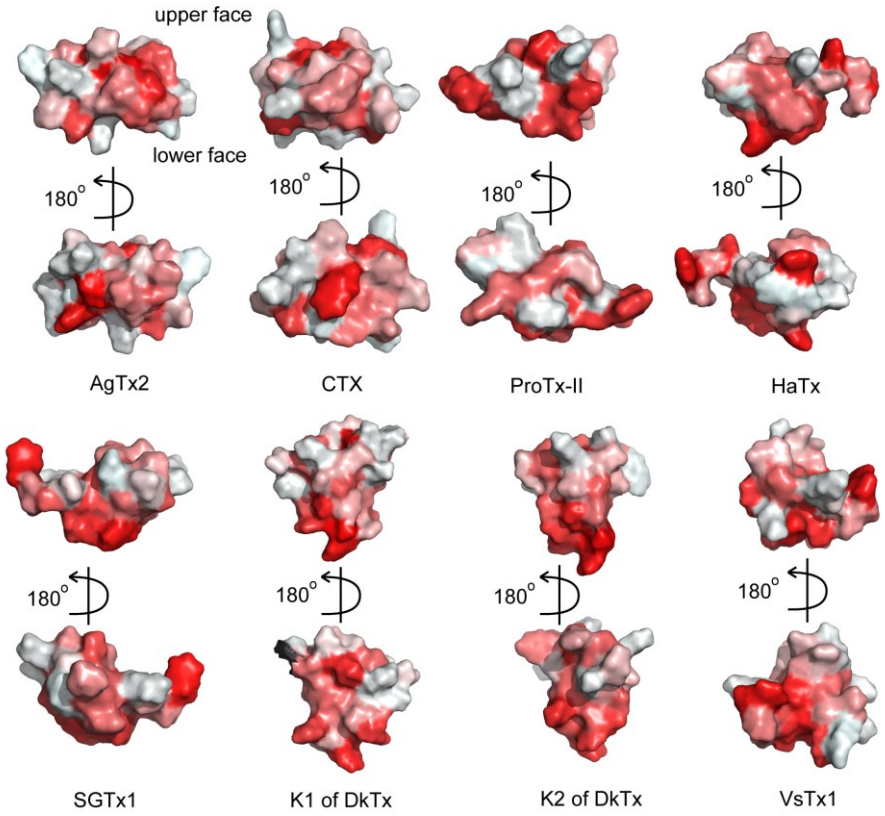

Figure 1.8. Surface renditions of ICK toxins in the Eisenberg hydrophobicity scale wherein the intensity of the red color is proportional to the hydrophobicity of residues. The lower face of the AgTx2 (PDB: 1agt) and CTX (PDB: 2crd) represents the channel-binding surface, whereas for ProTx-II (PDB: 2n9t), HaTx (PDB: 1d1h), SGTx1 (PDB: 1la4) and VsTx1 (PDB: 2n1n), the lower face represents the membrane-interacting surface (Bontems et al., 1992; Henriques et al., 2016; Krezel et al., 1995; Lau et al., 2016; Lee et al., 2004; Takahashi et al., 2000). For the K1 knot (PDB: 2n9z) and the K2 knot (PDB: 2naj) of DkTx, the lower face depicts the surface that forms a tripartite complex with the TRPV1 channel and membrane lipids (Bae et al., 2016).

partitioning paddle toxins HaTx, SGTx1, VsTx1, ProTx-II predominantly contain hydrophobic residues on their membrane-interacting surfaces (Figure 1.8). Interestingly, a hydrophobic surface akin to the ones identified in the paddle toxins was also observed in each of the knots of DkTx, as shown in Figure 1.8 (bottom panel) despite the fact that DkTx binds to its target channel's pore domain. This observation suggests that DkTx possesses high membrane partitioning propensity similar to that demonstrated by the paddle toxins. This hypothesis was demonstrated to be correct by the results obtained from membrane partitioning studies performed on DkTx by the Swartz laboratory (Bae et al., 2016).

1.2.4. Studies on the interactions of toxins with membrane lipids

Mechanistic studies on paddle toxins, particularly those on HaTx by the Mackinnon and Swartz laboratories discussed above that demonstrated that these toxins bind to membrane-embedded paddle motifs of channels at the resting state of the voltage sensor implied that these toxins were somehow partitioning into the membrane to reach their binding sites. This observation set the stage for detailed studies on membrane partitioning properties of these toxins by employing the intrinsic fluorescence of the Trp amino acid residues present in these toxins. Perhaps the most insightful studies on membrane partitioning of toxins were performed by the Swartz laboratory on the paddle toxin, HaTx (Phillips et al., 2005; Phillips et al., 2009) that revealed that the surface-exposed W30 residue of the toxin shows a blue shift of ~11 nm in its fluorescence emission when it is incubated with large unilamellar vesicles composed of a 1:1 mixture of 1-palmitoyl-2-oleoyl-sn-glycero-3-phosphocholine (POPC) and 1-palmitoyl-2-oleoyl-snglycero-3-[phospho-rac-(1-glycerol)] (POPG) (Figure 1.9a). Increase in tryptophan fluorescence intensity with concomitant blue shift of the emission spectra is characteristic of a peptide that partitions well into membranes (Ladokhin et al., 2000). Fitting a defined partition function to the plots of relative fluorescence intensity (F/F_o) at 320 nm yields the mol. fraction partitioning coefficient or K_x of the toxin—a high K_x value is indicative of good membrane partitioning. A K_x value of 1.8×10^6 reported for HaTx (Swartz, 2007), for instance, suggests that this toxin partitions well into the membrane. Similar analysis performed on yet another gating modifier toxin, SGTx, yielded a K_x value of 3.6×10^6, suggestive of a HaTx-like mechanism of action (Milescu et al., 2007). Earlier reports from the Mackinnon laboratory also demonstrated that the K_vAP channel targeting toxin, VsTx1, partitions well into artificial membranes (Lee and MacKinnon, 2004).

More recently, Swartz and coworkers have demonstrated using similar tryptophan-based membrane partitioning experiments that the TRPV1-targeting toxin, DkTx, partitions well into large unilamellar vesicles (LUVs) made of POPC/POPG (K_x of 2.3×10^6) (Bae et al., 2016) which portends an important role of the membrane in functional modalities of DkTx (Figure 1.9b).

In addition to the experiments summarized above, another type of partitioning analysis is performed to estimate the depth to which peptides penetrate into the membrane. These experiments entail the use of di-brominated lipids possessing bromo substituents at different position on the lipidic tail that are known to quench Trp fluorescence (Ladokhin, 1999; McIntosh and Holloway, 1987). This approach when applied on HaTx by the Swartz laboratory revealed that the fluorescence of the Trp residue of HaTx was most effectively quenched by 9, 10-diBr lipids (Figure 1.9a, right panel) suggesting that the W30 residue of HaTx protrudes into the membrane to a distance of about 8.5 Å from the center of the membrane bilayer (Phillips et al., 2005).

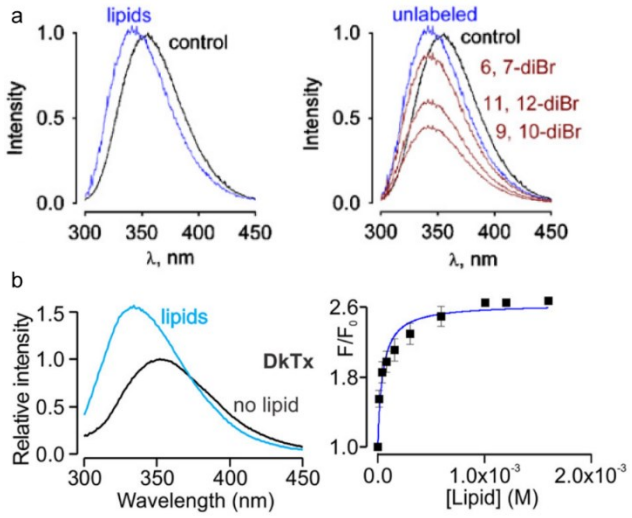

Figure 1.9. Partitioning of ICK toxins into artificial membranes. a) The left panel depicts fluorescence emission spectrum of HaTx in LUVs made up of POPC/POPG lipids and that obtained in buffer without LUVs. The right panel shows the emission spectra of HaTx in LUVs containing dibrominated lipids. Figures adapted from Swartz, 2007. b) The left panel depicts the fluorescence emission spectra of DkTx in presence and absence of LUVs. The right panel shows the partitioning function plot corresponding to the DkTx. Figures adapted from Bae et al., 2016.

In addition to these membrane partitioning studies, experiments based on the treatment of membranes with lipases have also made important contributions in understanding the roles of membrane lipids in toxin-modulation of channel function. Building on the work of Zhe Lu and coworkers that demonstrated that the treatment of $K_v2.1$ channel-expressing *Xenopus laevis* oocytes with the lipase, Sphingomyelinase D (SMase D), leads to channel activation at lower than usual depolarization voltages (Ramu et al., 2006; Xu et al., 2008), Swartz and coworkers studied the effects of this enzymatic treatment on paddle toxin-modulation of the channel. These studies demonstrated that toxin-modulation was perturbed upon this alteration of the membrane lipid properties. Indeed, the potency of a variant of the $K_v2.1$ channel (V282A) that weakens the affinity of the GxTx-1E paddle toxin towards the channel was restored to wild-type toxin affinity when the oocyte membrane was modified by SMase D application. The authors also reported that the residues of the channel that are most sensitive to SMase D-mediated changes in the membrane lie on the S3b helix facing the external lipid environment (Milescu et al., 2009). Another fascinating study on the role of lipids in toxin-modulation of channel function involved chemically induced depalmitoylation of the $Na_v1.2$ channel that demonstrated that removal of the palmitoyl group from the channel increased its affinity for the paddle toxins PaurTx3 and ProTx-II (Bosmans et al., 2011). This study also reported that in addition to altering the toxin's channel binding affinity, depalmitoylation also delayed the fast inactivation kinetics as well as recovery from fast inactivation of the $Na_v1.2$ channel.

Taken together, the results from these multifaceted studies employing different approaches convincingly demonstrate that the membrane plays an important role in the channel-modulatory activity of a variety of toxins. Consequently, studying the membrane-interaction properties of toxins is of paramount importance in fully understanding their mechanism of action.

1.3. Applications of toxins outside of the biophysics spectrum.

1.3.1. Toxins as imaging tools.

The ability of toxins to specifically bind to ion channels renders them attractive for applications that involve channel imaging (Sinai et al., 2006). Towards this goal, toxins have been labeled either site-specifically or randomly with fluorophores by employing a variety of approaches including *N*-hydroxy succinimidyl ester chemistry for labeling the ε-amino groups of lysine

residues, maleimide chemistry for labeling cysteinyl thiols, and via iodination of the tyrosine residues of toxins (Bingham et al., 2006; Hafidi et al., 2005; Massensini et al., 2002; Pragl et al., 2002). Jon Sack's group fluorescently labeled GxTx using thiol bioconjugation chemistry that allowed temporal imaging of binding and unbinding events of the fluorescent toxin on the $K_v2.1$ channel in live Chinese hamster ovary cells (Tilley et al., 2014). Du Bois and coworkers fluorescently labeled the small molecule toxin, saxitoxin, and used it to image Na_v channels in live neurons (Ondrus et al., 2012). In addition to these thiol and amine bioconjugation approaches, fluorophores have also been appended to toxins by employing biorthogonal chemistry on suitable chemical handles installed into toxins (Dang et al., 2014; Tilley et al., 2014). In addition to imaging, another application of fluorescently labeled toxins involves developing flow-cytometry based assays for sorting matured T-lymphocytes from naïve T-lymphocyte population based on their $K_v1.3$ channel expression (Beeton et al., 2003).

1.3.2. Toxins as therapeutic agents.

Considering that ion channels are extremely attractive targets for therapeutic intervention, the specificity of toxins for specific channel subtypes renders them ideal drug candidates (Kintzing and Cochran, 2016; Peigneur and Tytgat, 2018). Several toxins and toxin derivatives have demonstrated promise in the treatment of chronic pain, cerebral stroke, diabetes, autoimmune diseases and cancer (Bogin, 2005). For example, two variants of the chloride channel-targeting toxin, chlorotoxin, with trade names of TM-601 and TM-701 are currently in clinical trials for brain tumor and cancer therapy. Ziconitide, a variant of the ω-conotoxin that targets $Ca_v2.2$ channels, has obtained FDA approval for severe or chronic pain medication in the year 2004 (Prommer, 2006). Over the past decade, significant efforts have been put into developing toxins as therapeutic agents. For example, the GpTx-I toxin has been investigated in detail and has been subjected to mutagenesis-based studies and has also been appended with polyethyleneglycol derivatives and antibodies leading to the development of toxin derivatives possessing higher selectivity, potency and *in vivo* half-life for targeting $Na_v1.7$ channels present in peripheral pain receptors (Biswas et al., 2017; Murray et al., 2015a; Murray et al., 2015b; Murray et al., 2016). Another promising recent example of the therapeutic promise of toxins is that of development of a potent and selective HwTx-IV variant by Astrazeneca Pharmaceuticals for targeting $Na_v1.7$ for the treatment of peripheral pain (Revell et al., 2013). Unfortunately, however, despite all these

efforts towards the development of peptide toxin-based therapeutic agents, the number of approved peptide drugs in market remain significantly low.

1.3.3. Tethered toxins as tools for modulating cell autonomous functions of channels.

The use of toxins as tools for ion channel and receptor modulation *in vivo* have emerged over the past couple of decades. For example, Heintz and coworkers have been successful in expressing α-bungarotoxin appended to a glycosylphosphatidylinositol (GPI)-anchored mammalian prototoxin *lynx1* in zebrafish cell membranes to modulate nicotinic AChR (nAChR) function *in vivo* allowing them to achieve targeted inhibition of nAChR thereby inhibiting synaptic transmission without perturbing synapse formation (Ibanez-Tallon et al., 2004). Using a similar approach, ω-conotoxin MVIIA, an inhibitor of $Ca_v2.2$ channel, was expressed appended to a GPI-anchor in the peripheral nociceptor neurons in transgenic mice. When subjected to inflammatory pain inducing stimuli, these animals exhibited reduced pain response as compared to those elicited in wild-type mice (Auer et al., 2010).

1.4. Future prospects

One of the most prominent emerging themes from the recent structural and functional studies on toxin-modulation of channel function is the dominant roles of membrane lipids in this process. Indeed, the presence of lipids bound to functionally important sites of ion channels (Gao et al., 2016; Matthies et al., 2018; Nury et al., 2011; Payandeh et al., 2012; Payandeh et al., 2011) including those where toxins bind (Gao et al., 2016) portends a central importance of lipids in channel function. Although these structures have provided significant insights on protein-lipid interfaces, it is imperative to not over-interpret their functional roles just on the basis of these structures. Instead, these structures should be considered as templates for the design and execution of electrophysiology-based structure-function studies focused on interrogating the roles of these interfaces in channel function. Additionally, the development of precise binding assays that enable the measurement of the dissociation constants of membrane-toxin complexes in native cellular membranes is necessary. This multipronged approach combining structural biology, functional studies and binding assays is required for an in-depth understanding of the roles of lipids in ion channel function.

In addition to the recent structural biology revolution, recent breakthroughs in studying protein-lipid interaction by employing native mass spectrometry (Bolla et al., 2018; Laganowsky et al., 2014; Zhou et al., 2011) have tremendous potential in contributing towards understanding the roles of lipids in toxin-modulation of channel function. Additionally, recent advances in technologies for incorporating UV-crosslinkable groups on cellular lipids that have enabled the discovery of lipid-interacting proteomes (Gubbens et al., 2009; Niphakis et al., 2015; Wang et al., 2017) constitute one of the most promising new approaches for mapping protein-lipid interfaces of membrane-interacting proteins. Application of these modern approaches on toxins and on toxin-channel complexes can provide novel insights on the mechanisms underlying toxin-activation of ion channels, and by extension, on ion channel gating.

1.5 References.

Ahern, C.A., Payandeh, J., Bosmans, F., and Chanda, B. (2016). The hitchhiker's guide to the voltage-gated sodium channel galaxy. J Gen Physiol *147*, 1-24.

Alabi, A.A., Bahamonde, M.I., Jung, H.J., Kim, J.I., and Swartz, K.J. (2007). Portability of paddle motif function and pharmacology in voltage sensors. Nature *450*, 370-375.

Alessandri-Haber, N., Dina, O.A., Chen, X., and Levine, J.D. (2009). TRPC1 and TRPC6 channels cooperate with TRPV4 to mediate mechanical hyperalgesia and nociceptor sensitization. J Neurosci *29*, 6217-6228.

Anderson, C.S., MacKinnon, R., Smith, C., and Miller, C. (1988). Charybdotoxin block of single Ca2+-activated K+ channels. Effects of channel gating, voltage, and ionic strength. J Gen Physiol *91*, 317-333.

Andreev, Y.A., Kozlov, S.A., Korolkova, Y.V., Dyachenko, I.A., Bondarenko, D.A., Skobtsov, D.I., Murashev, A.N., Kotova, P.D., Rogachevskaja, O.A., Kabanova, N.V.*, et al.* (2013). Polypeptide modulators of TRPV1 produce analgesia without hyperthermia. Mar Drugs *11*, 5100-5115.

Auer, S., Sturzebecher, A.S., Juttner, R., Santos-Torres, J., Hanack, C., Frahm, S., Liehl, B., and Ibanez-Tallon, I. (2010). Silencing neurotransmission with membrane-tethered toxins. Nat Methods *7*, 229-236.

Bae, C., Anselmi, C., Kalia, J., Jara-Oseguera, A., Schwieters, C.D., Krepkiy, D., Won Lee, C., Kim, E.H., Kim, J.I., Faraldo-Gomez, J.D.*, et al.* (2016). Structural insights into the mechanism of activation of the TRPV1 channel by a membrane-bound tarantula toxin. Elife *5*.

Bae, C., Kalia, J., Song, I., Yu, J., Kim, H.H., Swartz, K.J., and Kim, J.I. (2012). High yield production and refolding of the double-knot toxin, an activator of TRPV1 channels. PLoS One *7*, e51516.

Bae, C., Sachs, F., and Gottlieb, P.A. (2011). The mechanosensitive ion channel Piezo1 is inhibited by the peptide GsMTx4. Biochemistry *50*, 6295-6300.

Bajaj, S., and Han, J. (2019). Venom-Derived Peptide Modulators of Cation-Selective Channels: Friend, Foe or Frenemy. Front Pharmacol *10*, 58.

Banerjee, A., Lee, A., Campbell, E., and Mackinnon, R. (2013). Structure of a pore-blocking toxin in complex with a eukaryotic voltage-dependent K(+) channel. Elife *2*, e00594.

Beeton, C., Wulff, H., Singh, S., Botsko, S., Crossley, G., Gutman, G.A., Cahalan, M.D., Pennington, M., and Chandy, K.G. (2003). A novel fluorescent toxin to detect and investigate Kv1.3 channel up-regulation in chronically activated T lymphocytes. J Biol Chem *278*, 9928-9937.

Benzinger, G.R., Kyle, J.W., Blumenthal, K.M., and Hanck, D.A. (1998). A specific interaction between the cardiac sodium channel and site-3 toxin anthopleurin B. J Biol Chem *273*, 80-84.

Bingham, J.P., Bian, S., Tan, Z.Y., Takacs, Z., and Moczydlowski, E. (2006). Synthesis of a biotin derivative of iberiotoxin: binding interactions with streptavidin and the BK Ca2+-activated K+ channel expressed in a human cell line. Bioconjug Chem *17*, 689-699.

Biswas, K., Nixey, T.E., Murray, J.K., Falsey, J.R., Yin, L., Liu, H., Gingras, J., Hall, B.E., Herberich, B., Holder, J.R.*, et al.* (2017). Engineering Antibody Reactivity for Efficient Derivatization to Generate NaV1.7 Inhibitory GpTx-1 Peptide-Antibody Conjugates. ACS Chem Biol *12*, 2427-2435.

Bogin, O. (2005). Venom Peptides and their Mimetics as Potential Drugs. In Modulator Issue (www.alomone.com), pp. 14-20.

Bohlen, C.J., Priel, A., Zhou, S., King, D., Siemens, J., and Julius, D. (2010). A bivalent tarantula toxin activates the capsaicin receptor, TRPV1, by targeting the outer pore domain. Cell *141*, 834-845.

Bolla, J.R., Sauer, J.B., Wu, D., Mehmood, S., Allison, T.M., and Robinson, C.V. (2018). Direct observation of the influence of cardiolipin and antibiotics on lipid II binding to MurJ. Nat Chem *10*, 363−371.

Bontems, F., Gilquin, B., Roumestand, C., Menez, A., and Toma, F. (1992). Analysis of side-chain organization on a refined model of charybdotoxin: structural and functional implications. Biochemistry *31*, 7756-7764.

Bosmans, F., Martin-Eauclaire, M.F., and Swartz, K.J. (2008). Deconstructing voltage sensor function and pharmacology in sodium channels. Nature *456*, 202-208.

Bosmans, F., Milescu, M., and Swartz, K.J. (2011). Palmitoylation influences the function and pharmacology of sodium channels. Proc Natl Acad Sci U S A *108*, 20213-20218.

Bosmans, F., and Swartz, K.J. (2010). Targeting voltage sensors in sodium channels with spider toxins. Trends Pharmacol Sci *31*, 175-182.

Bosmans, F., and Tytgat, J. (2007). Voltage-gated sodium channel modulation by scorpion alpha-toxins. Toxicon *49*, 142-158.

Campos, F.V., Chanda, B., Beirao, P.S., and Bezanilla, F. (2007). beta-Scorpion toxin modifies gating transitions in all four voltage sensors of the sodium channel. J Gen Physiol *130*, 257-268.

Cao, E., Liao, M., Cheng, Y., and Julius, D. (2013). TRPV1 structures in distinct conformations reveal activation mechanisms. Nature *504*, 113-118.

Cardoso, F.C., and Lewis, R.J. (2019). Structure-Function and Therapeutic Potential of Spider Venom-Derived Cysteine Knot Peptides Targeting Sodium Channels. Front Pharmacol *10*, 366.

Caterina, M.J., Schumacher, M.A., Tominaga, M., Rosen, T.A., Levine, J.D., and Julius, D. (1997). The capsaicin receptor: a heat-activated ion channel in the pain pathway. Nature *389*, 816-824.

Cestele, S., Qu, Y., Rogers, J.C., Rochat, H., Scheuer, T., and Catterall, W.A. (1998). Voltage sensor-trapping: enhanced activation of sodium channels by beta-scorpion toxin bound to the S3-S4 loop in domain II. Neuron *21*, 919-931.

Cestele, S., Yarov-Yarovoy, V., Qu, Y., Sampieri, F., Scheuer, T., and Catterall, W.A. (2006). Structure and function of the voltage sensor of sodium channels probed by a beta-scorpion toxin. J Biol Chem *281*, 21332-21344.

Chang, C.C., and Lee, C.Y. (1963). Isolation of neurotoxins from the venom of Bungarus multicinctus and their modes of neuromuscular blocking action. Archs int Pharmacodyn Ther *184*, 241-257.

Chang, S.C., Bajaj, S., and Chandy, K.G. (2018). ShK toxin: history, structure and therapeutic applications for autoimmune diseases. WikiJournal of Science *1*.

Chassagnon, I.R., McCarthy, C.A., Chin, Y.K., Pineda, S.S., Keramidas, A., Mobli, M., Pham, V., De Silva, T.M., Lynch, J.W., Widdop, R.E.*, et al.* (2017). Potent neuroprotection after stroke afforded by a double-knot spider-venom peptide that inhibits acid-sensing ion channel 1a. Proc Natl Acad Sci U S A *114*, 3750-3755.

Clairfeuille, T., Cloake, A., Infield, D.T., Llongueras, J.P., Arthur, C.P., Li, Z.R., Jian, Y., Martin-Eauclaire, M.F., Bougis, P.E., Ciferri, C.*, et al.* (2019). Structural basis of alpha-scorpion toxin action on Nav channels. Science *363*.

Corzo, G., Sabo, J.K., Bosmans, F., Billen, B., Villegas, E., Tytgat, J., and Norton, R.S. (2007). Solution structure and alanine scan of a spider toxin that affects the activation of mammalian voltage-gated sodium channels. J Biol Chem *282*, 4643-4652.

Cosens, D.J., and Manning, A. (1969). Abnormal electroretinogram from a Drosophila mutant. Nature *224*, 285-287.

Dang, B., Kubota, T., Correa, A.M., Bezanilla, F., and Kent, S.B. (2014). Total chemical synthesis of biologically active fluorescent dye-labeled Ts1 toxin. Angew Chem Int Ed Engl *53*, 8970-8974.

Dauplais, M., Gilquin, B., Possani, L.D., Gurrola-Briones, G., Roumestand, C., and Menez, A. (1995). Determination of the three-dimensional solution structure of noxiustoxin: analysis of structural differences with related short-chain scorpion toxins. Biochemistry *34*, 16563-16573.

Edgerton, G.B., Blumenthal, K.M., and Hanck, D.A. (2008). Evidence for multiple effects of ProTxII on activation gating in Na(V)1.5. Toxicon *52*, 489-500.

Eisenberg, D., Schwarz, E., Komaromy, M., and Wall, R. (1984). Analysis of membrane and surface protein sequences with the hydrophobic moment plot. J Mol Biol *179*, 125-142.

Escoubas, P., De Weille, J.R., Lecoq, A., Diochot, S., Waldmann, R., Champigny, G., Moinier, D., Menez, A., and Lazdunski, M. (2000). Isolation of a tarantula toxin specific for a class of proton-gated Na+ channels. J Biol Chem *275*, 25116-25121.

Escoubas, P., and Rash, L. (2004). Tarantulas: eight-legged pharmacists and combinatorial chemists. Toxicon *43*, 555-574.

Fertuck, H.C., and Salpeter, M.M. (1974). Localization of acetylcholine receptor by 125I-labeled α-bungarotoxin binding at mouse motor endplates. Proceedings of the National Academy of Sciences *71*, 1376-1378.

Gao, B., Peng, C., Yang, J., Yi, Y., Zhang, J., and Shi, Q. (2017). Cone Snails: A Big Store of Conotoxins for Novel Drug Discovery. Toxins (Basel) *9*, 397.

Gao, Y., Cao, E., Julius, D., and Cheng, Y. (2016). TRPV1 structures in nanodiscs reveal mechanisms of ligand and lipid action. Nature *534*, 347-351.

Garcia, M.L., Garcia-Calvo, M., Hidalgo, P., Lee, A., and MacKinnon, R. (1994). Purification and characterization of three inhibitors of voltage-dependent K+ channels from Leiurus quinquestriatus var. hebraeus venom. Biochemistry *33*, 6834-6839.

Geron, M., Hazan, A., and Priel, A. (2017). Animal Toxins Providing Insights into TRPV1 Activation Mechanism. Toxins (Basel) *9*, 326.

Gross, A., and MacKinnon, R. (1996). Agitoxin footprinting the shaker potassium channel pore. Neuron *16*, 399-406.

Gubbens, J., Ruijter, E., de Fays, L.E., Damen, J.M., de Kruijff, B., Slijper, M., Rijkers, D.T., Liskamp, R.M., and de Kroon, A.I. (2009). Photocrosslinking and click chemistry enable the specific detection of proteins interacting with phospholipids at the membrane interface. Chem Biol *16*, 3-14.

Gur, M., Kahn, R., Karbat, I., Regev, N., Wang, J., Catterall, W.A., Gordon, D., and Gurevitz, M. (2011). Elucidation of the molecular basis of selective recognition uncovers the interaction site for the core domain of scorpion alpha-toxins on sodium channels. J Biol Chem *286*, 35209-35217.

Hafidi, A., Beurg, M., and Dulon, D. (2005). Localization and developmental expression of BK channels in mammalian cochlear hair cells. Neuroscience *130*, 475-484.

Hakim, M.A., Jiang, W., Luo, L., Li, B., Yang, S., Song, Y., and Lai, R. (2015). Scorpion Toxin, BmP01, Induces Pain by Targeting TRPV1 Channel. Toxins (Basel) *7*, 3671-3687.

Hanck, D.A., and Sheets, M.F. (2007). Site-3 toxins and cardiac sodium channels. Toxicon *49*, 181-193.

Henriques, S.T., Deplazes, E., Lawrence, N., Cheneval, O., Chaousis, S., Inserra, M., Thongyoo, P., King, G.F., Mark, A.E., Vetter, I.*, et al.* (2016). Interaction of Tarantula Venom Peptide ProTx-II with Lipid Membranes Is a Prerequisite for Its Inhibition of Human Voltage-gated Sodium Channel NaV1.7. J Biol Chem *291*, 17049-17065.

Herzig, V., and King, G.F. (2015). The Cystine Knot Is Responsible for the Exceptional Stability of the Insecticidal Spider Toxin omega-Hexatoxin-Hv1a. Toxins (Basel) *7*, 4366-4380.

Hill, K., and Schaefer, M. (2007). TRPA1 is differentially modulated by the amphipathic molecules trinitrophenol and chlorpromazine. J Biol Chem *282*, 7145-7153.

Hille, B. (2001). Ionic channels of excitable membranes., Third edn (Sinauer Associates Inc.).

Holmes, D. (2014). Conotoxins: how a deadly snail could help ease pain. The Lancet *13*, 867-868.

Ibanez-Tallon, I., Wen, H., Miwa, J.M., Xing, J., Tekinay, A.B., Ono, F., Brehm, P., and Heintz, N. (2004). Tethering naturally occurring peptide toxins for cell-autonomous modulation of ion channels and receptors in vivo. Neuron *43*, 305-311.

Jung, H.J., Lee, J.Y., Kim, S.H., Eu, Y.J., Shin, S.Y., Milescu, M., Swartz, K.J., and Kim, J.I. (2005). Solution structure and lipid membrane partitioning of VSTx1, an inhibitor of the KvAP potassium channel. Biochemistry *44*, 6015-6023.

Kalia, J., Milescu, M., Salvatierra, J., Wagner, J., Klint, J.K., King, G.F., Olivera, B.M., and Bosmans, F. (2015). From foe to friend: using animal toxins to investigate ion channel function. J Mol Biol *427*, 158-175.

Karbat, I., Altman-Gueta, H., Fine, S., Szanto, T., Hamer-Rogotner, S., Dym, O., Frolow, F., Gordon, D., Panyi, G., Gurevitz, M.*, et al.* (2019). Pore-modulating toxins exploit inherent slow inactivation to block K(+) channels. Proc Natl Acad Sci U S A *116*, 18700-18709.

Kintzing, J.R., and Cochran, J.R. (2016). Engineered knottin peptides as diagnostics, therapeutics, and drug delivery vehicles. Curr Opin Chem Biol *34*, 143-150.

Krezel, A.M., Kasibhatla, C., Hidalgo, P., MacKinnon, R., and Wagner, G. (1995). Solution structure of the potassium channel inhibitor agitoxin 2: caliper for probing channel geometry. Protein Sci *4*, 1478-1489.

Kuang, Q., Purhonen, P., and Hebert, H. (2015). Structure of potassium channels. Cell Mol Life Sci *72*, 3677-3693.

Ladokhin, A.S. (1999). Evaluation of lipid exposure of tryptophan residues in membrane peptides and proteins. Anal Biochem *276*, 65-71.

Ladokhin, A.S., Jayasinghe, S., and White, S.H. (2000). How to Measure and Analyze Tryptophan Fluorescence in Membranes Properly, and Why Bother? . Anal biochem *285*, 235-245.

Laganowsky, A., Reading, E., Allison, T.M., Ulmschneider, M.B., Degiacomi, M.T., Baldwin, A.J., and Robinson, C.V. (2014). Membrane proteins bind lipids selectively to modulate their structure and function. Nature *510*, 172-175.

Lau, C.H.Y., King, G.F., and Mobli, M. (2016). Molecular basis of the interaction between gating modifier spider toxins and the voltage sensor of voltage-gated ion channels. Sci Rep *6*, 34333.

Lee, C.W., Kim, S., Roh, S.H., Endoh, H., Kodera, Y., Maeda, T., Kohno, T., Wang, J.M., Swartz, K.J., and Kim, J.I. (2004). Solution structure and functional characterization of SGTx1, a modifier of Kv2.1 channel gating. Biochemistry *43*, 890-897.

Lee, H.C., Wang, J.M., and Swartz, K.J. (2003). Interaction between Extracellular Hanatoxin and the Resting Conformation of the Voltage-Sensor Paddle in Kv Channels. Neuron *40*, 527-536.

Lee, S.Y., and MacKinnon, R. (2004). A membrane-access mechanism of ion channel inhibition by voltage sensor toxins from spider venom. Nature *430*, 232-235.

Leipold, E., Borges, A., and Heinemann, S.H. (2012). Scorpion beta-toxin interference with NaV channel voltage sensor gives rise to excitatory and depressant modes. J Gen Physiol *139*, 305-319.

Li-Smerin, Y., and Swartz, K.J. (2000). Localization and molecular determinants of the Hanatoxin receptors on the voltage-sensing domains of a K(+) channel. J Gen Physiol *115*, 673-684.

Long, S.B., Tao, X., Campbell, E.B., and MacKinnon, R. (2007). Atomic structure of a voltage-dependent K+ channel in a lipid membrane-like environment. Nature *450*, 376-382.

MacKinnon, R., and Miller, C. (1988). Mechanism of charybdotoxin block of the high-conductance, Ca2+-activated K+ channel. J Gen Physiol *91*, 335-349.
MacKinnon, R., and Miller, C. (1989). Mutant potassium channels with altered binding of charybdotoxin, a pore-blocking peptide inhibitor. Science *245*, 1382-1385.

Marcotte, P., Chen, L.Q., Kallen, R.G., and Chahine, M. (1997). Effects of Tityus serrulatus scorpion toxin gamma on voltage-gated Na+ channels. Circ Res *80*, 363-369.

Massensini, A.R., Suckling, J., Brammer, M.J., Moraes-Santos, T., Gomez, M.V., and Romano-Silva, M.A. (2002). Tracking sodium channels in live cells: confocal imaging using fluorescently labeled toxins. J Neurosci Methods *116*, 189-196.

Matthies, D., Bae, C., Toombes, G.E., Fox, T., Bartesaghi, A., Subramaniam, S., and Swartz, K.J. (2018). Single-particle cryo-EM structure of a voltage-activated potassium channel in lipid nanodiscs. Elife *7*.

Mazzuca, M., Heurteaux, C., Alloui, A., Diochot, S., Baron, A., Voilley, N., Blondeau, N., Escoubas, P., Gelot, A., Cupo, A.*, et al.* (2007). A tarantula peptide against pain via ASIC1a channels and opioid mechanisms. Nat Neurosci *10*, 943-945.

McIntosh, T.J., and Holloway, P.W. (1987). Determination of the depth of bromine atoms in bilayers formed from bromolipid probes. Biochemistry *26*, 1783-1788.

Milescu, M., Bosmans, F., Lee, S., Alabi, A.A., Kim, J.I., and Swartz, K.J. (2009). Interactions between lipids and voltage sensor paddles detected with tarantula toxins. Nat Struct Mol Biol *16*, 1080-1085.

Milescu, M., Vobecky, J., Roh, S.H., Kim, S.H., Jung, H.J., Kim, J.I., and Swartz, K.J. (2007). Tarantula toxins interact with voltage sensors within lipid membranes. J Gen Physiol *130*, 497-511.

Miller, C., Moczydlowski, E., Latorre, R., and Phillips, M. (1985). Charybdotoxin, a protein inhibitor of single Ca2+-activated K+ channels from mammalian skeletal muscle. Nature *313*, 316-318.

Montell, C., and Rubin, G.M. (1989). Molecular characterization of the drosophila trp locus: A putative integral membrane protein required for phototransduction. Neuron *2*, 1313-1323.

Morales Duque, H., Campos Dias, S., and Franco, O.L. (2019). Structural and Functional Analyses of Cone Snail Toxins. Mar Drugs *17*.

Moran, M.M. (2018). TRP Channels as Potential Drug Targets. Annu Rev Pharmacol Toxicol *58*, 309-330.

Murray, J.K., Biswas, K., Holder, J.R., Zou, A., Ligutti, J., Liu, D., Poppe, L., Andrews, K.L., Lin, F.F., Meng, S.Y.*, et al.* (2015a). Sustained inhibition of the NaV1.7 sodium channel by engineered dimers of the domain II binding peptide GpTx-1. Bioorg Med Chem Lett *25*, 4866-4871.

Murray, J.K., Ligutti, J., Liu, D., Zou, A., Poppe, L., Li, H., Andrews, K.L., Moyer, B.D., McDonough, S.I., Favreau, P.*, et al.* (2015b). Engineering potent and selective analogues of GpTx-1, a tarantula venom peptide antagonist of the Na(V)1.7 sodium channel. J Med Chem *58*, 2299-2314.

Murray, J.K., Long, J., Zou, A., Ligutti, J., Andrews, K.L., Poppe, L., Biswas, K., Moyer, B.D., McDonough, S.I., and Miranda, L.P. (2016). Single Residue Substitutions That Confer Voltage-Gated Sodium Ion Channel Subtype Selectivity in the NaV1.7 Inhibitory Peptide GpTx-1. J Med Chem *59*, 2704-2717.

Niphakis, M.J., Lum, K.M., Cognetta, A.B., 3rd, Correia, B.E., Ichu, T.A., Olucha, J., Brown, S.J., Kundu, S., Piscitelli, F., Rosen, H.*, et al.* (2015). A Global Map of Lipid-Binding Proteins and Their Ligandability in Cells. Cell *161*, 1668-1680.

Nury, H., Van Renterghem, C., Weng, Y., Tran, A., Baaden, M., Dufresne, V., Changeux, J.P., Sonner, J.M., Delarue, M., and Corringer, P.J. (2011). X-ray structures of general anaesthetics bound to a pentameric ligand-gated ion channel. Nature *469*, 428-431.

Ondrus, A.E., Lee, H.L., Iwanaga, S., Parsons, W.H., Andresen, B.M., Moerner, W.E., and Du Bois, J. (2012). Fluorescent saxitoxins for live cell imaging of single voltage-gated sodium ion channels beyond the optical diffraction limit. Chem Biol *19*, 902-912.

Ostrow, K.L., Mammoser, A., Suchyna, T., Sachs, F., Oswald, R., Kubo, S., Chino, N., and Gottlieb, P.A. (2003). cDNA sequence and in vitro folding of GsMTx4, a specific peptide inhibitor of mechanosensitive channels. Toxicon *42*, 263-274.

Oswald, R.E., Suchyna, T.M., McFeeters, R., Gottlieb, P., and Sachs, F. (2002). Solution structure of peptide toxins that block mechanosensitive ion channels. J Biol Chem *277*, 34443-34450.

Payandeh, J., Gamal El-Din, T.M., Scheuer, T., Zheng, N., and Catterall, W.A. (2012). Crystal structure of a voltage-gated sodium channel in two potentially inactivated states. Nature *486*, 135-139.

Payandeh, J., Scheuer, T., Zheng, N., and Catterall, W.A. (2011). The crystal structure of a voltage-gated sodium channel. Nature *475*, 353-358.

Peigneur, S., and Tytgat, J. (2018). Toxins in Drug Discovery and Pharmacology. Toxins (Basel) *10*, 126.

Peng, K., Shu, Q., Liu, Z., and Liang, S. (2002). Function and solution structure of huwentoxin-IV, a potent neuronal tetrodotoxin (TTX)-sensitive sodium channel antagonist from Chinese bird spider Selenocosmia huwena. J Biol Chem *277*, 47564-47571.

Phillips, L.R., Milescu, M., Li-Smerin, Y.Y., Mindell, J.A., Kim, J.I., and Swartz, K.J. (2005). Voltage-sensor activation with a tarantula toxin as cargo. Nature *436*, 857-860.

Phillips, R., Ursell, T., Wiggins, P., and Sens, P. (2009). Emerging roles for lipids in shaping membrane-protein function. Nature *459*, 379-385.

Porter, C.W., Chiu, T.H., Wieckowski, J., and Barnard, E.A. (1973). Types and locations of cholinergic receptor-like molecules in muscle fibres. Nat New Biol *241*, 3-7.

Possani, L.D., Becerril, B., Delepierre, M., and Tytgat, J. (1999). Scorpion toxins specific for Na+-channels. Eur J Biochem *264*, 287-300.

Pragl, B., Koschak, A., Trieb, M., Obermair, G., Kaufmann, W.A., Gerster, U., Blanc, E., Hahn, C., Prinz, H., Schütz, G.*, et al.* (2002). Synthesis, Characterization, and Application of Cy-Dye- and Alexa-Dye-Labeled Hongotoxin1Analogues. The First High Affinity Fluorescence Probes for Voltage-Gated K+Channels. Bioconjugate Chemistry *13*, 416-425.

Prommer, E. (2006). Ziconotide: a new option for refractory pain. Drugs Today (Barc) *42*, 369-378.

Ramu, Y., Xu, Y., and Lu, Z. (2006). Enzymatic activation of voltage-gated potassium channels. Nature *442*, 696-699.

Redaelli, E., Cassulini, R.R., Silva, D.F., Clement, H., Schiavon, E., Zamudio, F.Z., Odell, G., Arcangeli, A., Clare, J.J., Alagon, A.*, et al.* (2010). Target promiscuity and heterogeneous effects of tarantula venom peptides affecting Na+ and K+ ion channels. J Biol Chem *285*, 4130-4142.

Revell, J.D., Lund, P.E., Linley, J.E., Metcalfe, J., Burmeister, N., Sridharan, S., Jones, C., Jermutus, L., and Bednarek, M.A. (2013). Potency optimization of Huwentoxin-IV on hNav1.7: a neurotoxin TTX-S sodium-channel antagonist from the venom of the Chinese bird-eating spider Selenocosmia huwena. Peptides *44*, 40-46.

Robinson, S.D., and Norton, R.S. (2014). Conotoxin gene superfamilies. Mar Drugs *12*, 6058-6101.

Schmalhofer, W.A., Calhoun, J., Burrows, R., Bailey, T., Kohler, M.G., Weinglass, A.B., Kaczorowski, G.J., Garcia, M.L., Koltzenburg, M., and Priest, B.T. (2008). ProTx-II, a selective inhibitor of NaV1.7 sodium channels, blocks action potential propagation in nociceptors. Mol Pharmacol *74*, 1476-1484.

Shen, H., Li, Z., Jiang, Y., Pan, X., Wu, J., Cristofori-Armstrong, B., Smith, J.J., Chin, Y.K.Y., Lei, J., Zhou, Q.*, et al.* (2018). Structural basis for the modulation of voltage-gated sodium channels by animal toxins. Science *362*.

Shen, H., Liu, D., Wu, K., Lei, J., and Yan, N. (2019). Structures of human Nav1.7 channel in complex with auxiliary subunits and animal toxins. Science *363*, 1303-1308.

Siemens, J., Zhou, S., Piskorowski, R., Nikai, T., Lumpkin, E.A., Basbaum, A.I., King, D., and Julius, D. (2006). Spider toxins activate the capsaicin receptor to produce inflammatory pain. Nature *444*, 208-212.

Sinai, N., Meir, A., and Bogin, O. (2006). Fluorescently-labeled Toxins: Novel tools for Working with Live Cells. In Modulator Issue (www.alomone.com), pp. 22-24.

Sokolov, S., Kraus, R.L., Scheuer, T., and Catterall, W.A. (2008). Inhibition of sodium channel gating by trapping the domain II voltage sensor with protoxin II. Mol Pharmacol *73*, 1020-1028.

Spassova, M.A., Hewavitharana, T., Xu, W., Soboloff, J., and Gill, D.L. (2006). A common mechanism underlies stretch activation and receptor activation of TRPC6 channels. Proc Natl Acad Sci U S A *103*, 16586-16591.

Swartz, K.J. (2007). Tarantula toxins interacting with voltage sensors in potassium channels. Toxicon *49*, 213-230.
Swartz, K.J. (2008). Sensing voltage across lipid membranes. Nature *456*, 891-897.

Swartz, K.J., and MacKinnon, R. (1995). An inhibitor of the Kv2.1 potassium channel isolated from the venom of a Chilean tarantula. Neuron *15*, 941-949.

Swartz, K.J., and MacKinnon, R. (1997). Mapping the receptor site for hanatoxin, a gating modifier of voltage-dependent K+ channels. Neuron *18*, 675-682.

Takahashi, H., Kim, J.I., Min, H.J., Sato, K., Swartz, K.J., and Shimada, I. (2000). Solution structure of hanatoxin1, a gating modifier of voltage-dependent K(+) channels: common surface features of gating modifier toxins. J Mol Biol *297*, 771-780.

Tejedor, F.J., and Catterall, W.A. (1988). Site of covalent attachment of alpha-scorpion toxin derivatives in domain I of the sodium channel alpha subunit. Proc Natl Acad Sci U S A *85*, 8742-8746.

Thomsen, W.J., and Catterall, W.A. (1989). Localization of the receptor site for alpha-scorpion toxins by antibody mapping: implications for sodium channel topology. Proc Natl Acad Sci U S A *86*, 10161-10165.

Tilley, D.C., Eum, K.S., Fletcher-Taylor, S., Austin, D.C., Dupre, C., Patron, L.A., Garcia, R.L., Lam, K., Yarov-Yarovoy, V., Cohen, B.E.*, et al.* (2014). Chemoselective tarantula toxins report

voltage activation of wild-type ion channels in live cells. Proc Natl Acad Sci U S A *111*, E4789-4796.

Wang, D., Du, S., Cazenave-Gassiot, A., Ge, J., Lee, J.S., Wenk, M.R., and Yao, S.Q. (2017). Global Mapping of Protein-Lipid Interactions by Using Modified Choline-Containing Phospholipids Metabolically Synthesized in Live Cells. Angew Chem Int Ed Engl *56*, 5829-5833.

Wang, J., Yarov-Yarovoy, V., Kahn, R., Gordon, D., Gurevitz, M., Scheuer, T., and Catterall, W.A. (2011). Mapping the receptor site for alpha-scorpion toxins on a Na+ channel voltage sensor. Proc Natl Acad Sci U S A *108*, 15426-15431.

Wang, M., Diao, J., Li, J., Tang, J., Lin, Y., Hu, W., Zhang, Y., Xiao, Y., and Liang, S. (2008). JZTX-IV, a unique acidic sodium channel toxin isolated from the spider Chilobrachys jingzhao. Toxicon *52*, 871-880.

Wu, G., Li, Y., Wei, D., He, F., Jiang, S., Hu, G., and Wu, H. (2000). Solution structure of BmP01 from the venom of scorpion Buthus martensii Karsch. Biochem Biophys Res Commun *276*, 1148-1154.

Xu, H., Li, T., Rohou, A., Arthur, C.P., Tzakoniati, F., Wong, E., Estevez, A., Kugel, C., Franke, Y., Chen, J.*, et al.* (2019). Structural Basis of Nav1.7 Inhibition by a Gating-Modifier Spider Toxin. Cell *176*, 702-715 e714.

Xu, Y., Ramu, Y., and Lu, Z. (2008). Removal of phospho-head groups of membrane lipids immobilizes voltage sensors of K+ channels. Nature *451*, 826-829.

Yang, S., Yang, F., Wei, N., Hong, J., Li, B., Luo, L., Rong, M., Yarov-Yarovoy, V., Zheng, J., Wang, K.*, et al.* (2015). A pain-inducing centipede toxin targets the heat activation machinery of nociceptor TRPV1. Nat Commun *6*, 8297.

Yang, S., Yang, F., Zhang, B., Lee, B.H., Li, B., Luo, L., Zheng, J., and Lai, R. (2017). A bimodal activation mechanism underlies scorpion toxin-induced pain. Sci Adv *3*, e1700810.
Zheng, J. (2013). Molecular mechanism of TRP channels. Compr Physiol *3*, 221-242.

Zhou, M., Morgner, N., Barrera, N.P., Politis, A., Isaacson, S.C., Matak-Vinkovic, D., Murata, T., Bernal, R.A., Stock, D., and Robinson, C.V. (2011). Mass spectrometry of intact V-type ATPases reveals bound lipids and the effects of nucleotide binding. Science *334*, 380-385.

Chapter 2:

Investigating the roles of the TRPV1-DkTx and membrane-DkTx interfaces in TRPV1 activation

This chapter has been published:

Sarkar, D., Singh, Y. and Kalia, J.* (2018). Protein–Lipid Interfaces Can Drive the Functions of Membrane-Embedded Protein–Protein Complexes. *ACS Chemical Biology* 13, 2689-2698.

[Note: Contents of the published article have been used for this thesis after obtaining permission from the publisher.]

2.1. Introduction.

The role of the membrane in membrane protein function has long been a subject of investigation. For example, the role of membrane fluidity on the function of the transferrin and concanavalin A receptors was reported in the 1970s by Meir Shinitzky's group (Muller and Shinitzky, 1979; Shinitzky and Inbar, 1976). These efforts have received a major impetus recently due to advances in structural biology (Autzen et al., 2018; Bae et al., 2016; Gao et al., 2016; Long et al., 2007; Nury et al., 2011; Payandeh et al., 2011) and mass spectroscopy (Bolla et al., 2018; Cong et al., 2017; Laganowsky et al., 2014; Zhou et al., 2011) that reveal that lipids engage in intimate and specific interactions with a diverse range of membrane proteins including ion channels, transporters and membrane enzymes, suggesting that protein–lipid interfaces may play important roles in protein function (Contreras et al., 2012; Coskun et al., 2011; Hunte and Richers, 2008; Lee, 2011; Li et al., 1992; Phillips et al., 2009; Polley et al., 2017). A detailed understanding of the functional roles of these protein–lipid interfaces, therefore, is imperative to fully understand the function of both integral and peripheral membrane proteins.

Recent structural work on the complex of the homotetrameric rat TRPV1 ion channel protein and its potent agonist, the double-knot spider toxin (DkTx) (Bae et al., 2016; Gao et al., 2016) (Figure 2.1a) provides one of the best available snapshots of protein–protein complexes in a native membrane-like milieu. These studies have demonstrated that each of the two lobes (cystine knots K1 and K2) of the toxin interacts with the channel by inserting two of their loops (loops 2 and 4) into the membrane to form a toxin–lipid–channel tripartite complex (Figure 2.1a and b). DkTx (Bohlen et al., 2010) belongs to the family of the inhibitory cystine-knot (ICK) toxins (Bohlen and Julius, 2012; Kalia et al., 2015; Swartz, 2007) known to target several types of ion channels, and is the only member of this family of toxins that contains two ICK motifs (K1 and K2 separated by a seven amino acids-long linker). Another unique aspect of DkTx is that it is the only pore-binding toxin that is known to partition into the membrane (Bae et al., 2016). Indeed, other membrane-partitioning toxins such as Hanatoxin (Blouin et al., 2016; Rissanen et al., 2017; Swartz and MacKinnon, 1995, 1997a, b) inhibit voltage-activated ion channels by targeting their voltage sensors that are far removed from, yet, tightly coupled to the pore. In contrast to the DkTx–TRPV1 complex, no structural information is available currently on the toxin–channel complexes formed by these voltage sensor-binding toxins, thereby

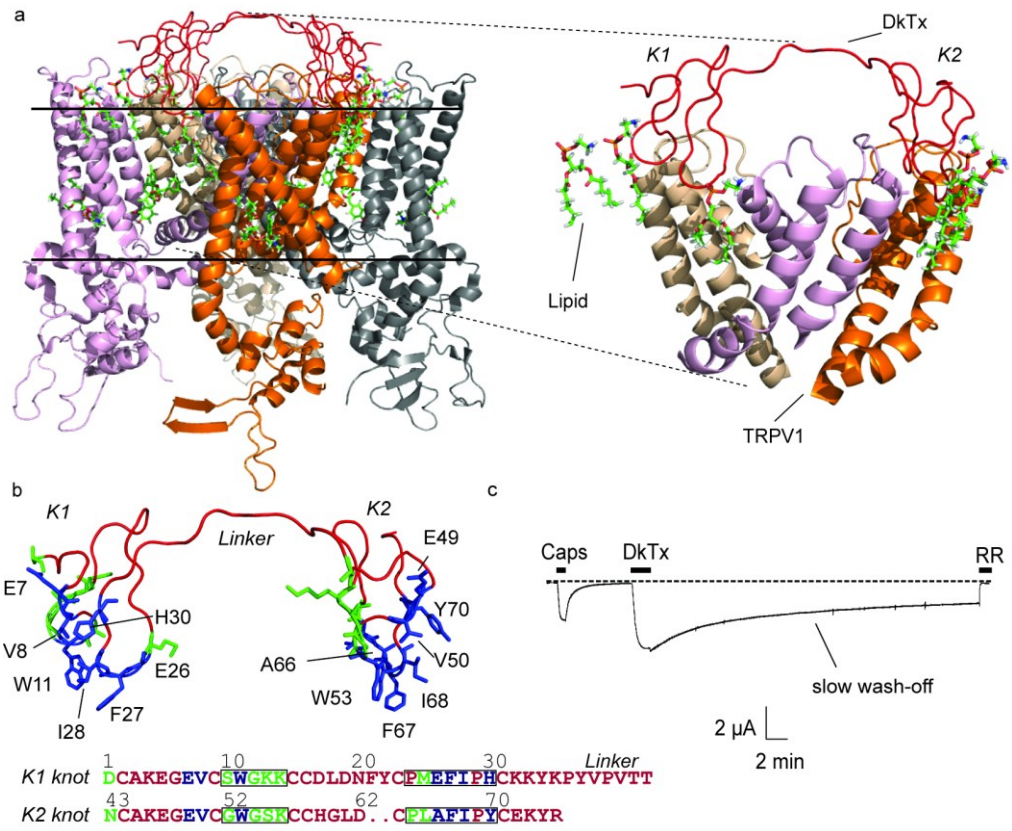

Figure 2.1. The DkTx–TRPV1 complex. a) The DkTx–lipid–TRPV1 tripartite complex viewed sideways from within the membrane, PDB: 5irx (Gao et al., 2016), and a zoomed-in view of the complex depicting the pore domains of three channel monomers (right panel) (the fourth monomer is not depicted to enhance clarity). The solid horizontal lines represent the membrane boundaries (the region above the top line is extracellular and the region below the bottom line is intracellular). b) Structure of DkTx depicting residues that interact exclusively with TRPV1 residues and not with lipids in green, and those that interact with lipids in blue. Only the lipid-interacting residues are labeled. The same color code is used to denote the sequence of the K1 and K2 knots of DkTx at the bottom. The residues of loops 2 and 4 of each knot are boxed. c) A two-electrode voltage clamp electrophysiology recording of TRPV1 depicting activation by capsaicin (Caps, 5 µM) and subsequently by DkTx (3.3 µM), followed by wash-off for 30 min, and ultimately, complete channel block by ruthenium red (RR, 7 µM). The dotted line represents zero current.

obviating molecular-level investigations into the role of toxin–lipid interfaces in channel modulation.

A notable feature of DkTx is that it demonstrates extremely slow wash-off of the toxin after channel activation (Bae et al., 2012; Bohlen et al., 2010) (Figure 2.1c)—an intriguing observation considering that the TRPV1–DkTx complex structures (Bae et al., 2016; Gao et al., 2016) do not reveal any electrostatic (Sheinerman et al., 2000) , cation–pi (Crowley and Golovin, 2005) or pi stacking (McGaughey et al., 1998) interactions between the residues of the toxin and those of the channel that commonly underlie tight complex-formation between proteins (Stites, 1997). In contrast to this relatively sparse protein–protein interaction landscape, the structures depict two intimate protein–lipid interfaces, one formed by the K1 knot of DkTx and the other one formed by its K2 knot (Figure 2.1a, right panel). This observation engenders the hypothesis that protein–lipid interfaces play a major role in the binding and potency of the toxin. Taken together, these structural and functional attributes of the DkTx–TRPV1 complex render it an ideal model system for mechanistic investigations into the poorly understood roles of protein–lipid interfaces in the function of protein–protein complexes present within membranes.

2.2. Results.

DkTx–TRPV1 structures enable generation of protein–lipid and protein–protein interaction maps. To compare and contrast the roles of protein–protein interactions with protein–lipid interactions in DkTx-mediated activation of TRPV1, we performed systematic site-directed mutagenesis to generate DkTx variants and characterized their TRPV1 activation properties electrophysiologically. Our selection of toxin residues for substitution was guided by the recent cryo-EM structure of the rat TRPV1–DkTx complex solved in a lipidic environment (Gao et al., 2016) and by another recent study (Bae et al., 2016) that utilized molecular dynamics simulations to predict lipid-binding sites on the toxin and also reported a molecular model of the DkTx–TRPV1 complex structure. Yashaswi Singh, a graduate student from Dr. Jeet Kalia's laboratory utilized these two structural frameworks to build an interaction map of the TRPV1-DkTx-membrane lipid tripartite complex and classified the toxin residues lying within 4.4 Å of the atoms of the nearby channel residues/lipid molecules as "interacting". The summary of this interaction map depicting all DkTx residues obtained from these analyses is depicted in Figure 2.1b. This structural analysis enabled us to pinpoint 27 toxin residues that interact with the

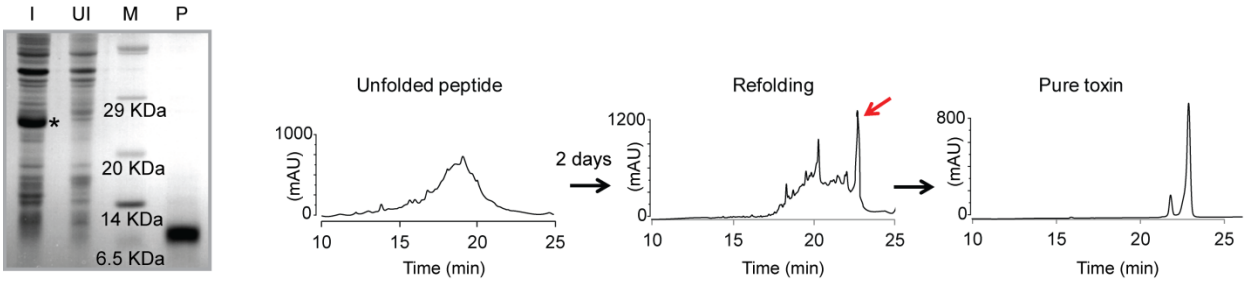

Figure 2.2. Representative DkTx purification data. DkTx variants were produced as described above. The band for the overexpressed DkTx-KSI fusion protein (depicted by an asterisk in the gel picture below) was expected at 24 kDa. Gel lanes have been labeled as followed: I: induced; UI: uninduced; M: molecular weight markers; P: DkTx protein purified by HPLC after refolding (expected at 9 kDa). The red arrow below denotes the peak for the correctly folded toxin in the HPLC chromatogram.

channel or/and lipids, 13 of which were observed to be exclusively channel-interacting (no lipid contacts) and 14 were identified as lipid-interacting, depicted in green and blue respectively in Figure 2.1b. Among the lipid-interacting residues, 8 (E7, V8, I28 and H30 of the K1 knot of the toxin, and E49, V50, I68 and Y70 of the K2 knot) were observed to directly interact only with lipids and not with the channel, whereas 6 (W11, E26 and F27 of K1, and W53, A66, and F67 of K2) were identified as interacting both with lipids and channel residues.

DkTx–lipid interfaces play crucial roles in the efficacy of the toxin for TRPV1 activation. After identifying channel or/and lipid-interacting DkTx residues, we generated alanine variants of each of these residues, except for A66 which was substituted to serine. Wild-type DkTx and its variants were expressed recombinantly in *E. coli* inclusion bodies and refolded and purified to homogeneity by HPLC (representative protein purification data are depicted in Figure 2.2; HPLC traces for purity evaluation of each of the variants except for E49A that did not refold under the conditions tested are depicted in Figure 2.3; and the MALDI mass characterization data of each variant is tabulated in Table 2.1). Subsequently, the toxin variants were characterized by performing two-electrode voltage clamp experiments on rat TRPV1 expressed in *Xenopus laevis* oocytes to yield dose-response curves that are depicted in Figure 2.5a (representative electrophysiological recordings obtained for each of the toxin variants are depicted in Figure

wild-type DkTx

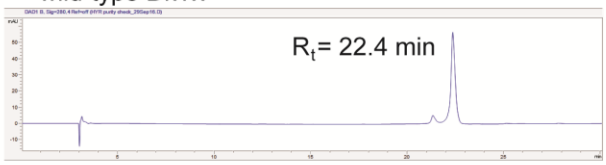

D1A DkTx

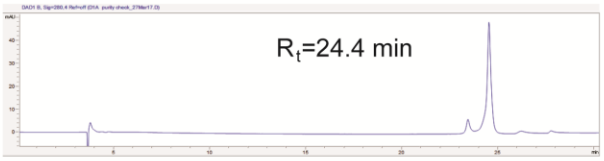

N43A DkTx

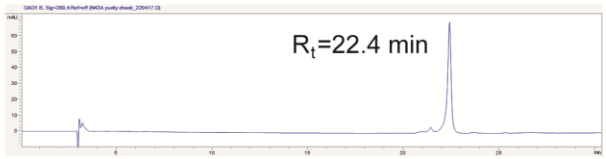

E7A DkTx

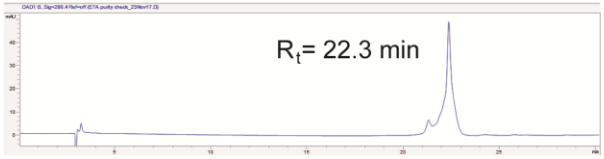

V8A DkTx

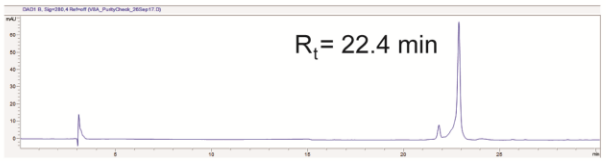

V50A DkTx

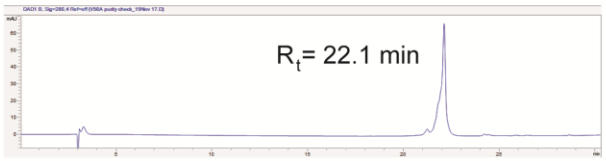

S10A DkTx

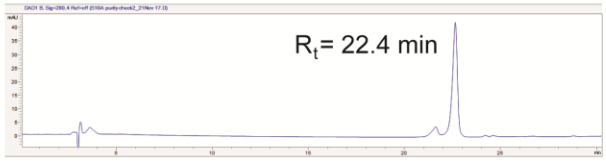

G52A DkTx

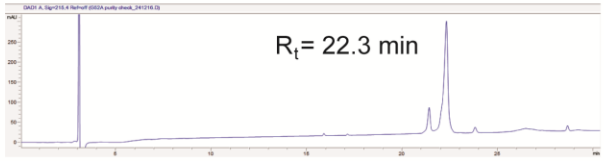

W11A DkTx

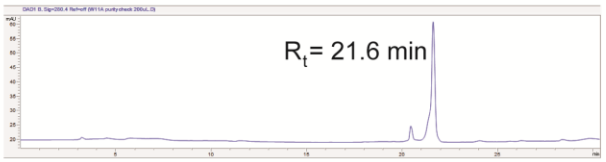

W53A DkTx

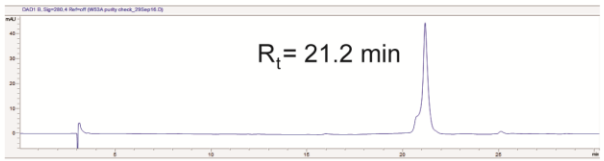

G12A DkTx

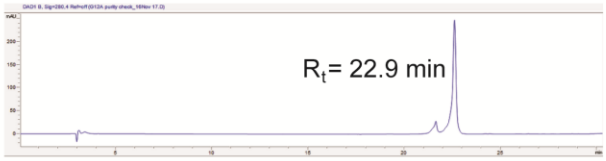

G54A DkTx

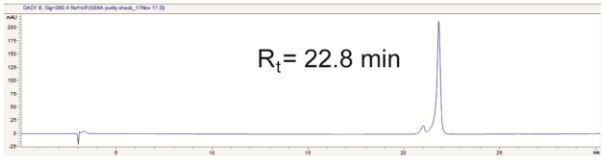

K13A DkTx

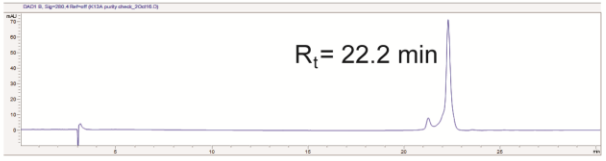

S55A DkTx

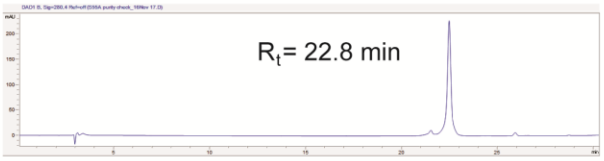

K14A DkTx

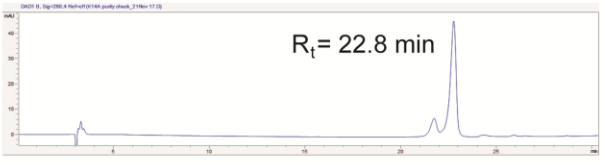

K56A DkTx

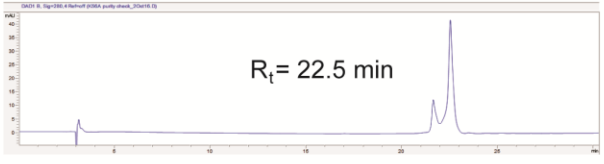

(Continued on next page)

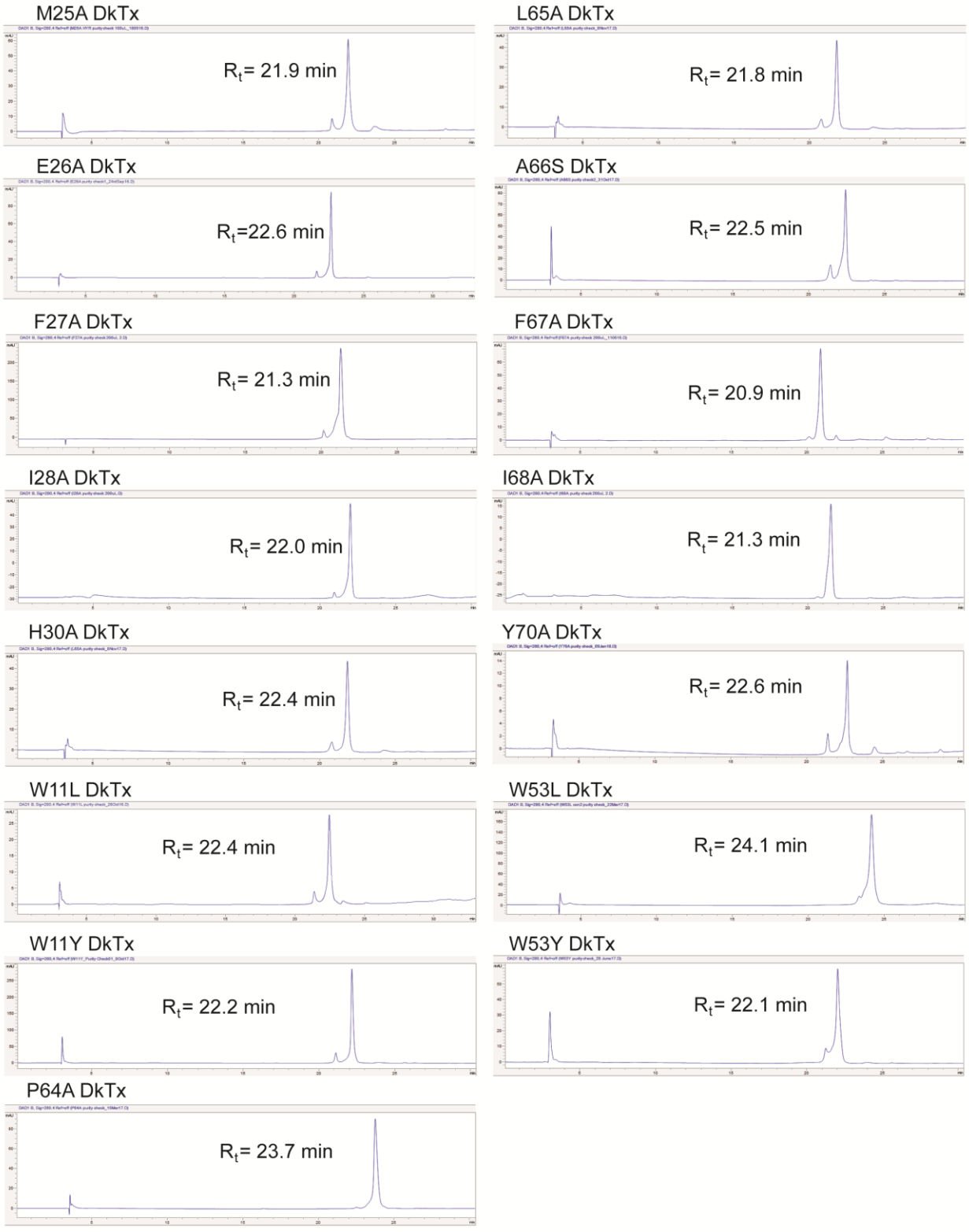

Figure 2.3. HPLC traces for purity evaluation of all our DkTx variants. The absorbance has been measured at 280 nm.

Representative current traces for variants of lipid-interacting DkTx residues

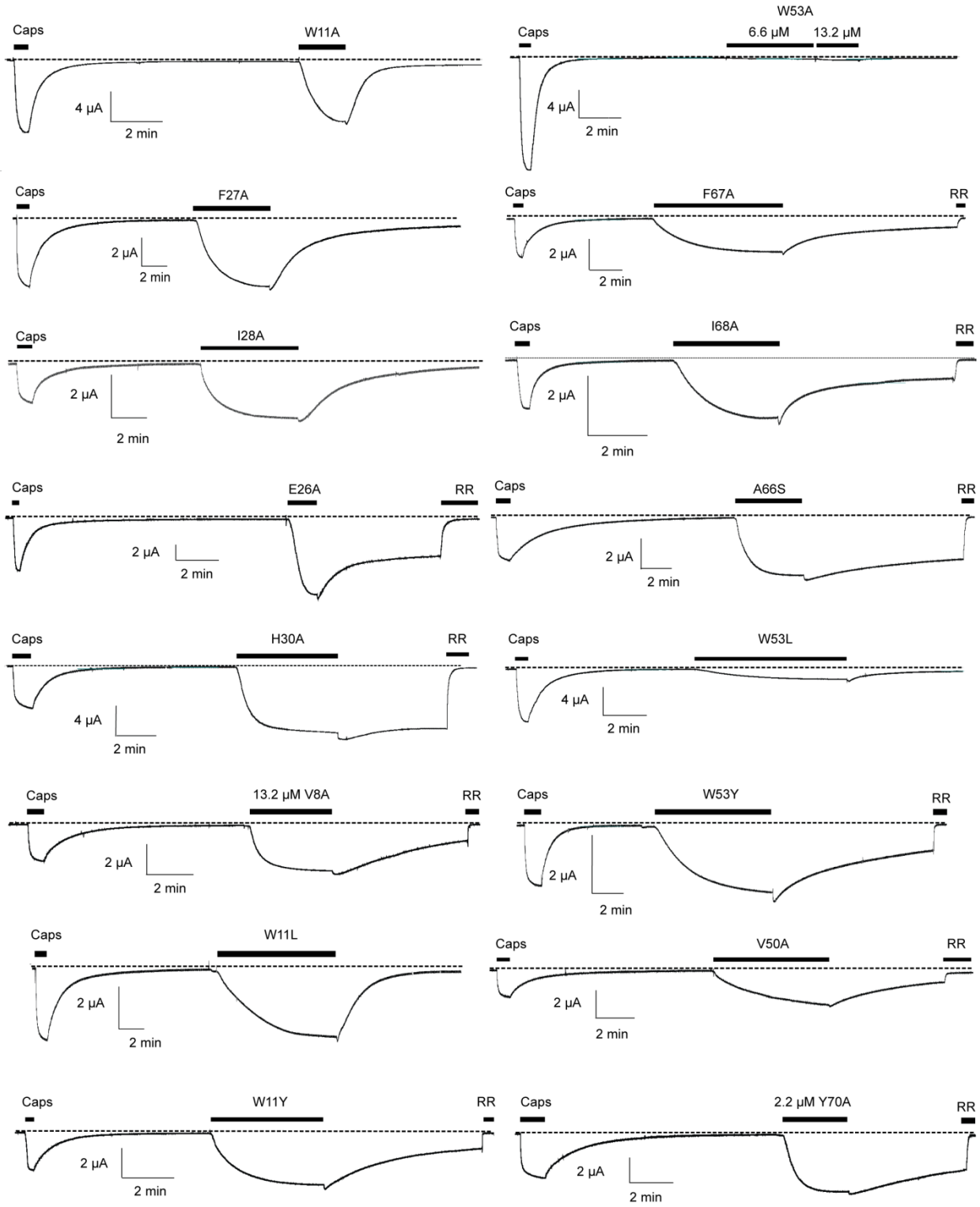

(Continued on next page)

Representative current traces for variants of exclusively channel-interacting DkTx residues

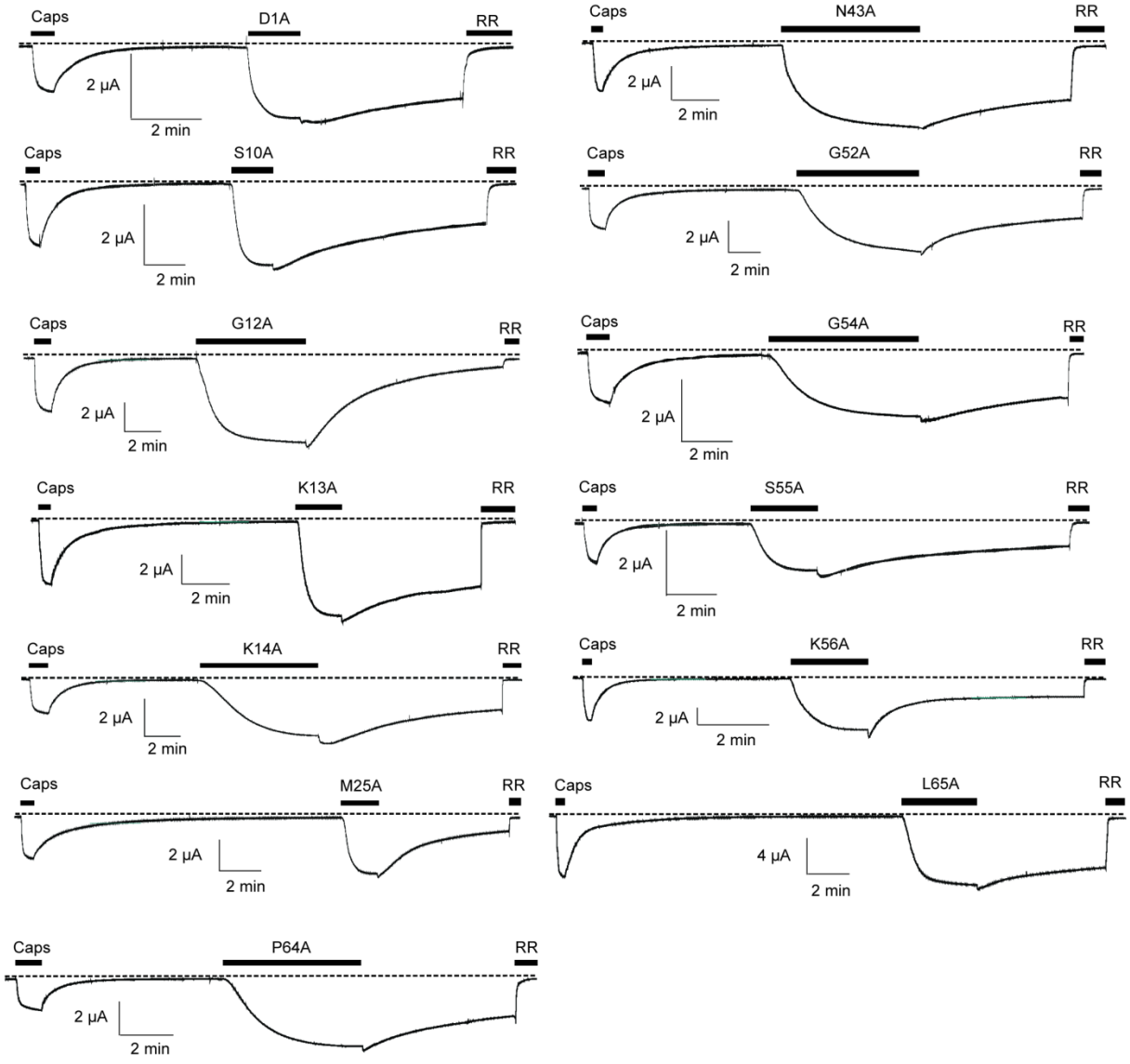

Figure 2.4. Representative electrophysiological recordings of the DkTx variants. All traces depicted below were obtained by applying 6.6 µM of toxin (unless otherwise mentioned).

2.4). These dose-response curves clearly show that the variants of DkTx residues that interact with channel residues independent of lipids (Figure 2.5a, top panel) demonstrate at best, a moderate effect on the potency of the toxin. Indeed, except for the alanine variants of the G12 and G54 residues of DkTx present at similar positions of the K1 and K2 knots (sequence

alignment of K1 and K2 is provided at the bottom of Figure 2.1b) that yielded an 8 and 9-fold increase in the EC_{50} values respectively as compared to the wild-type toxin (Table 2.1), the other 11 exclusively channel-interacting variants gave EC_{50} values that were within 2-4 fold of that of the wild-type toxin (bars in green in Figure 2.5b and Table 2.1). In contrast, variants of several of the lipid-interacting toxin residues demonstrated a profound abrogation of toxin potency (bottom panel of Figure 2.5a and blue bars in Figure 2.5b). In particular, the W11A and W53A DkTx variants of the K1 and K2 knot respectively demonstrated a substantially reduced potency—whereas the W11A variant yielded an 80-fold higher EC_{50} value (Table 2.1) than the wild-type

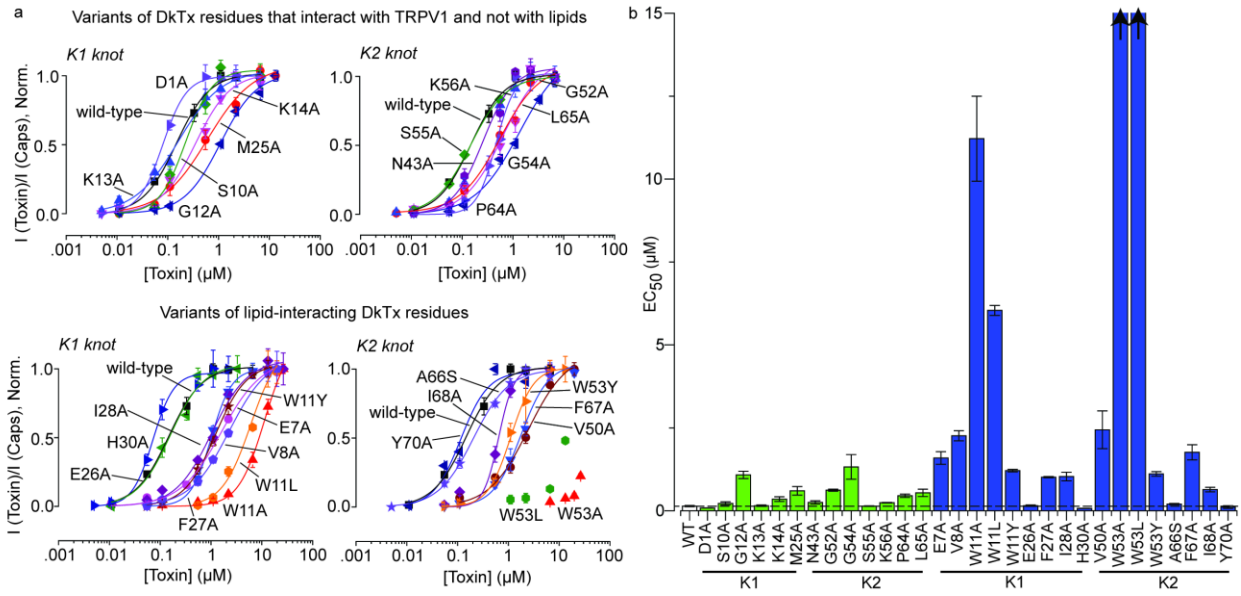

Figure 2.5. Effects on the potency of DkTx for TRPV1 activation upon alteration of protein–protein and protein–lipid interfaces. a) Dose-response plots of the variants of exclusively channel-interacting (top) and lipid-interacting (bottom) residues of DkTx. The K1 knot variants of DkTx are depicted on the left and K2 variants on the right. b) EC_{50} values of all DkTx variants. The bars in green correspond to variants of exclusively channel-interacting DkTx residues, and the ones in blue are of those that interact with lipids. The EC_{50} values for the W53A and W53L variants could not be obtained owing to their extremely low potency (this is denoted by the arrows on the top of the bars corresponding to these variants). "WT" is an abbreviation for "wild-type". Each data point is an average of 3-5 recordings and the error bars correspond to standard deviation values.

toxin, the W53A variant was such a poor TRPV1 agonist that we were unable to generate its complete dose response curve due to lack of solubility of the toxin at the high concentrations required to achieve full channel activation (Figure 2.5a), demonstrating that the EC_{50} value of this variant was well above 100-fold higher than that of the wild-type toxin. Our interaction maps (summarized in Figure 2.1b) show that these tryptophan residues interact intimately with both the channel residues and also with lipid molecules. To investigate the importance of the W11 and W53 residues further, we generated their leucine and tyrosine variants and characterized their activity. Similar to the alanine variants of these residues, their leucine variants also demonstrated poor TRPV1 activation properties, whereas their tyrosine variants demonstrated significant rescue of toxin activity (EC_{50} values obtained for the W11Y and W53Y variants were ~10-fold higher than that of the wild-type toxin; Figures 2.5a-b) suggesting that an aromatic side chain is important for toxin activity at these positions. The alanine variant of another DkTx residue that constitutes the toxin–lipid interface, V8, located in loop 1 of the K1 knot, demonstrated an appreciably-reduced potency (~16-fold higher EC_{50} value) as compared to the wild-type toxin (Figure 2.5 and Table 2.1). The alanine substituent of the corresponding residue of the K2 knot, V50, also demonstrated a similarly significant loss of toxin potency (Figure 2.5b). Interestingly, neither of our two interaction maps (Table 2.1) depicts these two valine residues in the proximity of any channel residues, and instead, shows both of them as exclusively lipid-interacting. Strikingly, except for the lipid-interacting residue E7 of loop 1 of the K1 knot whose alanine substituent demonstrated an 11-fold higher EC_{50} value as compared to the wild-type toxin (Figure 2.5 and Table 2.1), not a single charged or polar residue of the toxin was observed to play an important role in the toxin's activity. Indeed, the residues that were found to be most important for toxin-activity were hydrophobic—whereas some of them were aliphatic (V8, I28, V50 and I68), the others were aromatic (W11, F27, W53 and F67).

Protein–lipid interfaces formed by the K1 knot of DkTx are responsible for slow toxin wash-off. A prominent observation from our electrophysiological recordings was that several of our DkTx variants demonstrate enhanced wash-off rates as compared to the wild-type toxin (Figure 2.6a). Interestingly, all the DkTx residues whose variants demonstrated fast wash-off (W11, F27, I28 and V8) are lipid-interacting residues of the K1 knot. Moreover, none of the variants of the exclusively channel-interacting DkTx residues, except G12 (another K1 residue), and none of the K2 knot DkTx variants demonstrated this phenotype (Figure 2.4). The fastest

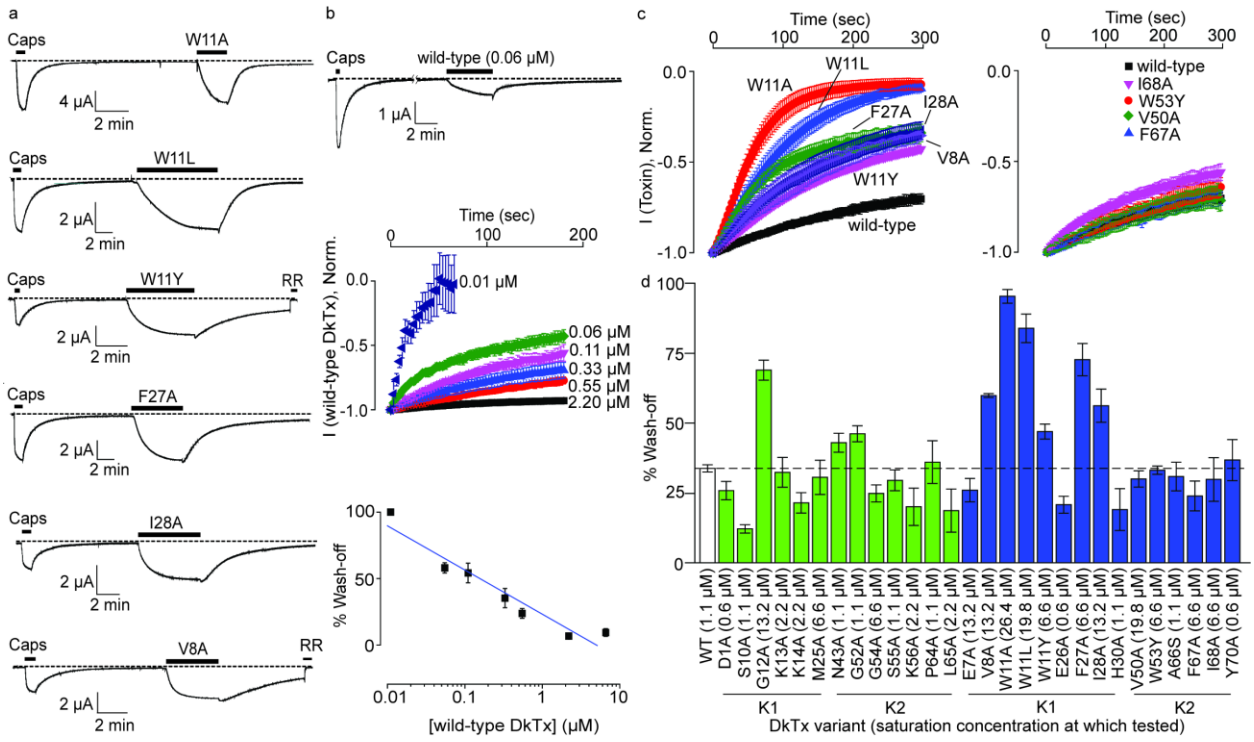

Figure 2.6. Toxin wash-off studies. a) Electrophysiological recordings obtained for fast washing-off DkTx variants. Capsaicin was applied at a concentration of 5 μM and the toxins were applied at 6.6 μM, except for V8A which was tested at 13.2 μM. b) Wash-off studies on wild-type DkTx showing fast wash-off when applied at a low concentration (top panel), and concentration-dependence of wash-off kinetics (middle and bottom panels). The *y*-axis of the plot on the bottom panel depicts % reduction in current after 3 min of buffer perfusion post wild-type DkTx-mediated channel activation. The blue line shown was generated by fitting a linear equation to the data. c) Averaged wash-off current traces obtained for wild-type DkTx and fast washing-off lipid-interacting K1 variants of DkTx (left panel) and those of their corresponding K2 variants (right panel). d) Bar graph depicting the percentage reduction in current after 3 min of buffer perfusion post toxin-mediated channel activation for all variants (bars corresponding to the variants of lipid-independent channel-interacting residues are depicted in green and those for lipid-interacting residues are depicted in blue). The experiments (in both c and d) were performed at saturation concentrations of the respective toxins denoted within parenthesis in Figure 2.6d. Each current trace/data point is an average of 3-5 recordings and the error bars correspond to standard deviation values.

wash-off rates were observed for the W11A variant that washed off completely within ~3 min (Figure 2.6a), in contrast to the wild-type toxin that does not wash-off completely even after 30 min of buffer perfusion (Figure 2.1c).

The large differences in the wash-off kinetics demonstrated by DkTx variants motivated us to study toxin wash-off in more detail. We began our studies by first determining whether toxin wash-off rates were dependent on the concentration of the applied toxin. We observed that when a low concentration (0.06 μM) of wild-type DkTx was employed to activate TRPV1, the toxin washed off completely in 12 min (Figure 2.6b, top panel), in contrast to the much slower wash-off observed with 3.3 μM of the toxin (Figure 2.1c). Wash-off studies with a range of concentrations of DkTx revealed that wash-off kinetics was indeed concentration dependent—when 0.01 μM of wild-type DkTx was employed to activate TRPV1, the wash-off was complete within 1 min, in stark contrast to the negligible wash-off in 3 min observed upon channel activation with 2.2 μM toxin (Figures 2.6b, middle panel). These studies established an inverse correlation between the wash-off rates and the concentration of the toxin used in the experiment (Figure 2.6b, bottom panel; Pearson's $r = -0.90$). The observation that wash-off kinetics depends on the concentration of the toxin used for channel activation suggests the possibility that wash-off kinetics vary as a function of channel-occupancy. Consequently, we reasoned that a valid comparison of wash-off kinetics between the toxin variants can only be performed at toxin concentrations where the channel-occupancy is the same in each case, for example at the top of each variant's dose response curve, where all channels would be toxin-bound resulting in 100% channel-occupancy before wash-off. All subsequent wash-off experiments were therefore performed with saturating concentrations of each of the toxin variants.

The wash-off current traces obtained over a 5 min buffer perfusion time-period subsequent to channel activation with saturating concentrations of our fast washing-off DkTx variants, W11A, W11L, W11Y, V8A, F27A and I28A, are depicted in Figure 2.6c (left panel). Notably, none of the DkTx variants of the K2 knot demonstrated fast wash-off (see Figure 2.4 for representative traces). Indeed, the wash-off kinetics obtained with saturation concentrations of W53Y, F67A and I68A and the V50A variants overlapped with that of the wild-type toxin (right panel of Figure 2.6c). Toxin variants W53A and W53L were not amenable to these experiments as their poor potency obviated preparation of toxin solutions at concentrations

required to attain saturation of their dose-response curves (Figure 2.5). Our entire wash-off dataset for both the channel-interacting and lipid-interacting residues of the DkTx depicted in Figure 2.6d shows that none of the residues of the toxin that interact with the channel residues exclusively via protein–protein interactions (green bars), except for G12A, demonstrated significantly faster wash-off rates as compared to that of the wild-type toxin.

K1 knot-driven efficient membrane partitioning of DkTx underlies its slow wash-off. The observation that the fast washing-off toxin variants were generated by substituting lipid-interacting residues suggests that the wash-off kinetics are linked to toxin–membrane lipid interactions. To compare the intrinsic membrane lipid-interacting properties of our toxin variants, Yashaswi Singh in Dr. Jeet Kalia's lab subjected them to tryptophan fluorescence-based membrane partitioning experiments on POPC-POPG (1:1) large unilamellar vesicles (LUVs) by employing approaches similar to the ones previously reported (Bae et al., 2016; Gupta et al., 2015; Lee and MacKinnon, 2004; Milescu et al., 2007). Consistent with the results of a previous study (Bae et al., 2016), our experiments with wild-type DkTx revealed that it partitions well into vesicles. Indeed, in presence of LUVs generated at a particular lipid concentration, a robust increase in fluorescence emission with a concomitant blue shift of >10 nm was noted (data not shown here), characteristic of proteins that interact favorably with membrane lipids and partition into the membrane. In comparison, the W11A variant demonstrated a small blue shift, and a modest increase in emission intensity in presence of vesicles generated with the same concentration of lipids (data not shown here). A plot of normalized relative fluorescence versus lipid concentration plots was made for each of these variants from K1 and K2 knots tested and by fitting a partition function to it yielded their mol. fraction partitioning coefficients (K_x) values (Table 2.1 for their K_x values). It was found that fast washing-off K1 knot variants of DkTx, W11L and F27A also demonstrated greatly abrogated membrane partitioning as compared to the wild-type toxin. The variants of analogous K2 knot residues of DkTx, W53A and F67A, on the other hand, yielded K_x values that were similar to that of the wild-type toxin demonstrating that they partition very well into membranes. Plotting the K_x values of the wild-type toxin and those of the K2 and fast washing-off K1 variants versus the % wash-off yielded the plot shown in Figure 2.7c and fitting a linear equation to the plot for the fast washing-off K1 variants gave a good correlation (Pearson's $r = –0.90$). The K2 variants of DkTx such as W53Y, I68A and F67A that wash-off slowly demonstrated efficient membrane partitioning (open squares in Figure 2.7c)

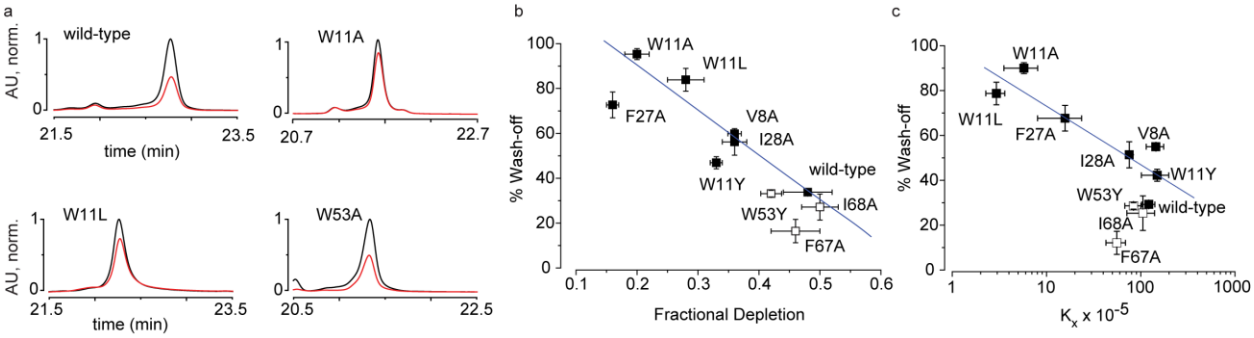

Figure 2.7. Toxin–membrane interaction studies on DkTx and its variants. a) HPLC traces depicting toxin depletion upon incubation of DkTx and its variants with *Xenopus laevis* oocytes. Traces in black correspond to the controls wherein the toxins solubilized in buffer devoid of oocytes were subjected to HPLC analysis, whereas those in red were obtained when the supernatant of toxin solutions incubated with 100 oocytes were subjected to HPLC. b) Plot of % wash-off of wild-type DkTx and K1 variants (solid squares) and K2 variants (open squares) after 3 min of buffer perfusion post TRPV1 activation by saturation concentrations of the toxins (obtained from the electrophysiology experiments) versus fractional depletion (obtained from HPLC peak areas as described in the Materials and Methods section 2.4.3). The blue line shown was generated by fitting a linear equation to the data for the K1 variants. Each data point is an average of 3-5 recordings/assays and the error bars correspond to standard deviation values. c) Plot of % wash-off of wild-type DkTx and K1 variants (solid squares), and those of K2 variants (open squares) after 3 min of buffer perfusion post TRPV1 activation by saturation concentrations of the toxins (obtained from the electrophysiology experiments) versus mol. fraction partitioning coefficients (K_x) values (obtained from the tryptophan fluorescence experiments) (Courtesy: Yashaswi Singh). The blue line shown was generated by fitting a linear equation to the data for the K1 variants.

similar to wild-type DkTx. These results are consistent with the notion that the slow wash-off demonstrated by DkTx is a consequence of its high intrinsic affinity for the membrane that is orchestrated by the protein–lipid interactions of the K1 knot, and not the K2 knot.

To investigate the interactions of DkTx and its variants with more physiologically-representative membranes, we characterized their binding to *Xenopus laevis* oocytes. These

experiments were performed by following previously reported protocols developed by Swartz and co-workers for studying the membrane-interacting properties of toxins that target voltage-activated ion channels (Milescu et al., 2007). Oocytes were incubated in toxin solutions and the unbound toxin was quantitated by subjecting the supernatant to HPLC. The depletion in the concentration of DkTx and its variants due to partitioning into oocyte plasma membranes was calculated by using the areas under the HPLC peaks corresponding to the toxins as a measure of the amount of the unbound toxin (details in the supporting information section). The results of these experiments (Figure 2.7a, b) revealed that whereas the slow washing-off toxins (wild-type DkTx and the variants of the K2 knot residues W53, F67 and I68) were substantially depleted, the fast washing-off K1 variants (W11A, W11L and F27A) demonstrated significantly lower

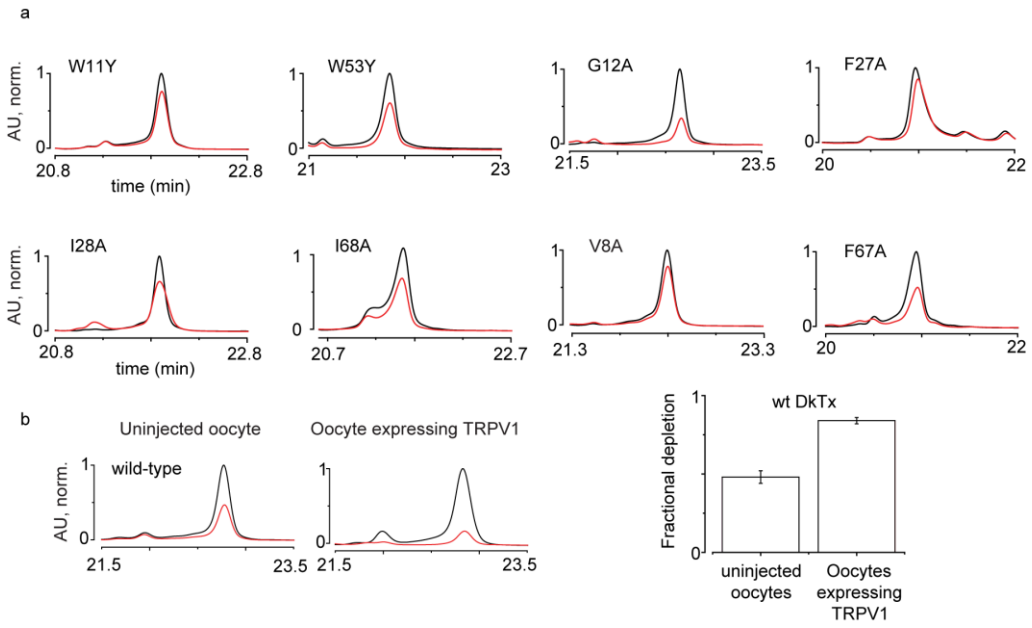

Figure 2.8. Toxin depletion assays performed with DkTx and its variants. a**)** Overlay of normalized HPLC chromatograms for toxin depletion experiments on DkTx variants on uninjected *Xenopus laevis* oocytes. Control traces are depicted in black and the experimental ones are depicted in red. b) Overlay chromatograms (left panel) for the depletion experiments performed with wild-type DkTx on uninjected and TRPV1-expressing oocytes. A bar graph depicting the fractional depletion obtained from the HPLC traces on the left panel is shown on the right panel. Error bars correspond to standard deviation values (n=3-5)

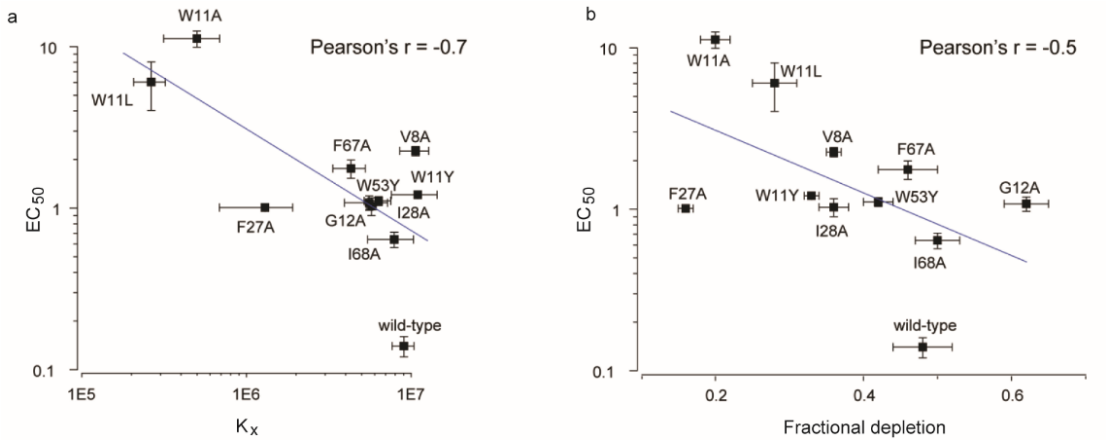

Figure 2.9. Correlation plot of potency vs. membrane partitioning of DkTx variants. a) Potency (EC_{50}) vs. mol. partitioning coefficient (K_x), and b) Potency (EC_{50}) vs. fractional depletion plots.

depletion. The HPLC chromatograms for the depletion of the variants not depicted in Figure 2.7a are provided in Figure 2.8a and the results of a control experiment demonstrating enhanced DkTx depletion upon incubation with TRPV1-expressing oocytes is shown in Figure 2.8b. Plotting % wash-off vs fractional depletion for the fast washing-off K1 variants (akin to the analysis depicted in Figure 2.7c for membrane partitioning) and fitting a linear equation to this plot gave a good correlation (Pearson's r = –0.94) (Figure 2.7b). In contrast, the EC_{50} values of DkTx and its variants did not correlate well with their membrane partitioning parameters (K_x, Figure 2.9a; and fractional depletion, Figure 2.9b), suggesting that bulk membrane partitioning properties of DkTx do not contribute substantially to the toxin's potency. Taken together, the results of these depletion experiments performed on physiological membranes are consistent with those of the fluorescence-based membrane partitioning experiments on LUVs and implicate the high membrane affinity of DkTx for its slow washing-off feature.

2.3. Discussion.

The overarching goal of this study was to elucidate the functional roles of protein–membrane lipid interfaces by leveraging the power of electrophysiology that enables the characterization of the function of ion channel membrane proteins under physiological conditions. By complementing these studies with fluorescence-based membrane partitioning and cellular depletion experiments, we have dissected the functional contributions of protein–lipid and

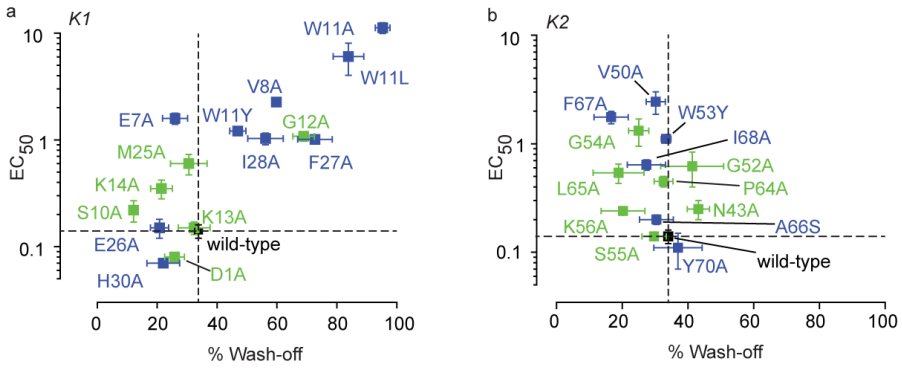

Figure 2.10. Plots of potency for TRPV1 activation (EC_{50} values) versus channel-dissociation rates (% wash-off), of DkTx variants. a) DkTx variants of the K1 knot residues, and b) those of the K2 knot residues. Data points for the variants of lipid-interacting residues are depicted in blue, those of channel-interacting residues in green, and that for the wild-type toxin in black. Percentage wash-off depicts the % reduction in current after 3 min of buffer perfusion post channel activation with saturation concentrations of the toxin variants. The dotted lines represent the data for wild-type DkTx.

protein–protein interactions orchestrated by the spider toxin, DkTx, to its TRPV1 ion channel activation properties.

An important insight that our results provide is that protein–lipid interactions do not merely subtly modulate, but rather, can drive protein function. To illustrate this point, the entire dataset obtained from our electrophysiology experiments on DkTx is summarized in the potency (EC_{50} values) versus channel-dissociation rates (% wash-off) plots depicted in Figure 2.10, separately for the K1 and K2 knots (except for the lipid-interacting K2 knot variants, W53A and W53L, that could not be fully characterized owing to their low potency). The plot for the K1 knot variants depicts several data points (corresponding to the W11A, W11L, V8A, G12A, W11Y, I28A and F27A variants) that are localized at its top-right portion, implying that substituting these K1 knot residues of the toxin resulted in a substantial increase in channel-dissociation rates of the toxin as well as appreciable ablation of the toxin's potency. Except for G12, all of these residues are lipid-interacting. On the other hand, the majority of the data points for the K2 knot variants are clustered towards the left side of the plot, highlighting that these

variants demonstrate slow wash-off similar to the wild-type toxin. Several K2 knot variants, however, demonstrate a considerably reduced potency for activating TRPV1 including the W53A, W53L, V50A, F67A, W53Y, G54A and I68A variants, among which, all except G54A are variants of lipid-interacting toxin residues (Figure 2.10b). This observation that the lipid-interacting K1 residues contribute profoundly to both the toxin's potency and in endowing it with slow channel-dissociation rates, whereas those of the K2 knot contribute substantially to the former but negligibly to the latter, reveals the ability of protein–lipid interactions to fine tune protein function in different ways. This functional dichotomy of the K1 and K2 lipid-interacting interfaces is particularly noteworthy considering that both map to similar regions of two structurally similar motifs (K1 and K2 knots) present within the same protein molecule.

Mapping of the functionally critical toxin residues identified in this study to the DkTx–TRPV1 complex structure reveals that the toxin activates the channel by employing a unique mechanism that entails the formation of two hydrophobic interfaces comprising membrane lipids, hydrophobic residues of the toxin, and those of the channel (Figure 2.11). The high degree of hydrophobicity of both of these tripartite complexes (one formed by the K1 knot and the other by the K2 knot) is prominently seen in their surface renditions colored by employing the Eisenberg hydrophobicity scale (Eisenberg et al., 1984) (right panels of Figures 2.11a and 2.11b). Each complex lies at the interface of and 3 for the K2 knot complex in Figure 2.11) such that the entire DkTx–TRPV1 complex spans three subunits of the tetrameric channel. Whereas one of the TRPV1 subunits of each complex adjacent channel subunits (labeled subunits 1 and 2 for the K1 knot complex, and subunits 2 contributes the hydrophobic F655, A657, V658 and I661 residues of its S6 helix, the other two contributes the Y631 residue of its pore helix. Consistent with our discovery that these toxin–lipid–channel interfaces play critical roles in toxin-activation of the channel, variants of two of these channel residues, A657 and Y631, have been shown to disrupt the DkTx-sensitivity of the channel (Bohlen et al., 2010). The complexes contain three putative phosphatidylethanolamine lipid molecules each, one of which (lipid 1of the K1 knot complex and lipid 4 of the K2 knot complex) is embedded deep in a hydrophobic pocket formed by the functionally critical toxin residues identified in this study—V8, W11, I28 and F27 of the K1 I661 (Figure 2.11). The tryptophan residues of the toxin form the floor of

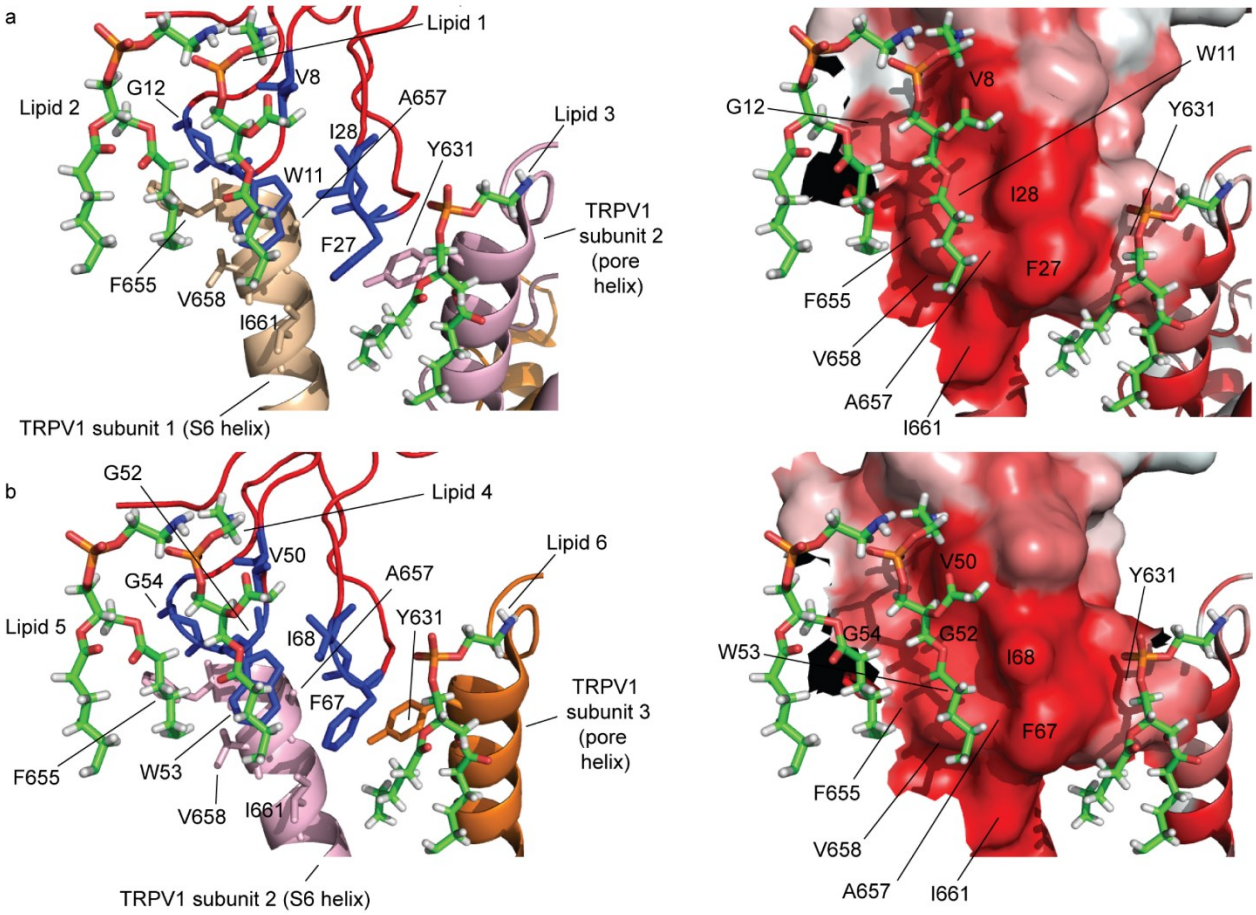

Figure 2.11. Functionally critical toxin residues of the a) K1 knot, and b) K2 knot, identified in this study mapped onto the structure (pdb:5irx (Gao et al., 2016)) along with the TRPV1 residues and lipid molecules they interact with. The left panels depict the toxin residues in blue, the lipids in the sticks representation, and the channel residues in the color employed to depict the channel subunit they belong to (the color scheme used to render the channel subunits is the same one that was used in Figure 2.1). The right panels depict the same interface shown on the left panel in the surface orientation rendered by employing the Eisenberg scale wherein the intensity of the red color is proportional to the hydrophobicity.

these hydrophobic pockets, whereas the walls of the pockets are formed by the hydrophobic side chains of the isoleucine and phenylalanine toxin residues on one side, and those of the channel residues, F655, V658 and A657 on the other, whereas the channel residue I661 forms the outer edge of the pocket. The tails of each of the lipid molecules in the pdb file for the structure are truncated and no structural information on their peripherally-located CH_2 groups is available. It

is, however, tempting to speculate that the hydrophobic valleys formed by the phenylalanine residues of the toxin (F27 in case of the K1 knot complex and F67 in case of the K2 knot complex) and I661 of the channel serve as hydrophobic conduits for one of the hydrophobic tails of lipid 1 and lipid 4 knot, and V50, W53, I68 and F67 of the K2 knot, and channel residues F655, A657, V658 and to thread through, and that the other hydrophobic tail of each of these lipids threads through the hydrophobic valleys formed by the side chains of the V8/V50 and I28/I68 residues of the toxin (right panels of Figure 2.11a and 2.11b). In addition to binding to the toxin and channel residues, lipids1 and 4 also engage in hydrophobic interactions with lipids 2 and 5 that are located nearby (Figure 2.11). The third lipid of each complex (lipid 3/lipid 6) forms a second hydrophobic patch adjacent to the one detailed above. Whereas lipid 1 and lipid 4 interact with loop 1 and loop 2 of the knots, lipid 3 and lipid 6 form hydrophobic patches with the I28/I68 and F27/F67 residues of loop 4 of the knots along with the Y631 residue of the pore helix of an adjacent TRPV1 subunit. Interestingly, one of the functionally important residues identified in this study, G12 (Figures 2.5b, 2.6d and 2.10), does not make direct contacts with any of the lipids in the structure (Figure 2.1b). Considering the unique property of glycine to confer conformational flexibility to protein structure (Krieger et al., 2005; Yan and Sun, 1997), it is possible that G12 enables the adjacent W11 residue to reach down into the membrane and form the heart of the tripartite complex. A similar logic may explain the functionally important roles of the G52 and G54 residues of the K2 knot that flank its critical W53 residue.

Previous work has demonstrated that the individual knots of DkTx can activate TRPV1 albeit with a lower potency than that of the double knot, and that the K1 knot's potency is much lower than that of the K2 knot (Bae et al., 2012; Bohlen et al., 2010). If the contributions of the individual knots towards the potency of the double knot are in accordance with their potency as single knots, variants of the K1 knot residues of DkTx would be expected to cause minimal alteration of the toxin's potency. In contrast to this expectation, we observed that several K1 knot variants dramatically disrupted TRPV1 activation properties. Indeed, among the 15 K1 knot variants we tested, 8 (W11A, W11L, V8A, E7A, W11Y, G12A, I28A and F27A in the order of increasing potency) demonstrated a >7-fold increase in the EC_{50} values as compared to that of the wild-type toxin (Figure 2.10a and Table 2.1). This dependence of the toxin's potency on K1 knot residues despite its low intrinsic potency as a single knot suggests that the knots on their own activate the channel by employing a different mechanism as compared to that of the double

knot. This notion is supported by the observation that whereas introducing the L65A substitution into the K2 single knot substantially reduces its potency (Bae et al., 2016), this substitution has only a moderate effect in the context of the double knot (Figure 2.5). Obtaining structures of single knots bound to the channel in lipidic environments coupled with mutagenesis-based structure-function studies on the individual knots akin to the one reported in this work on the double knot can enable testing of this intriguing hypothesis.

One of the most striking results we obtained in this study is that in contrast to wild-type DkTx, several variants of lipid-interacting residues of the K1 knot of DkTx demonstrate rapid wash-off rates (Figures 2.6 and 2.10a). Interestingly, these wash-off rates are inversely correlated with the membrane partitioning ability of these toxin variants measured both on artificial lipid vesicles (Figure 2.7c) and also on cells (Figure 2.7b). Since the partitioning experiments were performed on lipid vesicles/cells not containing the TRPV1 channel, this observation suggests that the high intrinsic membrane affinity of the wild-type toxin underlies its slow wash-off. Efficacious membrane partitioning of the toxin will lead to its accumulation at high concentrations within the membrane, suggesting that the slow wash-off phenotype of the toxin may be due to its presence at high concentrations in the membrane. These results are consistent with a "toxin relay mechanism" depicted in Figure 2.12. When the toxin is applied, it accumulates in the membrane at high concentrations owing to its highly efficient partitioning ability, and a few of these molecules bind to TRPV1 channels resulting in channel activation. Upon subsequent initiation of wash-off by buffer perfusion, the channel-bound toxin molecules (the knots of which are depicted as filled ellipses) begin to get dislodged and are rapidly replaced by the surrounding membrane-partitioned toxin molecules that are present at a high concentration. Buffer perfusion also causes toxin molecules within the membrane that are not bound to TRPV1 (whose knots are depicted as open ellipses) to wash-off resulting in depletion of the toxin in the vicinity of the channels, thereby slowing down the relay process leading to an increase in the population of the toxin-free closed channels that manifests itself as a slowly decreasing TRPV1 current in the electrophysiology recording. This model convincingly explains our observation that the toxin variants that partition poorly wash-off rapidly (Figure 2.6c) and can also explain the concentration-dependence of toxin wash-off kinetics (Figure 2.6b). The slow channel-dissociation rate of the toxin, is therefore, not merely due to a tight bimolecular binding

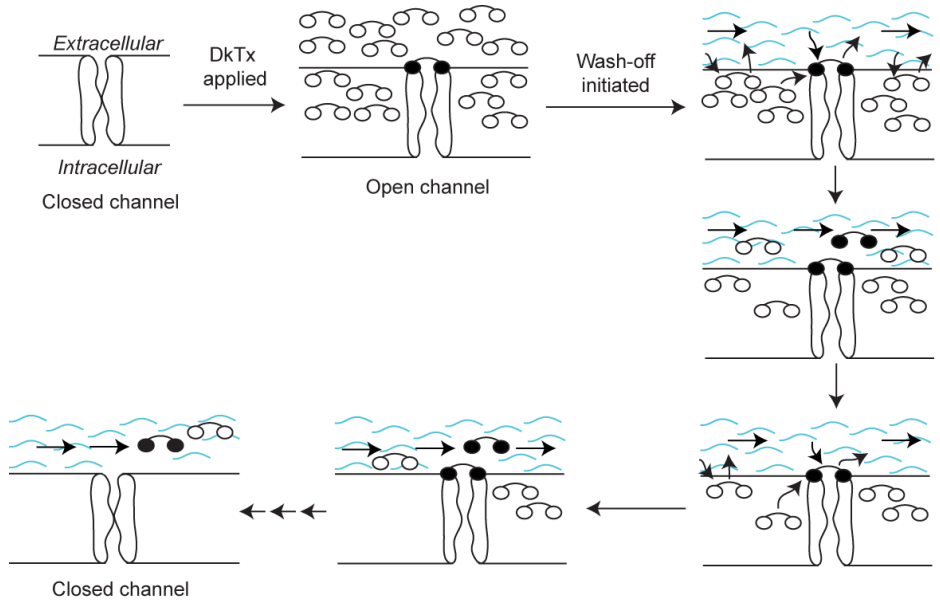

Figure 2.12. Our proposed "toxin relay" model that explains the slow wash-off feature of DkTx. DkTx is represented by a dumbbell-shaped object with its 2 ellipses denoting the two knots of the toxin. The knots of the toxin molecules that do not bind to the channel are depicted as empty ellipses, and those that bind to the channel as filled ellipses. The wavy blue curves depict buffer flow.

event but also due to the high concentration of neighboring toxin molecules in the membrane that are available to replace channel-bound toxin molecules as they are lost due to buffer perfusion.

Taken together, our studies on DkTx-activation of TRPV1 reveal that this process is driven primarily via protein–lipid interfaces, and minimally by lipid-independent protein–protein interactions. Furthermore, we report that DkTx activates the TRPV1 ion channel by employing a mechanism that entails the formation of hydrophobic toxin–lipid–channel interfaces, rather than by utilizing its charged amino acids to interact directly with the channel, as observed in case of the potassium channel-targeting pore-blocking toxins such as charybdotoxin (Banerjee et al., 2013; Goldstein et al., 1994), and also for the acid-sensing ion channel (ASIC)-activating toxin, psalmotoxin (Baconguis and Gouaux, 2012; Dawson et al., 2012). It remains to be seen whether a similar mechanism of action is employed by the voltage sensor-targeting toxins, the channel complexes of which await structural characterization. Finally, our functional and membrane

partitioning data supports a mechanistic model that posits that the high propensity of DkTx for membrane partitioning in addition to its bivalent mode of binding underlies its slow channel-unbinding property.

Table 2.1. Consolidated data summary for all DkTx site-directed variants

S. No.	Knot	DkTx variant	Expected mass (a.m.u.)	Observed mass (a.m.u.)	HPLC Retention time (min)	EC_{50} (μM)	Fold Change in EC_{50}	Hill Coefficient (n_H)	% Wash-off after 3 min of buffer perfusion post channel activation by saturation concentration of toxin	Mol. fraction partition coefficient (K_x) (Courtesy: Yashaswi Singh)	Fractional depletion (oocytes)
1		Wild-type	9042.5	9043.1	22.4	0.14 ± 0.02	1.0	1.32 ± 0.17	33.77 ± 1.26 (1.1 μM)	(9.03±1.38)E6	0.48 ± 0.04
2	K1	D1A	8998.5	8995.3	24.4	0.08 ± 0.00	0.6	1.84 ± 0.22	25.81 ± 3.29 (0.55 μM)	N.D	N.D
3		E7A	8984.4	8982.5	22.3	1.59 ± 0.19	11.4	1.32 ± 0.17	25.97 ± 4.17 (13.2 μM)	N.D.	N.D
4		V8A	9014.4	9012.5	22.4	2.26 ± 0.15	16.1	1.13 ± 0.06	59.81 ± 0.69 (13.2 μM)	(1.06±0.21)E7	0.36 ± 0.01
5		S10A	9026.5	9027.7	22.4	0.22 ± 0.05	1.6	1.67 ± 0.38	12.13 ± 1.50 (1.1 μM)	N.D	N.D
6		W11A	8927.4	8925.0	21.6	11.22 ± 1.3	80.1	1.68 ± 0.17	95.30 ± 2.45 (26.4 μM)	(4.99±1.86)E5	0.2 ± 0.02
7		W11L	8969.4	8970.1	22.4	6.04 ± 2.01	43.1	1.54 ± 0.43	83.87 ± 5.10 (19.8 μM)	(2.63±0.57)E5	0.28 ± 0.03
8		W11Y	9019.4	9020.9	22.2	1.21 ± 0.04	8.6	1.41 ± 0.07	46.92 ± 2.70 (6.6 μM)	(1.1±0.4)E7	0.33 ± 0.01
9		G12A	9056.5	9055.6	22.9	1.08 ± 0.11	7.7	1.21 ± 0.16	68.91 ± 3.58 (13.2 μM)	(5.55±1.62)E6	0.62 ± 0.03
10		K13A	8985.4	8986.9	22.2	0.15 ± 0.02	1.1	1.01 ± 0.11	32.35 ± 5.32 (2.2 μM)	N.D	N.D
11		K14A	8985.4	8986.1	22.8	0.35 ± 0.07	2.5	1.26 ± 0.22	21.44 ± 3.63 (2.2 μM)	N.D	N.D
12		M25A	8982.4	8980.6	21.9	0.60 ± 0.13	4.3	0.96 ± 0.14	30.56 ± 6.10 (6.6 μM)	N.D	N.D
13		E26A	8984.4	8983.9	22.6	0.15 ± 0.03	1.1	1.31 ± 0.39	20.78 ± 3.03 (0.55 μM)	N.D	N.D
14		F27A	8966.4	8966.3	21.3	1.01 ± 0.02	7.2	2.14 ± 0.09	72.67± 5.78 (6.6 μM)	(1.29±0.61)E6	0.16 ±0.01
15		I28A	9000.4	9000.7	22.0	1.03 ± 0.13	7.4	1.22 ± 0.20	56.18 ± 5.90 (13.2 μM)	(5.74±0.4)E6	0.36 ±0.02
16		H30A	8976.4	8976.9	22.4	0.07 ± 0.00	0.5	2.12 ± 0.42	22.05 ± 5.45 (1.1 μM)	N.D	N.D
17	K2	N43A	8999.4	8998.9	22.4	0.25 ± 0.05	1.8	1.47 ± 0.27	42.94 ± 3.39 (1.1 μM)	N.D	N.D
18		V50A	9014.4	9014.8	22.1	2.44 ± 0.57	17.4	1.13 ±0.20	29.99 ± 2.93 (19.8 μM)	N.D.	N.D
19		G52A	9056.5	9056.0	22.3	0.62 ± 0.22	4.4	1.14 ± 0.34	41.06 ± 9.56 (6.6 μM)	N.D	N.D
20		W53A	8927.4	8926.2	21.2	N.A.	>100	N.A.	N.A.	(4.6±0.65)E6	0.49 ± 0.04
21		W53L	8969.4	8968.2	24.1	N.A.	>100	N.A.	N.A.	N.D	N.D
22		W53Y	9019.4	9021.4	22.1	1.11 ± 0.07	7.4	1.92 ± 0.22	33.12 ± 1.48 (6.6 μM)	(6.34±1.16)E6	0.42 ± 0.02
23		G54A	9056.5	9056.6	22.8	1.32 ± 0.37	9.4	0.99 ± 0.16	24.80 ± 3.07 (6.6 μM)	N.D	N.D
24		S55A	9026.5	9025.7	22.8	0.14 ± 0.01	1.0	1.24 ± 0.07	29.48 ± 3.72 (1.1 μM)	N.D	N.D
25		K56A	8985.4	8985.2	22.5	0.24 ± 0.01	1.7	1.55 ± 0.07	20.02 ± 6.66 (2.2 μM)	N.D	N.D
26		P64A	9016.4	9013.4	23.7	0.45 ± 0.05	3.2	2.30 ± 0.63	32.37 ± 2.83 (1.1 μM)	N.D	N.D
27		L65A	9000.4	9000.0	21.8	0.54 ± 0.11	3.9	1.05 ± 0.18	18.67 ± 7.73 (2.2 μM)	N.D	N.D
28		A66S	9058.4	9059.1	22.5	0.20 ± 0.02	1.4	1.25 ± 0.14	30.20 ± 5.13 (1.1 μM)	N.D	N.D
29		F67A	8966.4	8966.3	20.9	1.76 ± 0.23	12.6	1.59 ± 0.28	16.43 ± 5.20 (13.2 μM)	(4.30±0.95)E6	0.46 ± 0.04
30		I68A	9000.4	9002.1	21.3	0.64 ± 0.07	4.6	2.93 ± 0.98	27.15 ± 5.80 (6.6 μM)	(7.88±2.44)E6	0.5 ± 0.03
31		Y70A	8950.4	8950.3	22.6	0.11 ± 0.04	0.8	1.61 ± 0.83	36.75 ± 7.34 (0.55 μM)	N.D	N.D

2.4. Materials and Methods.

2.4.1. Detailed procedure for the production of DkTx and its variants.

Mutagenesis and cloning:

DkTx variants were generated by performing whole-plasmid PCR on a plasmid provided by Dr. Kenton Swartz' laboratory at the NIH that contained the DkTx gene downstream of the ketosteroid isomerase (KSI) gene in a pET31b vector (Bae et al., 2012). PCR products were digested with *Dpn I* to remove methylated parental plasmid and the digested reaction mixture was transformed into *E.coli* NEB Turbo chemically competent cells.

Transformation and linear protein preparation:

Mutant DkTx clones were confirmed by sending sequencing samples to 1st Base, Malaysia. Positive clones were transformed into chemically competent *E. coli* BL21 (DE3) cells. LB broth cultures (1 L) containing ampicillin (100 µg/mL) were inoculated with transformed *E. coli* BL21 (DE3) cells and induced with IPTG (0.5 mM) on reaching an O.D. (600 nm) of 0.4-0.6 at 37°C. The induced culture was pelleted after 6 h of growth and lysed by sonication in Tris-HCl buffer (20 mM at pH 8.0). The sonicated cell lysate was first centrifuged at 12000 rpm for 1 h and the pellet was dissolved in guanidine hydrochloride solution (6 M), supplemented with L-methionine (67 mM). Fusion protein cleavage was performed by adding the cell lysate to a solution of hydroxylamine hydrochloride (2 M at pH 9) and incubating the resulting mixture at 45°C for 4.5 h. Subsequently, dithiothreitol (66 mM) was added and the resulting mixture was incubated at 45°C for 1 h for performing protein denaturation. This solution was then titrated with conc. HCl to pH 4 and centrifuged to obtain the denatured proteins in the supernatant. Subsequently, the protein solution was dialyzed against water containing 0.1% TFA and then filtered through 0.45 µm syringe filters and lyophilized to yield the linear protein as a white powder.

Refolding of linear DkTx variants:

The lyophilized linear protein was dissolved in 50% acetonitrile containing 0.1% TFA at a concentration of 2 mg/mL. This protein solution was then added to a redox refolding buffer containing Tris-HCl (0.4 M), EDTA (1 mM), Triton X-100 (0.5%), GSH (2.5 mM), GSSG (0.25 mM) at pH 8.0 and incubated at 4°C for 2 d. Poorly folding DkTx variants, W53A, W53L and G52A required prolonged incubation of 14 d in the refolding buffer to give good yields. The progression of refolding was assessed by subjecting the refolding cocktail to analytical RPHPLC on a C18 column (300 Å pore size) with a linear acetonitrile-water (0.1% TFA) gradient

(5-65% acetonitrile over 30 min). Once refolded optimally, the refolding cocktail was titrated to pH 4 with conc. HCl to quench the refolding reaction. The refolding cocktail was then concentrated in a 3500 MWCO dialysis membrane (Thermo Fischer Inc.) against 400 g/L solution of PEG20. The refolded DkTx variants were then purified from the concentrated refolding cocktail by RP-HPLC on a C18 column (300 Å pore size) with a linear acetonitrile-water (0.1% TFA) gradient (5-65% acetonitrile over 30 min). Purified fractions were quantified by spectrophotometric analysis from the absorbance at 280 nm and then aliquoted in 1 nmol aliquots or 4 nmol aliquots, vacuum-dried and stored at -80°C until use for electrophysiological activity assays and partitioning experiments, respectively. Figure 2.2 depicts representative protein production data and Figure 2.3 depicts the purity evaluation HPLC runs for all variants. Wild-type and all DkTx variants had an additional glycine residue at their N-termini and three additional residues (HYR) in the linker region. The sequence of DkTx referred to as "wild-type" in the manuscript, therefore, is as follows:
GDCAKEGEVCSWGKKCCDLDNFYCPMEFIPHCKKYKPYVPVTTHYRNCAKEGEVCGW
GSKCCHGLDCPLAFIPYCEKYR

2.4.2. Electrophysiology and data analysis

Activity assays on DkTx variants by Two-Electrode Voltage Clamp recordings:

Stage 5 and 6 oocytes from adult female *Xenopus laevis* (the African clawed frog) were surgically removed from anesthetized frogs in accordance with a protocol approved by the Institutional Animal Ethics Committee (IAEC), IISER Pune. Oocytes were digested with collagenase type 2 enzyme (2 mg/mL) in calcium-free OR2 buffer containing NaCl (82.5 mM), KCl (2.5 mM), $MgCl_2$ (1 mM) and HEPES (5 mM) at pH 7.6 for 1 h at 18°C on an automated rocker and then de-folliculated with cut pipettes. Rat TRPV1 gene cloned in pGEM-HE vector was used to make TRPV1 cRNA by in vitro transcription using HiScribe T7 ARCA mRNA Kit (New England Biolabs Inc.) followed by plasmid linearization by *Not I* (New England Biolabs Inc.). De-folliculated oocytes were injected with rTRPV1 cRNA solution (50 nL) in different dilutions (full strength to 1:4 dilution with RNase-free water) and stored at 18ºC in ND96 solution containing NaCl (96 mM), KCl (2 mM), HEPES (5 mM), $MgCl_2$ (1 mM), $CaCl_2$ (1.8 mM) and gentamycin (50 µg/mL) at pH 7.6. TRPV1 channel recordings were performed on oocytes 1-2 d post-mRNA injection under voltage-clamp conditions by using a two-electrode voltage clamp instrument (Warner Instruments) in a 150 µL recording chamber. The recorded

data were filtered and digitized at 0.5 KHz and 2.5 KHz respectively using digidata analog to digital converter and pClamp software (Molecular Devices). Recording microelectrode resistances were between at 0.1-1 MΩ when filled with 3 M KCl solution. The recording buffer contained NaCl (50 mM), KCl (50 mM), $MgCl_2$ (1 mM), $BaCl_2$ (0.3 mM) and HEPES (20 mM) at pH 7.4. Oocytes were held at -60 mV during recording and activated by perfusing capsaicin (5 μM in recording buffer), and following complete capsaicin wash-off, different concentrations of the wild-type/variant toxins were pipetted into the recording chamber to trigger toxin-mediated channel activation. The normalized ratios of the toxin-evoked and capsaicin-evoked peak currents were plotted to generate dose response curves. For each concentration of toxin sampling was done at least 3 times.

Dose-response plots:

The normalized ratio of toxin-induced current to that of the capsaicin current was plotted against the concentration of the toxin and the Hill equation (below) was fit to the data using Origin 9.0:

$$y = A_{max} \{(x_n)/(k_n+x_n)\}$$

where A_{max} is the normalized maximum I(toxin)/I(5 μM Capsaicin) ratio, k is EC_{50} and n is the Hill coefficient.

Data analysis to obtain toxin wash-off kinetic plots depicted in Figures 2.6b (middle panel) and 2.6c (top panel):

Electrophysiological recordings were used to extract the wash-off traces for 3 or 5 min in axon test file (.atf) format using the "Clampfit 10.5" software. The extracted traces were subjected to data point extraction at every 7500th point interval using the R3.4.1 package and the extracted points from 3-5 normalized traces were used to obtain averaged representative traces for wash-off kinetic plots along with their respective standard deviation values (error bars).

2.4.3. Toxin depletion experiments on *Xenopus laevis* oocytes

Our toxin-depletion experiments involved incubation of 100 defolliculated stage 5 or 6 oocytes with 4 nmol of DkTx or its variants in 400 μL (final volume) of 20 mM HEPES buffer at pH 7.4 containing NaCl (50 mM), KCl (50 mM), $MgCl_2$ (1 mM) and $BaCl_2$ (0.3 mM) for 1 h at room temperature. In control experiments, the same concentration and volume of toxin solutions not containing oocytes were used. After incubation, 200 μL of the supernatant from each well was removed, spiked with 2-nitrophenol (2.5 μL of a 2.5 mg/mL solution in MilliQ water) that served as an internal standard, and 100 μL of this solution was subjected to HPLC by employing the

same protocol that was used for the purification of DkTx and its variants (described on pg. 64 above). Fractional depletion was calculated as follows:

$$\text{Fraction depletion} = (R_{control} - R_{oocytes})/R_{control}$$

where $R_{control}$ is the averaged ratio of the area under the peak for the toxin and the area under the peak for 2-nitrophenol in the control experiments, and $R_{oocytes}$ is the ratio of the same parameters obtained from the oocyte samples (n = 3-5). Depletion assays on TRPV1-expressing oocytes (Figure 2.7b) were performed by using an identical protocol on oocytes injected with the TRPV1 cRNA 4 d earlier.

References.

Autzen, H.E., Myasnikov, A.G., Campbell, M.G., Asarnow, D., Julius, D., and Cheng, Y. (2018). Structure of the human TRPM4 ion channel in a lipid nanodisc. Science *359*, 228-232.

Baconguis, I., and Gouaux, E. (2012). Structural plasticity and dynamic selectivity of acid-sensing ion channel-spider toxin complexes. Nature *489*, 400-405.

Bae, C., Anselmi, C., Kalia, J., Jara-Oseguera, A., Schwieters, C.D., Krepkiy, D., Won Lee, C., Kim, E.H., Kim, J.I., Faraldo-Gomez, J.D.*, et al.* (2016). Structural insights into the mechanism of activation of the TRPV1 channel by a membrane-bound tarantula toxin. Elife *5*.

Bae, C., Kalia, J., Song, I., Yu, J., Kim, H.H., Swartz, K.J., and Kim, J.I. (2012). High yield production and refolding of the double-knot toxin, an activator of TRPV1 channels. PLoS One *7*, e51516.

Banerjee, A., Lee, A., Campbell, E., and Mackinnon, R. (2013). Structure of a pore-blocking toxin in complex with a eukaryotic voltage-dependent K(+) channel. Elife *2*, e00594.

Blouin, C.M., Hamon, Y., Gonnord, P., Boularan, C., Kagan, J., de Lesegno, C.V., Ruez, R., Mailfert, S., Bertaux, N., and Loew, D. (2016). Glycosylation-dependent IFN-γR partitioning in lipid and actin nanodomains is critical for JAK activation. Cell *166*, 920-934.

Bohlen, C.J., and Julius, D. (2012). Receptor-targeting mechanisms of pain-causing toxins: How ow? Toxicon *60*, 254-264.

Bohlen, C.J., Priel, A., Zhou, S., King, D., Siemens, J., and Julius, D. (2010). A bivalent tarantula toxin activates the capsaicin receptor, TRPV1, by targeting the outer pore domain. Cell *141*, 834-845.

Bolla, J.R., Sauer, J.B., Wu, D., Mehmood, S., Allison, T.M., and Robinson, C.V. (2018). Direct observation of the influence of cardiolipin and antibiotics on lipid II binding to MurJ. Nat Chem *10*, 363−371.

Cong, X., Liu, Y., Liu, W., Liang, X., and Laganowsky, A. (2017). Allosteric modulation of protein-protein interactions by individual lipid binding events. Nat Commun *8*, 2203.

Contreras, F.X., Ernst, A.M., Haberkant, P., Bjorkholm, P., Lindahl, E., Gonen, B., Tischer, C., Elofsson, A., von Heijne, G., Thiele, C.*, et al.* (2012). Molecular recognition of a single sphingolipid species by a protein's transmembrane domain. Nature *481*, 525-529.

Coskun, Ü., Grzybek, M., Drechsel, D., and Simons, K. (2011). Regulation of human EGF receptor by lipids. Proc Natl Acad Sci *108*, 9044-9048.

Crowley, P.B., and Golovin, A. (2005). Cation-pi interactions in protein-protein interfaces. Proteins *59*, 231-239.

Dawson, R.J., Benz, J., Stohler, P., Tetaz, T., Joseph, C., Huber, S., Schmid, G., Hugin, D., Pflimlin, P., Trube, G.*, et al.* (2012). Structure of the acid-sensing ion channel 1 in complex with the gating modifier Psalmotoxin 1. Nat Commun *3*, 936.

Eisenberg, D., Schwarz, E., Komaromy, M., and Wall, R. (1984). Analysis of membrane and surface protein sequences with the hydrophobic moment plot. J Mol Biol *179*, 125-142.

Gao, Y., Cao, E., Julius, D., and Cheng, Y. (2016). TRPV1 structures in nanodiscs reveal mechanisms of ligand and lipid action. Nature *534*, 347-351.

Goldstein, S.A., Pheasant, D.J., and Miller, C. (1994). The charybdotoxin receptor of a Shaker K+ channel: peptide and channel residues mediating molecular recognition. Neuron *12*, 1377-1388.

Gupta, K., Zamanian, M., Bae, C., Milescu, M., Krepkiy, D., Tilley, D.C., Sack, J.T., Yarov-Yarovoy, V., Kim, J.I., and Swartz, K.J. (2015). Tarantula toxins use common surfaces for interacting with Kv and ASIC ion channels. Elife *4*, e06774.

Hunte, C., and Richers, S. (2008). Lipids and membrane protein structures. Curr Opin Struct Biol *18*, 406-411.

Kalia, J., Milescu, M., Salvatierra, J., Wagner, J., Klint, J.K., King, G.F., Olivera, B.M., and Bosmans, F. (2015). From foe to friend: using animal toxins to investigate ion channel function. J Mol Biol *427*, 158-175.

Krieger, F., Moglich, A., and Kiefhaber, T. (2005). Effect of proline and glycine residues on dynamics and barriers of loop formation in polypeptide chains. J Am Chem Soc *127*, 3346-3352.

Laganowsky, A., Reading, E., Allison, T.M., Ulmschneider, M.B., Degiacomi, M.T., Baldwin, A.J., and Robinson, C.V. (2014). Membrane proteins bind lipids selectively to modulate their structure and function. Nature *510*, 172-175.

Lee, A.G. (2011). Lipid-protein interactions. Biochem Soc Trans *39*, 761-766.

Lee, S.Y., and MacKinnon, R. (2004). A membrane-access mechanism of ion channel inhibition by voltage sensor toxins from spider venom. Nature *430*, 232-235.

Li, L., Lee, Y.-H., Pappone, P., Palma, A., and McNamee, M.G. (1992). Site-specific mutations of nicotinic acetylcholine receptor at the lipid-protein interface dramatically alter ion channel gating. Biophysical journal *62*, 61-63.

Long, S.B., Tao, X., Campbell, E.B., and MacKinnon, R. (2007). Atomic structure of a voltage-dependent K+ channel in a lipid membrane-like environment. Nature *450*, 376-382.

McGaughey, G.B., Gagne, M., and Rappe, A.K. (1998). pi-Stacking interactions. Alive and well in proteins. J Biol Chem *273*, 15458-15463.

Milescu, M., Vobecky, J., Roh, S.H., Kim, S.H., Jung, H.J., Kim, J.I., and Swartz, K.J. (2007). Tarantula toxins interact with voltage sensors within lipid membranes. J Gen Physiol *130*, 497-511.

Muller, C., and Shinitzky, M. (1979). Modulation of Transferrin Receptors in Bone Marrow Cells by Changes in Lipid Fluidity. Br J Haematol *42*, 355-362.

Nury, H., Van Renterghem, C., Weng, Y., Tran, A., Baaden, M., Dufresne, V., Changeux, J.P., Sonner, J.M., Delarue, M., and Corringer, P.J. (2011). X-ray structures of general anaesthetics bound to a pentameric ligand-gated ion channel. Nature *469*, 428-431.

Payandeh, J., Scheuer, T., Zheng, N., and Catterall, W.A. (2011). The crystal structure of a voltage-gated sodium channel. Nature *475*, 353-358.

Phillips, R., Ursell, T., Wiggins, P., and Sens, P. (2009). Emerging roles for lipids in shaping membrane-protein function. Nature *459*, 379-385.

Polley, A., Orłowski, A., Danne, R., Gurtovenko, A.A., Bernardino de la Serna, J., Eggeling, C., Davis, S.J., Róg, T., and Vattulainen, I. (2017). Glycosylation and lipids working in concert direct CD2 ectodomain orientation and presentation. The Journal of Physical Chemistry Letters *8*, 1060-1066.

Rissanen, S., Grzybek, M., Orłowski, A., Róg, T., Cramariuc, O., Levental, I., Eggeling, C., Sezgin, E., and Vattulainen, I. (2017). Phase Partitioning of GM1 and Its Bodipy-Labeled Analog Determine Their Different Binding to Cholera Toxin. Frontiers in physiology *8*, 252.

Sheinerman, F.B., Norel, R., and Honig, B. (2000). Electrostatic aspects of protein-protein interactions. Curr Opin Struct Biol *10*, 153-159.

Shinitzky, M., and Inbar, M. (1976). Microviscosity parameters and protein mobility in biological membranes. Biochim Biophys Acta *433*, 133-149.

Stites, W.E. (1997). Protein-Protein Interactions: Interface Structure, Binding Thermodynamics, and Mutational Analysis. Chem Rev *97*, 1233-1250.

Swartz, K.J. (2007). Tarantula toxins interacting with voltage sensors in potassium channels. Toxicon *49*, 213-230.

Swartz, K.J., and MacKinnon, R. (1995). An inhibitor of the Kv2.1 potassium channel isolated from the venom of a Chilean tarantula. Neuron *15*, 941-949.

Swartz, K.J., and MacKinnon, R. (1997a). Hanatoxin modifies the gating of a voltage-dependent K+ channel through multiple binding sites. Neuron *18*, 665-673.

Swartz, K.J., and MacKinnon, R. (1997b). Mapping the receptor site for hanatoxin, a gating modifier of voltage-dependent K+ channels. Neuron *18*, 675-682.

Yan, B.X., and Sun, Y.Q. (1997). Glycine residues provide flexibility for enzyme active sites. J Biol Chem *272*, 3190-3194.

Zhou, M., Morgner, N., Barrera, N.P., Politis, A., Isaacson, S.C., Matak-Vinkovic, D., Murata, T., Bernal, R.A., Stock, D., and Robinson, C.V. (2011). Mass spectrometry of intact V-type ATPases reveals bound lipids and the effects of nucleotide binding. Science *334*, 380-385.

Chapter 3:

Investigating the role of the linker region of DkTx in TRPV1 activation

3.1. Introduction.

Several multi-domain proteins contain linker regions that connect these domains (Figure 3.1) (Anthis and Clore, 2013; Bu et al., 2005; Cowan-Jacob et al., 2005). Linkers play important functional roles by facilitating inter-domain interactions and/or orienting the domains appropriately to achieve the desired functional output (Ma et al., 2011; Papaleo et al., 2016). For example, the calcium binding protein calmodulin relies on conformational changes in its linker region for transitioning from a compact to an extended conformation in order to bind Ca^{2+} ions (Figure 3.1a) (Anthis and Clore, 2013). Additionally, enzymes such as Src protein kinases rely on the hinged movement of their catalytic domains about a flexible linker that connects them to the SH2 domain of the enzyme (Figure 3.1b) which in turn allows allosteric functioning (Cowan-Jacob et al., 2005; Young et al., 2001). A linker region is also present in the diphtheria toxin that allows the dimeric toxin to achieve a domain-swapped conformation (Bennett et al., 1994). Linker properties such as its length and rigidity are evolutionarily finely tuned to enable the linker in functioning optimally and alterations in these parameters lead to disruption of protein function. For example, experiments on glycosyl hydrolase 5 cellulases demonstrate that alterations in the length of the linker between its glycosyl hydrolase 5 and carbohydrate-binding module 3 domains result in mitigation of enzyme activity (Ruiz et al., 2016).

The linker regions naturally present in various proteins such as those discussed above have motivated efforts towards the creation of proteins containing multiple domains attached to each other by artificially designed linker sequences. For example, two molecules of the human carbonic anhydrase enzyme were linked to each other by employing polyethyleneglycol linkers to achieve enhanced catalytic efficiency (Krishnamurthy et al., 2007; Mack et al., 2012). Polyethyleneglycol linkers were also used to connect two molecules of the $Na_v1.7$ channel-targeting toxin, GpTx-1, resulting in the generation of a dimeric toxin derivative that demonstrated potent and sustained channel inhibition (Murray et al., 2015). Examples of artificially introduced linkers composed of amino acids outnumber those containing non-natural moieties such as polyethyleneglycols due to the technical ease of their introduction via standard molecular cloning approaches. Indeed, flexible peptide linkers have been employed on a variety of ion channels for generating “concatemeric” constructs that enable the creation of channel variants with altered residue(s) present in a desired number of channel subunits, thereby

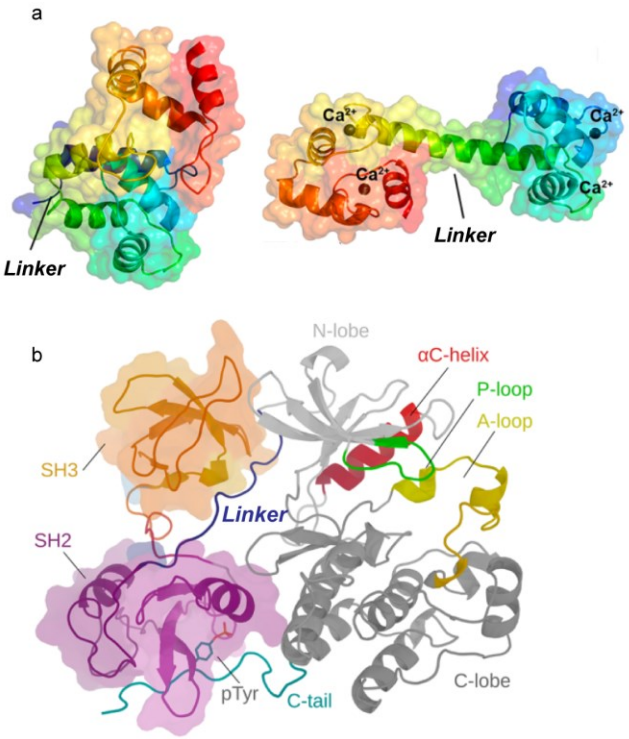

c

Enzyme/ Protein complex	Linker function	References
Calmodulin	Conformation change to allow binding of Ca^{2+} ions	Anthis and Clore, 2013
Src protein kinase	Hinged movement of polyproline type II linker of SH2 domain about catalytic domains	Cowan-Jacob et al., 2005; Young et al., 2001
GH5 cellulase	Optimal linker length is crucial for catalytic activity	Ruiz et al., 2016
Taq polymerase	Controlling movement between polymerase domain and exonuclease domain	Bu et al., 2005
Diphtheria toxin	Linker distends in open state allowing dimerization	Bennett et al., 1994

Figure 3.1. Linker regions in proteins. a) Crystal structure of calmodulin (PDB: 1qx5, 1exr) depicted in unbound (left panel) and Ca^{2+}-bound (right panel) states. The linker region attains rigid helical conformation in the extended Ca^{2+}-bound state of calmodulin. Figure adapted from Papaleo et al., 2016. b) Structure of the Src protein kinase (PDB: 2src) depicting functionally crucial linker region in dark blue. Figure adapted from Papaleo et al., 2016. c) Function of the linkers of multi-domain proteins.

facilitating mechanistic and biophysical studies. This approach has been extended to the TRPV1 ion channel as well (Hazan et al., 2015). In addition to facilitating basic science-centric studies, artificially designed peptide linkers have contributed to the development of novel therapeutic strategies and biotechnology-based applications. Peptide linkers connecting tumor marker-targeting antibodies to anticancer agents that undergo protease-mediated/chemical cleavage within cancer cells have been successfully used to fabricate antibody-drug conjugates for cancer therapy (Bargh et al., 2019). An important contribution of peptide linkers in biotechnology is for the creation of single-chain antibodies (scFvs) that are miniature antibodies composed of the variable heavy and light chains joined via flexible linkers comprising of glycine-serine repeats

(Ahmad et al., 2012; Yan and Sun, 1997).

DkTx naturally contains a seven amino acids-long linker region that connects its two cystine knots (Figure 3.2). The structure of the TRPV1-DkTx complex solved in lipid nanodiscs (PDB: 5irx) (Gao et al., 2016) depicts the linker at a poor resolution precluding discernment of the exact location of its side-chain residues. Nevertheless, the distance of the residues of the linker region of DkTx from the TRPV1 channel residues and the membrane appears to be greater than 11Å (refer Figure 3.2a left panel) rendering the possibility of specific interactions between the linker region residues and those of the channel and/or membrane lipids low.

The two knots of DkTx can individually activate the TRPV1 ion channel albeit with much poorer potency and faster wash-off kinetics as compared to DkTx (Bae et al., 2012; Bohlen et al., 2010). Indeed, the more potent of the two single knots (K2) demonstrates a ~30-fold

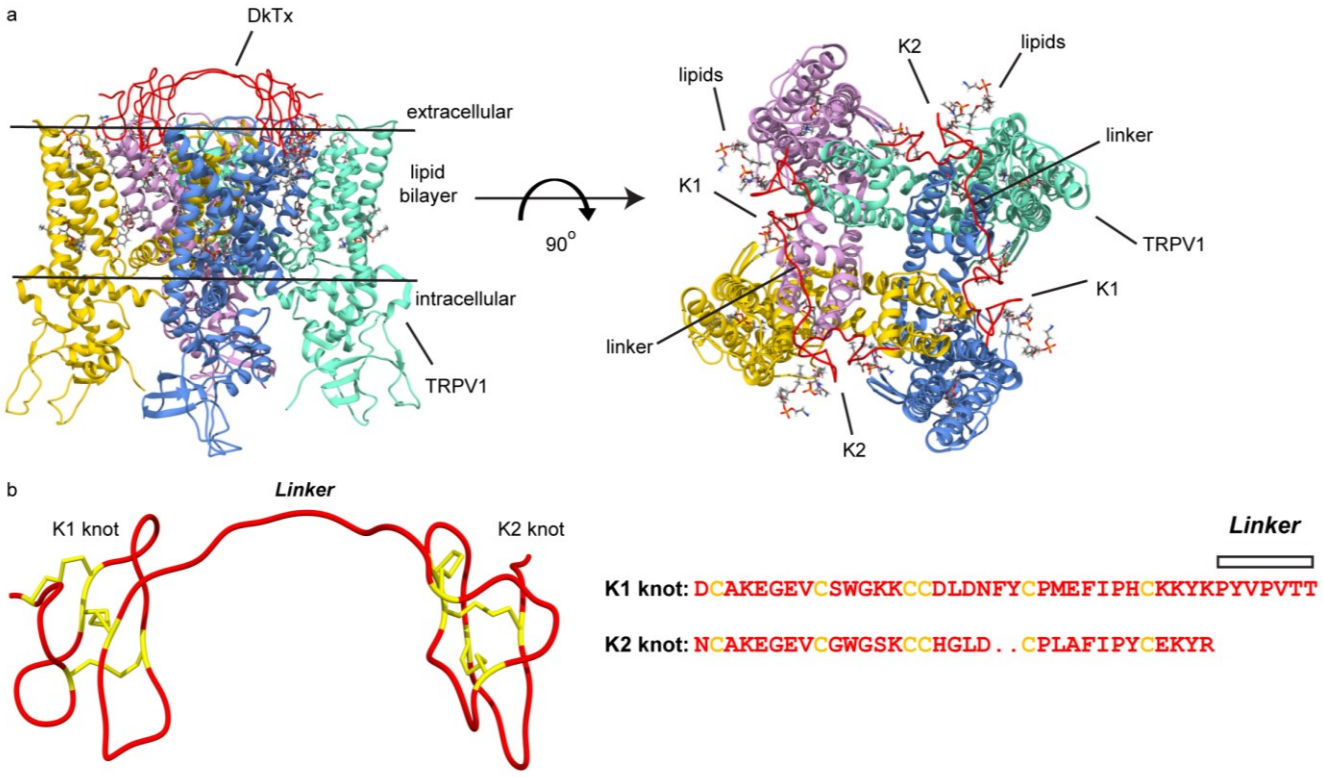

Figure 3.2. The linker region of DkTx. a) Side view (left panel) and top view (right panel) of the DkTx-bound TRPV1 ion channel structure (PDB: 5irx) (Gao et al., 2016). b) Structure and sequence of DkTx (PDB: 5irx) depicting its linker region connecting the K1 and K2 knots (left panel).

higher EC_{50} value (1.57 μM) for TRPV1 activation as compared to DkTx (0.05 μM). Furthermore, the double knot washes off much more slowly as compared to the single knots (Bae et al., 2012)—an observation that has been attributed to the absence of bivalency when the single knots act as TRPV1 agonists (Bae et al., 2012; Bohlen et al., 2010). Interestingly, tryptophan fluorescence-based membrane partitioning experiments identical to the ones described in Chapter 2 demonstrate that the K1 and the K2 single knots partition poorly into membranes (K_x of the K1 single knot is 3.9×10^5 whereas that of the K2 single knot is 2.0×10^4) as compared to wild-type DkTx ($K_x = 8.2\times10^6$) (Bae et al., 2016). When these partitioning data are viewed in the context of one of the main findings of my work described in Chapter 2 of this thesis that poorly partitioning toxin variants demonstrate faster wash-off kinetics (Sarkar et al., 2018), it sets up the following intriguing question: is it the bivalency or the membrane partitioning propensity of DkTx that is responsible for its slow wash-off kinetics? In other words, do single K1 and K2 knots wash-off much faster than DkTx because they partition poorly into the membrane as compared to DkTx or because they are inherently monovalent unlike the bivalent DkTx? With the long-term goal of teasing apart the contributions of bivalency and partitioning in DkTx-activation of TRPV1, we decided to study the linker region of the toxin in more detail as it is this domain that confers bivalency to the toxin. We reasoned that engineering linker regions possessing different lengths and/or rigidity may allow us to create toxin constructs that lack bivalency while retaining wild-type DkTx-like membrane partitioning properties, enabling us to tease apart the roles of bivalency and partitioning in DkTx-activation of TRPV1.

3.2. Results.

Altering linker rigidity significantly affects DkTx potency and minimally perturbs toxin wash-off kinetics. The linker region of DkTx contains two proline residues (P36 and P39) in a seven amino acids-long stretch (Figure 3.2b). Proline residues are commonly found in the linker regions of multi-domain proteins (George and Heringa, 2003; Papaleo et al., 2016; Wriggers et al., 2005) and are known to confer rigidity into protein secondary structures (Bhandari et al., 1986; Chen et al., 2013). Consequently, we began our studies into the role of linker rigidity in the toxin's function by generating the P36A and the P39A DkTx variants and characterizing their TRPV1-activation properties (HPLC profiles of all purified toxin variants depicted in Figure 3.3

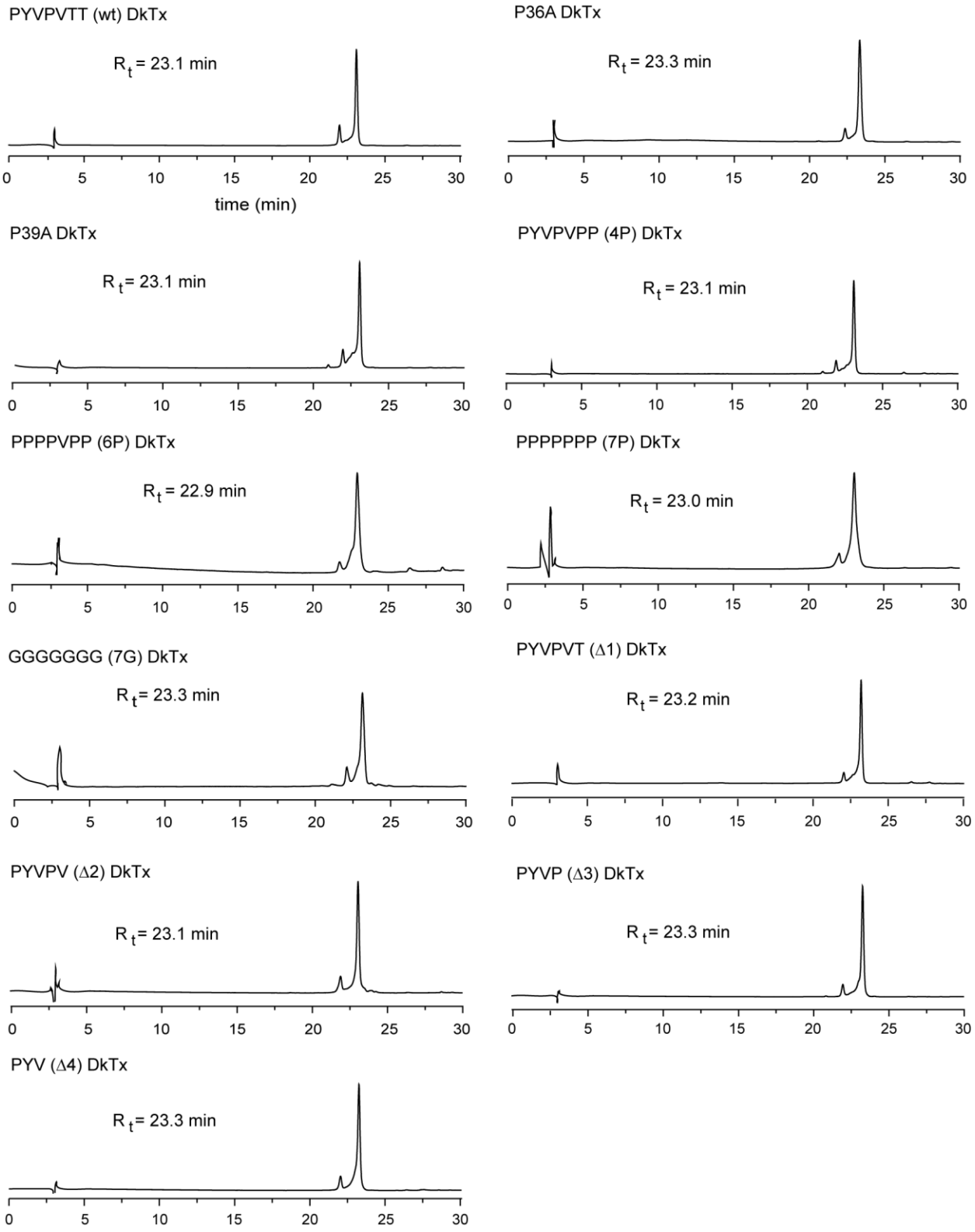

Figure 3.3. HPLC traces for the purity evaluation of all DkTx linker variants. The absorbance has been measured at 280 nm.

and their representative electrophysiological traces are shown in Figure 3.4). These experiments revealed that both these variants demonstrate only mildly-altered potency as compared to wild-type DkTx (upto 1.8-fold decrease) and no significant effects on the wash-off kinetics (Figure

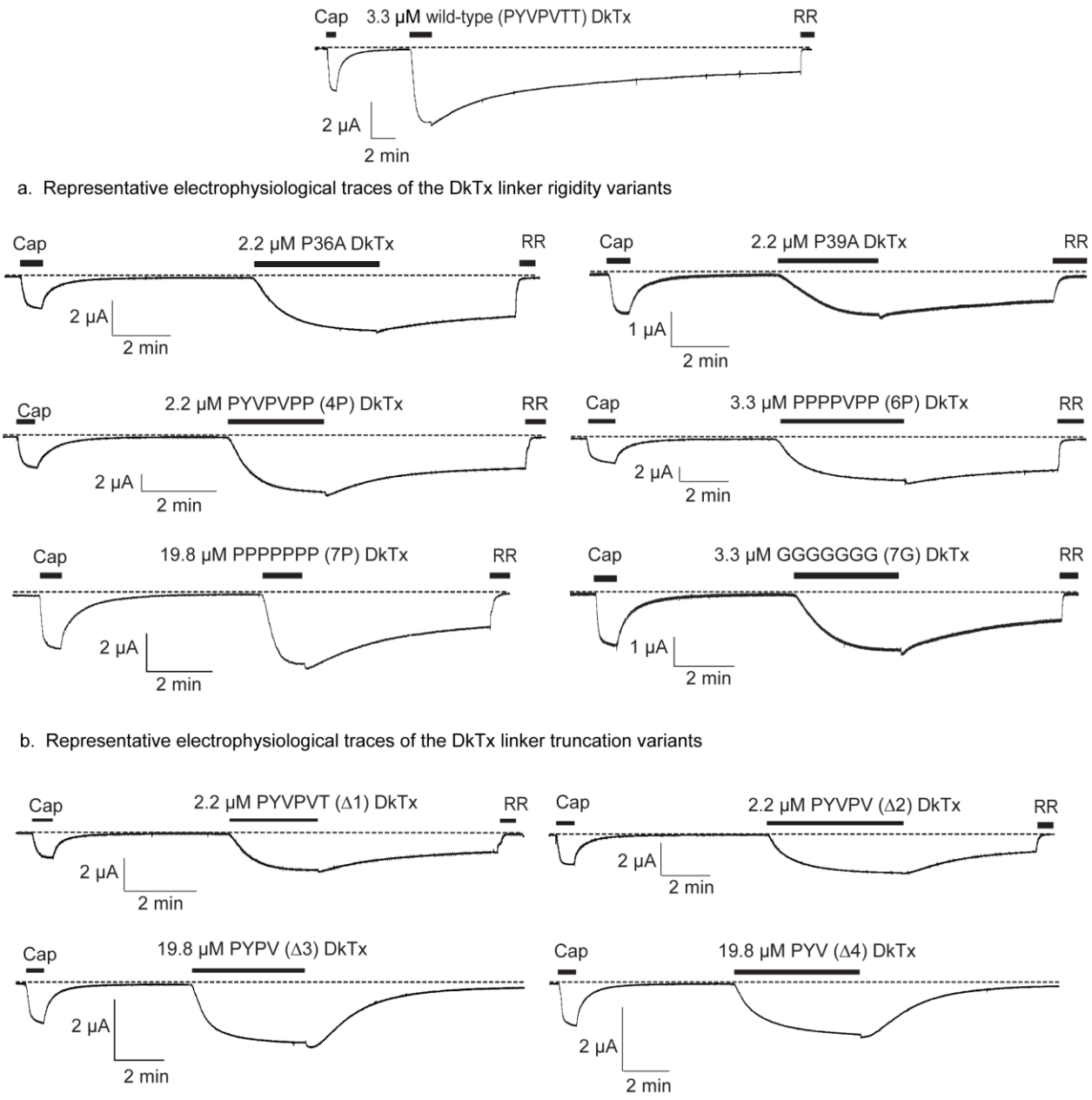

Figure 3.4. Representative electrophysiological recordings of wild-type DkTx and DkTx linker variants.

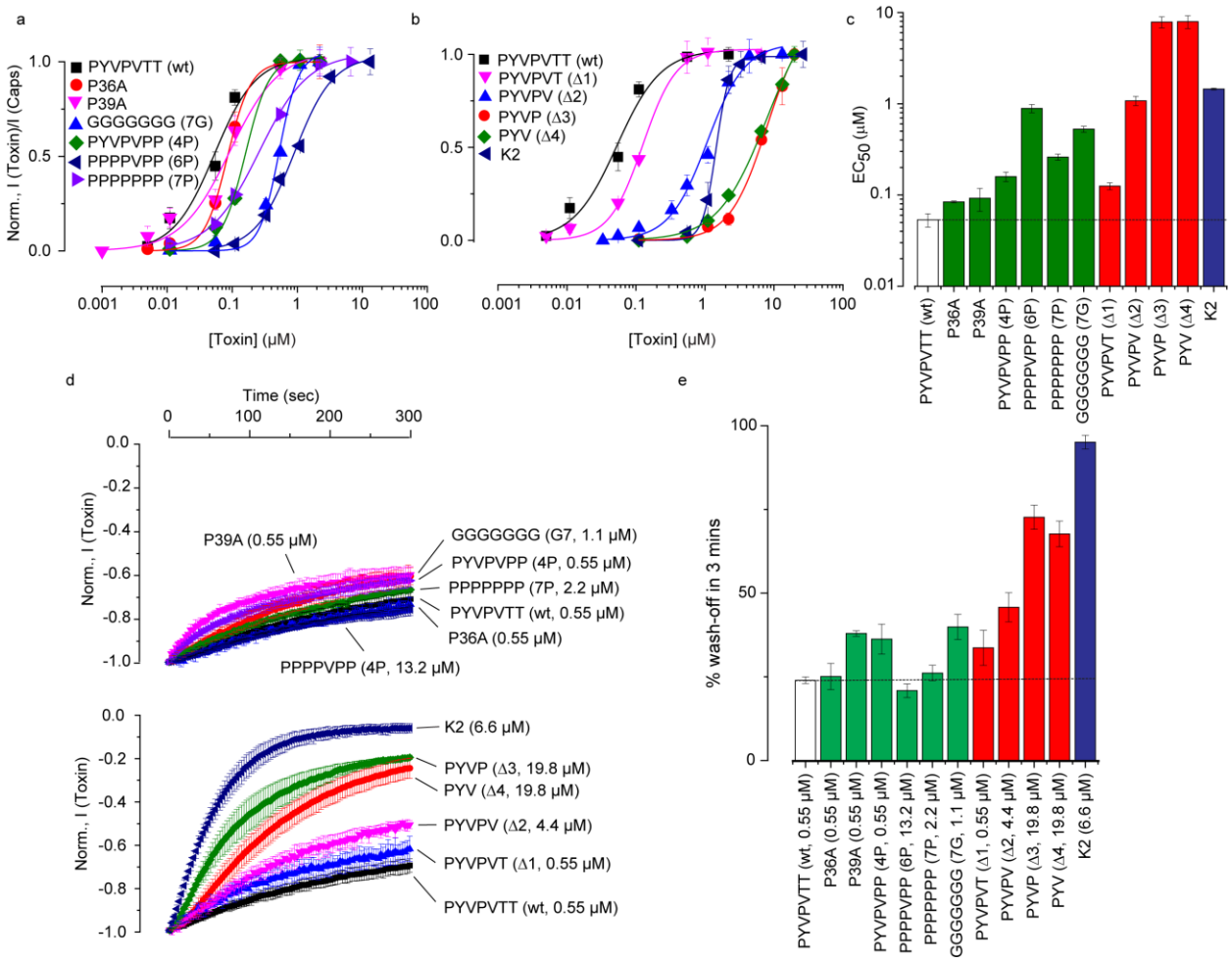

Figure 3.5. Effects on potency and wash-off properties of DkTx upon alterations in linker rigidity and length. a) Dose-response plots of the DkTx linker rigidity variants. b) Dose-response plots of the DkTx linker length variants and that of the K2 single knot. c) EC_{50} values for DkTx linker variants and K2. The bars in green correspond to linker rigidity variants and those in red represent the linker length variants. d) Averaged wash-off current traces for wild-type DkTx and DkTx linker rigidity variants (top panel), and linker length variants with those for wild-type DkTx and K2 (bottom panel). e) Bar graph depicting the % reduction in currents after 3 min of buffer perfusion post toxin-mediated channel activation for all variants (bars corresponding to the linker rigidity variants are depicted in green and those of the linker length variants in red). Experiments depicted in both d and e were performed at saturation concentrations of the respective toxins denoted within parentheses. Each current trace/data point is an average of 3-5 recordings and the error bars correspond to standard deviation values.

3.5a, c-e and Table 3.1). To more profoundly alter the rigidity of the linker, I next studied DkTx variants with more drastic changes in the linker sequence. In one of these variants, all the seven amino acids of the linker were substituted to glycine residues to generate a potentially highly flexible linker (the cDNA for this variant was a generous gift from Dr. Kenton J. Swartz' laboratory at NIH, USA). Additionally, I generated versions of the linker potentially possessing enhanced rigidity by increasing their proline content yielding toxin variants having linkers containing 4, 6 and 7 proline residues. As compared to the wild-type toxin, I observed a ~3-fold decrease in potency for the 4P DkTx variant (PYVPVPP linker) and a ~5-fold decrease for the 7P DkTx variant (PPPPPPP linker) which indicates at best moderate changes in potency (Figure 3.5a, c and Table 3.1). No considerable changes in wash-off kinetics were observed for these toxin variants (Figure 3.5e and top panel of Figure 3.5d). Interestingly, the DkTx variant having potentially the most flexible linker (7G) and the one containing potentially one of the most rigid linkers tested (PPPPVPP or the 6P variant) demonstrated the highest impact on the potency of the toxin. Indeed, whereas the 7G linker DkTx construct showed a ~10-fold decrease in potency, the 6P linker variant demonstrated ~18-fold decrease in potency. Both these constructs demonstrated only minimal changes in wash-off kinetics as compared to the wild-type toxin (Figure 3.5a, c-e and Table 3.1; see Figure 3.4a for representative current traces). These results demonstrate that the rigidity of the linker of DkTx plays a more important role in the toxin's potency than in its wash-off kinetics.

Truncating the linker diminishes potency of DkTx drastically and accelerates wash-off kinetics. Recently, a DkTx variant containing an elongated 14 amino acids-long linker was reported to demonstrate merely a 5-fold decrease in potency as compared to the wild-type toxin and the toxin wash-off kinetics remained unaltered (Geron et al., 2018). In light of the lack of significant functional differences between this elongated linker construct as compared to the wild-type toxin, I decided to focus my efforts on generating linker truncations. I designed linker truncation constructs wherein one through four amino acids of the linker were deleted (all HPLC traces for the purity evaluation of these truncated linker variants of DkTx are depicted in Figure 3.3). Electrophysiological characterization of these toxin variants revealed that whereas there was a gradual decline in the potency of the toxin variants with each amino acid deletion from one through three residues (the PYVPVT (Δ1), PYVPV (Δ2) and PYVP (Δ3) linker DkTx variants), the Δ3 and Δ4 (PYV) linker variants demonstrated a potency drop that was more drastic. Indeed,

a ~160-fold drop in potency was observed for both the Δ3 and the Δ4 DkTx variants as compared to the wild-type DkTx (Figure 3.5b, c and Table 3.1). This levelling-off effect suggests that reducing the linker length to 4 amino acids or lower (as in the Δ3 and the Δ4 variants) results in abrogation of bivalent binding of the toxin to the channel. Channel activation by these variants, therefore, entails the binding of either of the two knots (K1 or K2), rendering these variants monovalent despite possessing both the knots. Since the potency of the K1 knot is lower than that of the K2 knot, toxin binding events wherein the K1 knot binds to the channel shall elicit lower activation whereas the K2 knot-binding events shall results in higher channel activation. Consequently, the overall averaged potency of these monovalent double-knot toxins would be expected to be lower than that of K2 which is exactly what our results indicate (Figure 3.5b).

These potency studies were complemented by rigorous wash-off kinetics studies for each toxin variant. As in Chapter 2 (Figure 2.6), to ensure the same channel occupancy in each case, wash-off comparisons were performed at the saturating concentrations of each variant (Figure 3.5d, e). While the Δ1 and the Δ2 DkTx linkers variants demonstrated marginally faster wash-off rates as compared to the wild-type toxin, the Δ3 and Δ4 linker variants washed-off considerably faster (Figure 3.5d, e). Indeed, whereas the wild-type, the Δ1, and the Δ2 variants demonstrated 24%, 36% and 46% TRPV1-current reduction respectively after 3 min of buffer perfusion (Table 3.1), the Δ3 and the Δ4 linker variants demonstrated a 72% and 67% reduction of currents respectively over the same wash-off time period (Figure 3.5e and Table 3.1). This escalation in wash-off kinetics observed for the Δ3 and the Δ4 linker variants leading to complete toxin wash-off over 10 min of buffer perfusion (see representative traces in Figure 3.4) is reminiscent of the wash-off rates observed for the single K2 knot (Bae et al., 2012). To compare these wash off rates at 100% channel occupancy for these toxins, I generated wash-off traces for the K2 single knot at its saturation concentration and plotted the averaged traces alongside those of the linker truncated DkTx variants (bottom panel of Figure 3.5d). This comparison shows that the Δ3 and the Δ4 DkTx linker variants do not wash off as rapidly as the single K2 knot. If the enhanced wash-off kinetics of these truncated linker toxin variants was entirely due to the loss of bivalency, their wash-off kinetics should overlap with that of the single K2 knot as all these three toxins—the Δ3, Δ4 and the K2 single knot—are monovalent. Considering that membrane partitioning of DkTx and its variants is a major factor that contributes to toxin wash-off rates (Chapter 2), these data strongly suggest that these truncated toxins wash off slower than K2

despite lacking bivalency because they partition more favorably into the membrane than K2 which would be expected as the single knots are known to partition much poorer than the wild-type DkTx (Bae et al., 2016). To test this hypothesis, we next proceeded to perform membrane partitioning studies on these variants.

Linker truncation DkTx variants partition considerably better into membranes than the single knots but not as well as wild-type DkTx. I performed tryptophan fluorescence-based studies to characterize the partitioning of my DkTx linker variants into POPC/POPG vesicles similar to those reported in Chapter 2 (experimental details provided in section 3.4.1) As expected, these results demonstrated that the Δ3 and Δ4 variants partition much better into membranes (K_x values 3.3×10^6 and 1.9×10^6 respectively, Table 3.1) as compared to the K2 single knot that yields a K_x value of 2.0×10^4 (Bae et al., 2016) , supporting the hypothesis

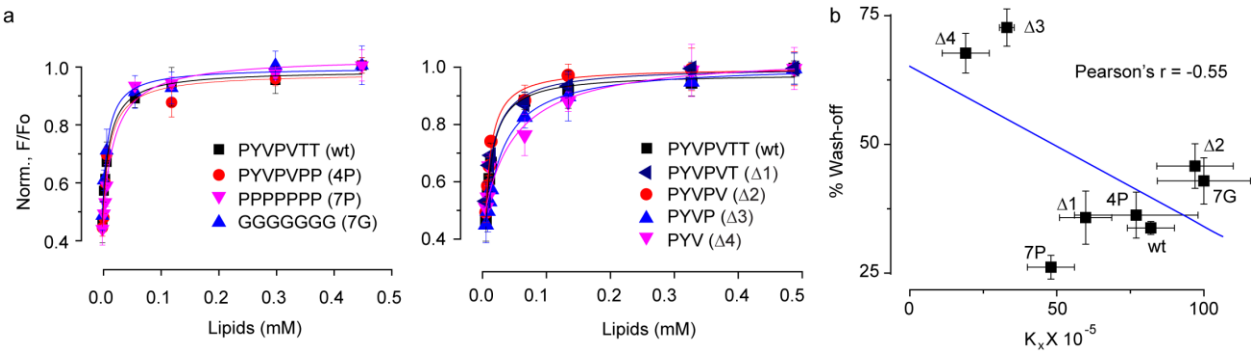

Figure 3.6. Toxin-membrane interaction studies on DkTx and its linker variants by employing tryptophan fluorescence. a) Plots of normalized relative fluorescence intensity (F/F_0) at 320 nm wild-type toxin and linker rigidity variants (left panel) and linker length variants (right panel) as a function of available lipid concentration. b) Plots of % wash-off of wild-type DkTx and linker variants (solid squares) after 3 min of buffer perfusion post TRPV1 activation at saturation concentration of the toxins (obtained from electrophysiological experiments) vs. mol. fraction partitioning coefficients (K_x) values (obtained from tryptophan fluorescence experiments). The blue line shown was obtained by fitting a linear equation to the data for the DkTx linker variants tested. Each data point is an average of 3-5 recordings/assays and the error bars correspond to standard deviation values.

that despite lacking bivalency, these truncated toxins wash-off slower than the K2 single knot (Figure 3.5d) because they partition better. Furthermore, these data demonstrate that variants that wash-off at rates similar to those of the wild-type toxin possess similar partitioning properties as wild-type DkTx (left panel of Figure 3.6a and Table 3.1). Indeed, the K_x values of the slow washing-off linker rigidity variants lie within the range of 4.8×10^6 (for the 7P variant) and 1.0×10^7 (for the 7G variant), whereas the wild-type DkTx yields a similar K_x value of 8.2×10^6. Among the linker truncation variants, the Δ1 and the Δ2 variants yielded K_x values (6.0×10^6 and 9.7×10^6, respectively) that were very similar to that of wild-type DkTx. In contrast, the membrane partitioning of the Δ3 and Δ4 variants were found to be diminished ~2.5- and ~4.3-fold respectively as compared to the wild-type toxin (Figure 3.6a right panel, Table 3.1). These results indicate that the linker length not only contributes to conferring bivalency to DkTx but also plays an as yet unappreciated role in optimizing the toxin's membrane partitioning. Plotting the % wash-off against the K_x values of the linker variants (Figure 3.6b) yielded a negative correlation (Pearson's r = -0.55) emphasizing that as observed for the site-directed variants of DkTx reported in Chapter 2, the linker variants that poorly partitioning into membranes wash-off faster than those that partition well. Considering this important role of membrane partitioning in toxin wash-off kinetics, the faster washing-off rates of the Δ3 and Δ4 DkTx variants as compared to the wild-type toxin cannot be entirely attributed to their lack of bivalency as their diminished membrane partitioning properties shall also contribute to the hastening of their wash-off rates.

To examine membrane partitioning under physiological settings, I performed toxin depletion experiments on *Xenopus laevis* oocytes by employing protocols identical to those reported in Chapter 2 (Materials and Methods, section 2.4.3). The results of these experiments yielded trends that were similar to those with the tryptophan fluorescence experiments described above. The linker rigidity variants yielded fractional toxin depletion values ranging from 0.30-0.38, which are similar to that for wild-type DkTx (0.42). The Δ3 and Δ4 variants demonstrated a ~2- and ~2.5-fold decrease respectively in depletion compared to the wild-type DkTx (Figure 3.7a and Table 3.1), thereby recapitulating the trends obtained from the partitioning data discussed above. Plotting % wash-off against fractional depletion values of the DkTx linker variants (Figure 3.7b) yielded a good negative correlation (Pearson's r = -0.83).

Taken together, the data from both Chapter 2 and this chapter provide compelling evidence that strongly supports the hypothesis that the high membrane partitioning ability of DkTx plays an important role in its activity especially with respect to its ability to activate the channel in a sustained fashion resulting in its very slow wash-off upon buffer perfusion. To summarize this feature of the toxin's function, I plotted the % wash-off after 3 min of buffer perfusion data for each of the toxin variants I characterized (those described in Chapter 2 as well as those discussed in this chapter) against their respective K_x values (Figure 3.8a). I also plotted the % wash-off against the toxins' fractional depletion values obtained from oocyte incubation assays (Figure 3.8b). Expectedly, the negative correlation between % wash-off and membrane-

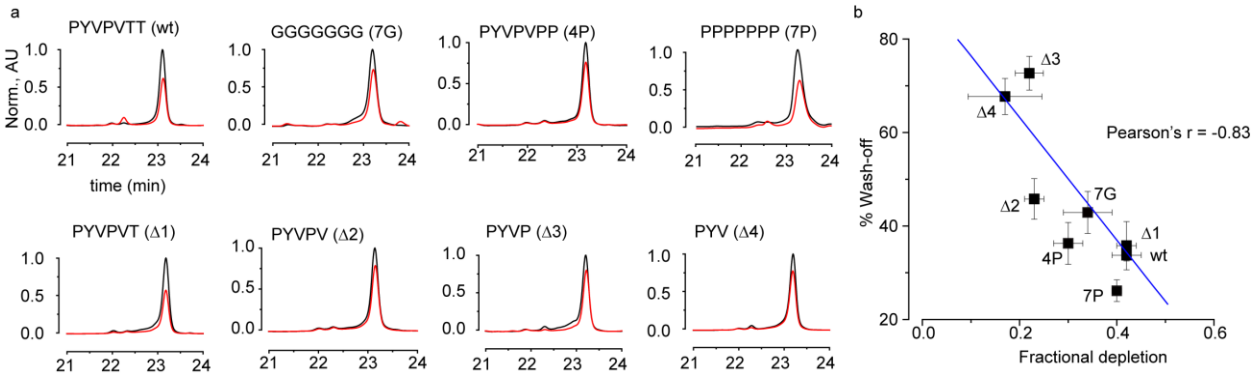

Figure 3.7. Toxin-membrane interaction studies on DkTx and its linker variants by employing oocyte depletion. a) HPLC traces depicting toxin depletion upon incubation of DkTx and its linker variants with *Xenopus laevis* oocytes. Traces in black correspond to the controls wherein the toxins solubilized in buffer devoid of oocytes were subjected to HPLC analysis, whereas those in red were obtained when the supernatant of toxin solutions incubated with 100 oocytes were subjected to HPLC. b) Plot of % wash-off of wild-type DkTx and linker variants (solid squares) after 3 min of buffer perfusion post TRPV1 activation by saturation concentrations of the toxins (obtained from the electrophysiology experiments) versus fractional depletion (obtained from HPLC peak areas as described in Materials and Methods section 2.4.3 in Chapter 2). The blue line shown was generated by fitting a linear equation to the data for the linker variants tested. Each data point is an average of 3-5 recordings/assays and the error bars correspond to standard deviation values.

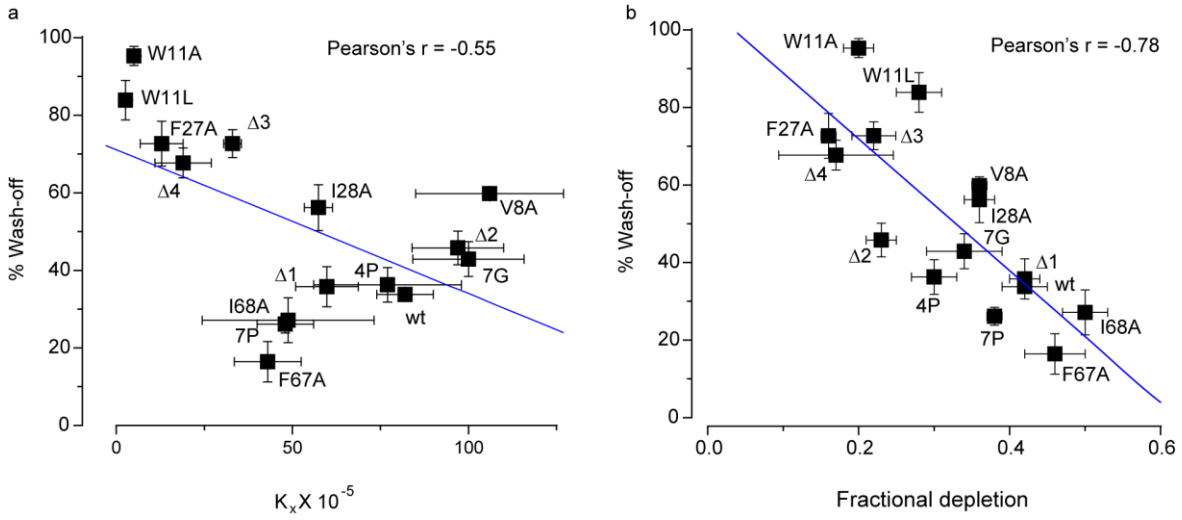

Figure 3.8. Correlation plot of % wash-off vs. membrane partitioning of all DkTx variants generated by side-directed mutagenesis and linker modification. (a) % Wash-off vs. mol. fraction partition coefficient (K_x) and (b) % Wash-off vs. fractional depletion plots.

interaction propensity remains consistent across all DkTx variants whether generated by site-directed mutagenesis or via linker modification. Notably, the plot obtained from data obtained under a more physiological setting (oocyte depletion assays, Figure 3.8b) yields a better correlation than that obtained from experiments in artificial vesicles (Figure 3.8a), highlighting the physiological relevance of our study.

3.3. Discussion.

The work described in this chapter was primarily aimed at using the linker region of DkTx to address some fundamental aspects of the mechanism of DkTx-activation of TRPV1. In particular, I was interested in answering the following questions: Does the linker play any role in the toxin's TRPV1-activation properties? Does it contribute to the partitioning of the toxin into the membrane? Can I disrupt the bivalency of DkTx by engineering toxin variants containing linkers possessing altered rigidity and lengths while retaining the toxin's high propensity for membrane partitioning? Can such linker variants enable us to tease apart the contributions of bivalency and membrane partitioning of DkTx in TRPV1-activation?

To address these questions, I generated a range of linker variants of DkTx possessing altered rigidity and lengths. In addition to the detailed electrophysiological characterization of these variants, I examined their propensity for membrane partitioning by employing tryptophan fluorescence experiments with LUVs and toxin depletion assays on *Xenopus laevis* oocytes. These studies demonstrate that the linker region of DkTx does not merely ensure that the two channel-binding knots of the toxin are held sufficiently apart to enable bivalent binding but also play an important role in ensuring optimal membrane partitioning of the toxin. Indeed, the Δ3 and Δ4 linker variants of DkTx partition ~2.5-4.3-fold poorly as compared to the wild-type toxin and also demonstrate ~2-2.5-fold lower depletion in oocyte assays. These truncated toxin variants also wash-off much faster than the wild-type toxin consistent with the conclusion from our alanine-scanning mutagenesis studies on DkTx (Chapter 2) that high membrane partitioning endows the toxin with its slow wash-off kinetics.

In light of the above assertion, an interesting question emerges: Can the fast washing-off property of the Δ3 and Δ4 linker truncations be attributed to loss of bivalency or to their reduced partitioning? To address this question, I compared the wash-off kinetics of the single K2 knot of the toxin that is not bivalent and also partitions ~100-fold poorer than the wild-type toxin. If the fast washing-off property of the truncation variants is entirely due to loss of bivalency, these variants should wash-off as quickly as the K2 single knot. I find that K2 washes off faster than either of these two truncation variants of DkTx demonstrating that bivalency alone cannot explain the slow wash-off feature of the wild-type toxin (Figure 3.5d, e) and that membrane partitioning also plays an important role. This notion is reaffirmed by our membrane partitioning experiments (Figure 3.6) that demonstrate that indeed, the Δ3 and Δ4 linker truncation DkTx variants partition much better than the K2 single knot (Table 3.1).

In our studies described in Chapter 2 of this thesis, I generated several variants at sites of the toxin that were seen to bind membrane lipids in the structure (Fig. 2.11). Therefore, it was not surprising that several of these variants demonstrated reduced membrane partitioning presumably due to their disrupted lipid-binding properties. In the study described in this chapter, however, I was focused on altering a portion of the toxin (the linker region) that is far-removed from the channel residues or the membrane (Figure 3.2a). Therefore, it was intriguing to observe that altering the linker region of the toxin resulted in significant alterations of the membrane

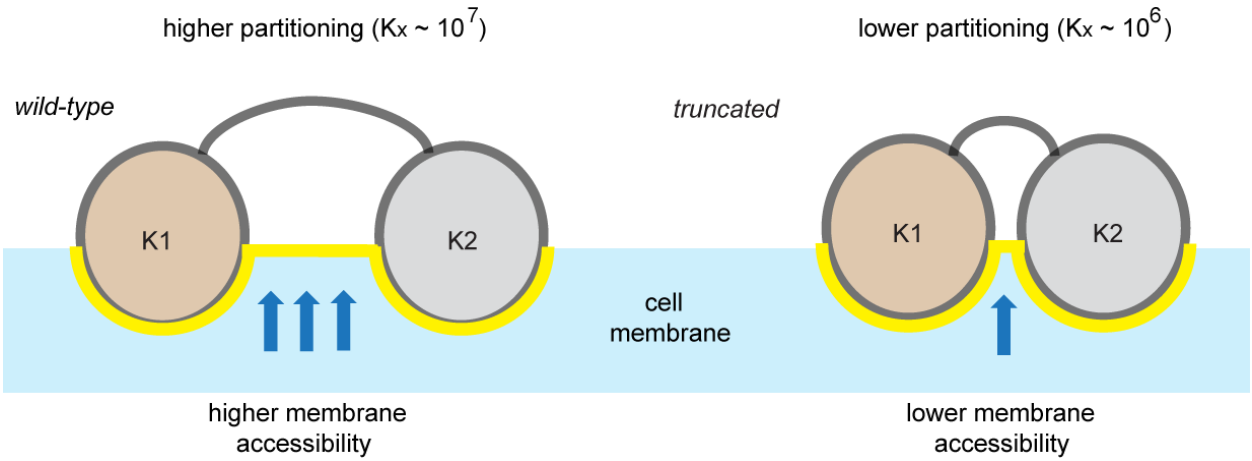

Figure 3.9. The reduced membrane accessibility model.

partitioning propensity (measured both in artificial vesicles as well as on cells, Figures 3.6 and 3.7 respectively). To explain this interesting observation, I propose a conceptual model that I refer to as the 'reduced membrane accessibility' model (Figure 3.9). In this model I propose that the seven amino acids-long linker present in wild-type DkTx allows the two knots to be spaced out far enough from each other such that maximum possible membrane solvation of each of the knots is achieved (Figure 3.9, left) leading to enhanced membrane partitioning properties. In contrast, when the linker is truncated to 4 or lesser number of amino acids, the two knots end up being located closer to each other and this close proximity reduces the surface area available for the membrane to solvate the toxin (Figure 3.9, right), thereby resulting in reduced membrane partitioning.

In conclusion, the results obtained from my studies reported in Chapter 2 and those reported in this chapter strongly suggest that the membrane plays a crucial role in the DkTx-mediated TRPV1 channel activation. I find that the poorer membrane partitioning toxin variants wash-off faster irrespective of how the toxin's partitioning is compromised (by making site-directed variants of the toxin at its lipid-interacting sites as in Chapter 2 or by truncating the linker to reduce membrane accessibility as in this chapter). Furthermore, comparisons between the wash-off kinetics and membrane partitioning values of the truncated monovalent DkTx variants with those of the monovalent single K2 knot demonstrate that both the high membrane partitioning ability of DkTx and its bivalency contribute to its slow washing-off property.

Another interesting insight from my studies on the linker truncation variants is that the naturally chosen linker length of seven amino acids not only ensures bivalent binding of the toxin to the channel, but also ensures optimal toxin partitioning. To the best of our knowledge, this aspect of the functional role of linkers in biological systems has previously not been reported and may be applied for engineering polyvalent membrane-partitioning ligands for targeting multiple membrane-embedded receptors simultaneously.

Table 3.1: Consolidated data summary for all DkTx linker variants

Serial no.	Linker variant	Expected mass (a.m.u)	Observed mass (a.m.u) (MALDI-TOF)	HPLC retention time (min)	EC_{50} (μM)	Fold change potency	Hill coefficient (nH)	% wash-off after 3 min of buffer perfusion post channel activation by saturation concentration of toxin	Mol. Fraction partition coefficient (K_x)	Fractional depletion (oocytes)
1	Wild-type	8586	8581.4	23.1	0.05±0.01	1	1.36±0.33	23.97±1.00	(8.2±0.8)E6	0.42±0.03
2	PYVPVT (Δ1)	8484.9	8482.9	23.2	0.13±0.01	2.6	1.78±0.28	35.78±5.16	(6.0±0.9)E6	0.42±0.03
3	PYVPV (Δ2)	8383.8	8386.1	23.1	1.08±0.12	21.6	1.58±0.22	45.79±4.33	(9.7±1.3)E6	0.23±0.02
4	PYVP (Δ3)	8284.6	8285.8	23.3	7.85±1.08	157	1.60±0.19	72.68±3.61	(3.3±0.3)E6	0.22±0.03
5	PYV (Δ4)	8187.5	8188.9	23.3	7.93±1.27	158.6	1.22±0.10	67.70±3.84	(1.9±0.4)E6	0.17±0.03
6	GGGGGGG	8227.5	8227.8	23.3	0.53±0.04	10.6	2.90±0.59	39.91±3.76	(1.0±0.2)E7	0.34±0.05
7	P36A	8559.9	8558.5	23.3	0.08±0.00	1.6	2.43±0.19	25.09±3.91	N.D.	N.D.
8	P39A	8559.9	8555.6	23.1	0.09±0.03	1.8	1.15±0.35	37.95±0.83	N.D.	N.D.
9	PYVPVPP	8578.0	8574.1	23.1	0.16±0.02	3.2	2.36±0.51	36.27±4.46	(7.7±2.1)E6	0.30±0.03
10	PPPPVPP	8509.9	8507.8	22.9	0.89±0.08	17.8	1.45±0.15	20.86±2.03	N.D.	N.D.
11	PPPPPPP	8507.9	8512.5	23.0	0.26±0.02	5.2	1.15±0.09	26.15±2.32	(4.8±0.8)E6	0.38±0.01

3.4. Materials and Methods.

DkTx mutagenesis, toxin production, electrophysiology experiments and their data analysis were performed as mentioned in Chapter 2.

3.4.1. Membrane partitioning experiments on LUVs

Fluorescence-based experiments on large unilamellar lipid vesicles (LUVs):

*LUV preparation:*1-palmitoyl-2-oleoyl-*sn*-glycero-3-phosphocholine (16:0-18:1 PC from Avanti Polar Lipids Inc.) and 1-palmitoyl-2-oleoyl-*sn*-glycero-3-phospho-(1'-rac-glycerol) (sodium salt) (16:0-18:1 PG from Avanti Polar Lipids Inc.) were mixed at a molar ratio of 1:1 from their chloroform stock solutions, dried under a gentle nitrogen stream and kept in a vacuum desiccator for 9 h. Dried lipid films were rehydrated in HEB buffer at pH 7.0 containing HEPES (10 mM) and EDTA (1 mM). The resulting solution was extruded through 100 nm pore-sized polycarbonate filters (Avanti Polar Lipids Inc.) to generate LUVs.

Tryptophan fluorescence spectroscopy: DkTx variants were dissolved in 2 mL of a buffer containing HEPES (10 mM) and EDTA (1 mM) at pH 7.0 to a concentration of 2 μM and the resulting solution was excited with 280 nm wavelength light by using a Horiba FluoroMax 4 spectrofluorometer. Emission spectra were recorded between 300 to 450 nm both in the presence and absence of LUVs. Scattering of light from lipid vesicles was corrected following earlier reported methods (Gupta et al., 2015; Ladokhin et al., 2000) and the data was subjected to a fitting analysis by employing the following equation:

$$F/F_0(L) = 1+(F/F_{0max}-1)K_x[L]/([W]+K_x[L])$$

where F is the fluorescence intensity at 320 nm for a given lipid concentration, F_0 is the fluorescence intensity at 320 nm in absence of lipids, F_{0max} is fluorescence intensity at 320 nm at a concentration of lipids where partitioning saturates, [L] is molar concentration of accessible lipid (60% of total lipid, corresponding to the outer leaflet), [W] is molar concentration of water (55.3 M), and K_x is mole-fraction partition coefficient of the DkTx variants.

3.5. References.

Ahmad, Z.A., Yeap, S.K., Ali, A.M., Ho, W.Y., Alitheen, N.B., and Hamid, M. (2012). scFv antibody: principles and clinical application. Clin Dev Immunol *2012*, 980250.

Anthis, N.J., and Clore, G.M. (2013). The length of the calmodulin linker determines the extent of transient interdomain association and target affinity. J Am Chem Soc *135*, 9648-9651.

Bae, C., Anselmi, C., Kalia, J., Jara-Oseguera, A., Schwieters, C.D., Krepkiy, D., Won Lee, C., Kim, E.H., Kim, J.I., Faraldo-Gomez, J.D*., et al.* (2016). Structural insights into the mechanism of activation of the TRPV1 channel by a membrane-bound tarantula toxin. Elife *5*.

Bae, C., Kalia, J., Song, I., Yu, J., Kim, H.H., Swartz, K.J., and Kim, J.I. (2012). High yield production and refolding of the double-knot toxin, an activator of TRPV1 channels. PLoS One *7*, e51516.

Bargh, J.D., Isidro-Llobet, A., Parker, J.S., and Spring, D.R. (2019). Cleavable linkers in antibody-drug conjugates. Chem Soc Rev *48*, 4361-4374.

Bennett, M.J., Choe, S., and Eisenberg, D. (1994). Domain swapping: entangling alliances between proteins. Proceedings of the National Academy of Sciences *91*, 3127-3131.

Bhandari, D.G., Levine, B.A., Trayer, I.P., and Yeadon, M.E. (1986). 1H-NMR study of mobility and conformational constraints within the proline-rich N-terminal of the LC1 alkali light chain of skeletal myosin. Correlation with similar segments in other protein systems. Eur J Biochem *160*, 349-356.

Bohlen, C.J., Priel, A., Zhou, S., King, D., Siemens, J., and Julius, D. (2010). A bivalent tarantula toxin activates the capsaicin receptor, TRPV1, by targeting the outer pore domain. Cell *141*, 834-845.

Bu, Z., Biehl, R., Monkenbusch, M., Richter, D., and Callaway, D.J. (2005). Coupled protein domain motion in Taq polymerase revealed by neutron spin-echo spectroscopy. Proc Natl Acad Sci U S A *102*, 17646-17651.

Chen, X., Zaro, J.L., and Shen, W.C. (2013). Fusion protein linkers: property, design and functionality. Adv Drug Deliv Rev *65*, 1357-1369.

Cowan-Jacob, S.W., Fendrich, G., Manley, P.W., Jahnke, W., Fabbro, D., Liebetanz, J., and Meyer, T. (2005). The crystal structure of a c-Src complex in an active conformation suggests possible steps in c-Src activation. Structure *13*, 861-871.

Gao, Y., Cao, E., Julius, D., and Cheng, Y. (2016). TRPV1 structures in nanodiscs reveal mechanisms of ligand and lipid action. Nature *534*, 347-351.

George, R.A., and Heringa, J. (2003). An analysis of protein domain linkers: their classification and role in protein folding. protein engineering *15*, 871-879.

Geron, M., Kumar, R., Zhou, W., Faraldo-Gomez, J.D., Vasquez, V., and Priel, A. (2018). TRPV1 pore turret dictates distinct DkTx and capsaicin gating. Proc Natl Acad Sci U S A *115*, E11837-E11846.

Gupta, K., Zamanian, M., Bae, C., Milescu, M., Krepkiy, D., Tilley, D.C., Sack, J.T., Yarov-Yarovoy, V., Kim, J.I., and Swartz, K.J. (2015). Tarantula toxins use common surfaces for interacting with Kv and ASIC ion channels. Elife *4*, e06774.

Hazan, A., Kumar, R., Matzner, H., and Priel, A. (2015). The pain receptor TRPV1 displays agonist-dependent activation stoichiometry. Sci Rep *5*, 12278.

Krishnamurthy, V.M., Semetey, V., Bracher, P.J., Shen, N., and Whitesides, G.M. (2007). Dependence of effective molarity on linker length for an intramolecular protein-ligand system. J Am Chem Soc *129*, 1312-1320.

Ladokhin, A.S., Jayasinghe, S., and White, S.H. (2000). How to Measure and Analyze Tryptophan Fluorescence in Membranes Properly, and Why Bother? . Anal biochem *285*, 235-245.

Ma, B., Tsai, C.J., Haliloglu, T., and Nussinov, R. (2011). Dynamic allostery: linkers are not merely flexible. Structure *19*, 907-917.

Mack, E.T., Snyder, P.W., Perez-Castillejos, R., Bilgicer, B., Moustakas, D.T., Butte, M.J., and Whitesides, G.M. (2012). Dependence of avidity on linker length for a bivalent ligand-bivalent receptor model system. J Am Chem Soc *134*, 333-345.

Murray, J.K., Biswas, K., Holder, J.R., Zou, A., Ligutti, J., Liu, D., Poppe, L., Andrews, K.L., Lin, F.F., Meng, S.Y.*, et al.* (2015). Sustained inhibition of the NaV1.7 sodium channel by engineered dimers of the domain II binding peptide GpTx-1. Bioorg Med Chem Lett *25*, 4866-4871.

Papaleo, E., Saladino, G., Lambrughi, M., Lindorff-Larsen, K., Gervasio, F.L., and Nussinov, R. (2016). The Role of Protein Loops and Linkers in Conformational Dynamics and Allostery. Chem Rev *116*, 6391-6423.

Ruiz, D.M., Turowski, V.R., and Murakami, M.T. (2016). Effects of the linker region on the structure and function of modular GH5 cellulases. Sci Rep *6*, 28504.

Sarkar, D., Singh, Y., and Kalia, J. (2018). Protein–Lipid Interfaces Can Drive the Functions of Membrane-Embedded Protein–Protein Complexes. ACS Chemical Biology *13*, 2689-2698.

Wriggers, W., Chakravarty, S., and Jennings, P.A. (2005). Control of protein functional dynamics by peptide linkers. Biopolymers *80*, 736-746.

Yan, B.X., and Sun, Y.Q. (1997). Glycine residues provide flexibility for enzyme active sites. J Biol Chem *272*, 3190-3194.

Young, M.A., Gonfloni, S., Superti-Furga, G., Roux, B., and Kuriyan, J. (2001). Dynamic Coupling between the SH2 and SH3 Domains of c-Src and Hck Underlies Their Inactivation by C-Terminal Tyrosine Phosphorylation. Cell *105*, 115-126.

Chapter 4:

Production of a fluorescently labeled DkTx bioconjugate

4.1. Introduction.

Agents that can target specific ion channel subtypes with high selectivity and potency possess tremendous potential not merely as pharmacological tools for physiology-centric studies but also for applications in channel imaging, cell sorting, and as therapeutic agents (Beeton et al., 2003; Bogin, 2005; Sinai et al., 2006). In this context, ion channel-targeting toxins are extremely attractive as they have evolved to selectively bind to their target ion channels and potently modulate their function.

The use of toxins for applications such as imaging and pull-down assays entails appending them with suitable probes or labels. The nicotinic acetyl choline receptor-targeting toxin, α-bungarotoxin, was one of the first toxins to be subjected to labeling (Chang and Lee, 1963; Porter et al., 1973). ^{3}H and ^{125}I labeled α-bungarotoxin was applied to muscles of anaesthetized mice and then subjected to electron microscope autoradiography to inform on the location of the receptor in the neuromuscular junction (Fertuck and Salpeter, 1974; Porter et al., 1973). Radiolabeled α-bungarotoxin also paved the way for developing insightful binding assays for studying the nicotinic acetylcholine receptors expressed in the membranes of different species ranging from rats to electric eels (Lukas et al., 1981). Another example of the development and use of radiolabeled toxins is tritiated saxitoxin (STX) that was used to design a competitive binding assay to screen for rat brain sodium channel-binding toxins implicated in paralytic shellfish poisoning (Usup et al., 2004). In a similar application, radiolabeled conotoxin ([^{125}I]-labeled ω-conotoxin GVIA), which was developed for identifying and studying the toxin's binding site on *N*-type calcium channels (Cruz et al., 1987; Cruz and Olivera, 1986; Marqueze et al., 1988), was more recently used as a reagent in high-throughput assays for the discovery of inhibitors of these channels (Zhang et al., 2006). Furthermore, an ^{125}I-labeled version of the $Na_v1.7$-targeting toxin, protoxin-II, which was originally utilized to provide insight into the binding site of the toxin on the channel (Schmalhofer et al., 2008), has been recently employed to obtain the binding affinity of the toxin with channel chimeras constructed by transferring the domain 2 voltage sensor from the human voltage-gated sodium channel ($hNa_v1.7$) to the Na_vAb channel of *Arcobacter butzleri* (Rajamani et al., 2017). Studies on the ion channel that is the focus of my thesis, TRPV1, have also utilized radiolabeled ligands. For example, a tritiated version of the vanilloid TRPV1 agonist, resiniferatoxin ([^{3}H]RTX), was used in binding assays

with membranes obtained from rat dorsal horn and trigeminal nerve neurons that express this channel (Acs et al., 1994; Szallasi and Blumberg, 1993). Moreover, Swartz and coworkers have recently utilized [^{3}H]RTX to characterize the binding affinity of RTX with channel variants expressed in yeast cells (Zhang et al., 2016b).

Although the radioisotope labeling-based studies discussed above provided valuable insights, there are some inherent limitations associated with this approach. One of the major issues with the use of radioisotopes is that the associated radioactive radiation is a safety hazard and handing these reagents requires expensive dedicated equipment. Moreover, this approach does not provide real time information and is not fully compatible with live cell-based assays. In comparison, although not as sensitive as radioactivity, fluorescence-based approaches are easier to execute, compatible with use in live cells, and extendable to applications that require monitoring two parameters concomitantly (for example, imaging by employing multi-colored dyes).

The small size of toxins (5-10 kDa) renders the use of fluorescent proteins fused to them unattractive as these fluorescent proteins are much larger than the toxins and can potentially disrupt the function of the toxin. In a recent study, however, the green-fluorescent protein (GFP) conjugate of the *Orthochirus scrobiculosus* toxin (OSK1) and the red fluorescent protein (RFP) conjugate of AgTx-2 were demonstrated to retain toxin activity and were employed to image $K_v1.3$ and $K_v1.1$ channels expressed in spheroplasts (Kuzmenkov et al., 2016). Despite this success, appending small molecule fluorophores remains the preferred strategy for toxin labeling as these fluorophores not only impose lesser alterations to the structure of the toxin but also possess better photochromic properties that have been synthetically fine-tuned for powerful imaging applications (Crivat and Taraska, 2012; Toseland, 2013). One challenging aspect of employing small molecule dyes for toxin labeling is that several of these toxins are cysteine-rich and their recombinant production involves careful optimization of redox refolding conditions to obtain correctly folded toxin that may not be compatible with classical bioconjugation methodologies such as thiol bioconjugation chemistry. This limitation has been overcome to a large extent due to the massive recent advances in the field of bioconjugation resulting in the development of a vast array of efficacious new approaches for protein bioconjugation (Boutureira and Bernardes, 2015; Kalia and Raines, 2010).

One of the first reports of the fluorescent labeling of a peptide toxin was that of fluorescein isothiocyanate labeling of the α-bungarotoxin which aided Anderson and Cohen to image the acetylcholine receptors in amphibian and rat neuromuscular junctions (Anderson and Cohen, 1974; Fambrough, 1979). About a decade later, synthesis and application of an α-scorpion toxin was reported for imaging sodium channels at the synapses of innervated chick muscle fibres (Angelides and Nutter, 1983; Angelides, 1986; Angelides, 1989). Angelides group further reported tetramethylrhodamine-labeling of the ω-conotoxin for imaging Ca_v channels in hippocampal neurons wherein toxin labeling was performed by treating the toxin with the amine-reactive succinimidyl ester derivative of the dye (Jones et al., 1989). Amine-based bioconjugation was also used for labeling tityustoxin with the Alexa Fluor 488 and 568 dyes enabling imaging of Na_v channels in rat pituitary tumor GH3 cell membranes (Massensini et al., 2002). The calcium-activated potassium (BK) channel-targeting toxin, iberiotoxin, was appended with fluorophores by employing both thiol and amine-based bioconjugation approaches and the resultant fluorescent toxin bioconjugates were used for imaging BK channels on cells (Bingham et al., 2006; Hafidi et al., 2005). Furthermore, fluorescently labeled hongotoxin generated via thiol chemistry was used to image $K_v1.2$ channels in brain slices and also in Jurkat T-cell lymphocytes (Pragl et al., 2002). Thiol bioconjugation was also employed for labeling Agitoxin-2 (AgTx-2) at its α-helical region which allowed the conjugated toxin to retain its full activity on $K_v1.3$ channels (Sinai et al., 2006). Another example of thiol bioconjugation of toxins is that of labeling guangxitoxin-1E (GxTx-1E) with tetramethylrhodamine maleimide and utilizing the resulting bioconjugate for the live cell imaging of $K_v2.1$ channels-expressing CHO-K1 cells (Tilley et al., 2014). A rare example of a fluorescent toxin conjugate generated by employing an approach other than thiol or amine bioconjugation is that of the $K_v1.3$ channel-targeting stichodactyla toxin (ShK) which was appended with a dye on its *N*-terminal arginine residue (Beeton et al., 2003). Labeled ShK was utilized for the sorting of activated versus naïve T-lymphocytes based on $K_v1.3$ channel expression.

We were interested in developing a robust approach for fluorescently labeling our toxin of interest, DkTx, and using this toxin conjugate for studying its membrane and channel-binding properties rigorously. Although our studies reported in Chapters 2 and 3 of this thesis describe the use of membrane partitioning experiments that we performed by using the intrinsic tryptophan fluorescence of the toxin as well as depletion experiments on *Xenopus laevis* oocytes,

both of these approaches have limitations. The tryptophan fluorescence-based experiments were performed in artificial vesicles that poorly mimic the cell membrane into which the toxin partitions in the physiological context. The depletion experiments performed on oocytes are physiologically relevant but are semi-quantitative at best as they do not provide K_d values of these complexes. Performing a single toxin-depletion experiment entails the use of ~300 *Xenopus laevis* oocytes rendering the obtainment of a titration curve by employing various toxin concentrations technically difficult. Considering these limitations in existing approaches, we decided to develop a fluorescence-based membrane partitioning assay to study DkTx-membrane interactions. Towards this goal, the first challenge that we had to overcome was to label DkTx with a fluorescent dye.

4.2. Results.

Thiol bioconjugation approaches lead to misfolding of DkTx. Thiol bioconjugation approaches require installing a free cysteine in a solvent-exposed region of the protein of interest followed by treatment with maleimide dyes to yield the desired bioconjugate. Installing an additional cysteine into a cysteine-rich protein such as DkTx that needs to be refolded from *E. coli* inclusion bodies in a redox buffer is tricky as it can result in the formation of non-native disulfide bridging patterns resulting in loss of protein function (Bae et al., 2012; Pi et al., 2007; Rudolph and Lilie, 1996; Zhang et al., 2005). Anticipating this potential hurdle, we decided to install a non-native cysteine into the linker region of the toxin—a region of the protein that does not contain any cysteine residues and is not part of the two cystine knots, K1 and K2, of DkTx. To achieve this goal, I generated two cysteine variants of DkTx-HYR —the DkTx construct I had utilized for my studies in Chapter 2 that contains an insertion of the three amino acid-long sequence 'HYR' that is recognized by the Genenase I enzyme. The idea behind using this construct was that if we could label this DkTx variant successfully with a fluorophore, we would be able to generate fluorophore-tagged single knots as well by treating these labeled proteins with the Genenase enzyme. I generated these two cysteine insertion variants using the molecular cloning strategies described in the Materials and Methods section 2.4.1 of Chapter 2. The cysteine residues were inserted such that in one construct the free cysteine would be present immediate prior to the 'HYR' cleavage sequence (i.e., CHYR) while in the other, the free

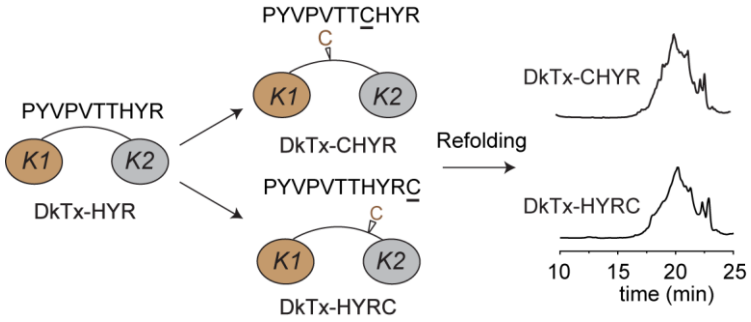

Figure 4.1. Maleimide bioconjugation attempts with free cysteine introduced in the DkTx linker. Single cysteine variants of the DkTx-HYR protein with the linker sequence shown above the cartoon for each variant. The right panel shows the HPLC refolding profiles of both the variants.

cysteine would be located immediately after the 'HYR' sequence (i.e., HYRC). To prevent free cysteine oxidation to sulfones or sulfoxides, the refolding buffers were purged with nitrogen gas for 2 h before the addition of the linear peptide solution, which was made in degassed 50% acetonitrile containing 0.1% TFA. Monitoring the progress of refolding of these cysteine variants by HPLC revealed that neither of these constructs yielded favorable refolding profiles. Indeed, in contrast to the folding profiles of wild-type DkTx and all our toxin variants reported in Chapters 2 and 3 of this thesis that gave a single major peak of properly folded active toxin (for example, see Figure 2.2 of Chapter 2), these two toxin constructs gave complicated folding profiles containing several overlapping peaks precluding the isolation of a major refolded product (Figure 4.1). These observations suggested that the non-native cysteines installed in the linker were forming disulfide linkages with the native cysteine residues located in the two knots of DkTx during refolding, thereby disrupting the refolding process and forming a mixture of misfolded species.

We reasoned that one potential solution to the refolding problem described above was to install the non-native cysteine residue at a site that was far-removed from the two knots of DkTx. To this end, we designed two rigid spacer constructs to be installed at the *N*-terminus of DkTx. In deciding which sequences to choose for creating the rigid spacer, we were guided by previous

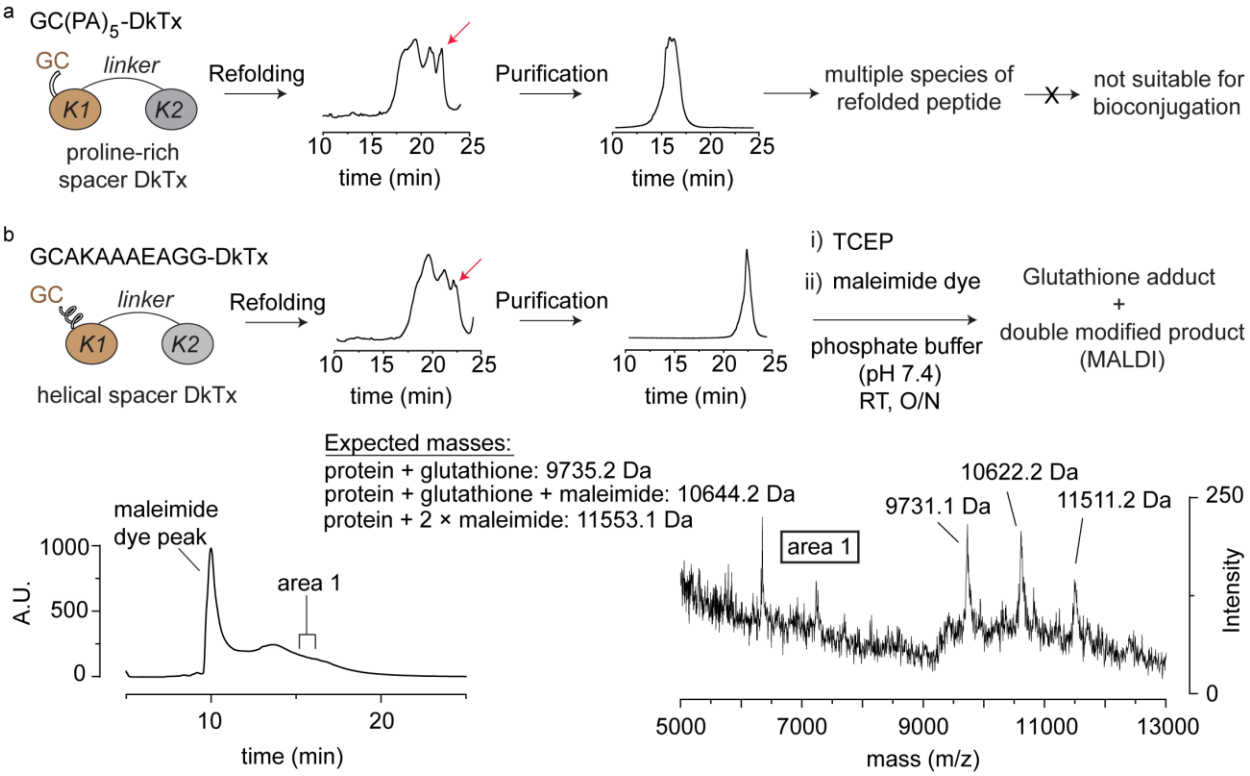

Figure 4.2. Rigid spacer-assisted cysteine bioconjugation attempts performed on DkTx. Expected rigid spacer shape depicted in cartoon representation in the left-most panel with the sequence of the spacer mentioned on the top of each cartoon (a and top panel of b). After refolding, HPLC peaks marked with red arrows were purified. Subsequently, for the helical spacer DkTx construct (see b), a bioconjugation reaction was performed by incubating the refolded peptide overnight with TCEP and the maleimide dye in phosphate buffer at room temperature. Bioconjugation reaction mixture yielded a peak for the unreacted maleimide dye and a broad chromatogram on HPLC (using a shorter HPLC protocol with an altered acetonitrile-water (0.1% TFA) gradient as described in section 4.4.2) as depicted in lower left panel of (b). MALDI spectrum of 'area 1' marked in the HPLC chromatogram is depicted on the lower right panel of (b). Low intensity peaks of the different products formed have been demarcated.

studies that demonstrated that the $(EAAAK)_n$ motif takes up an α-helical conformation (Chen et al., 2013), and $(XP)_n$ motifs such as $(AP)_n$ sequences assume stiff 'elbow'-like conformations (Bhandari et al., 1986). Consequently, we decided to generate two DkTx constructs—one containing a helical spacer separating the non-native cysteine residue from the rest of the toxin

(GCAKAAAEAGG-DkTx) and the other containing a proline-rich spacer (GCPAPAPAPAPA-DkTx). Unfortunately, both these variants did not serve their purpose. The proline-rich rigid spacer DkTx variant gave several merged peaks in the HPLC purification profiles suggestive of the formation of multiple misfolded species (Figure 4.2a, top panel). The variant with the helical spacer, on the other hand, gave a broad HPLC peak upon refolding (Figure 4.2b, top panel) which upon MALDI mass spectrometric analysis was found to contain the glutathione adduct of the desired protein. Treatment of this glutathione adduct with 3-fold molar excess of tris-carboxyethylphosphine (TCEP) to reductively cleave off the glutathione and release the reactive thiol group of cysteine, followed by addition of 5-fold molar excess of Alexa 594 C5 maleimide dye for performing thiol bioconjugation gave a broadened HPLC chromatogram (Figure 4.2b, lower left panel). All the portions of the chromatogram were subjected to MALDI mass spectroscopy, one of which (denoted as "area 1" in Figure 4.2b) yielded low intensity peak corresponding to two dye molecules appended to the protein and conjugates containing both the glutathione modification as well one dye molecule appended (Figure 4.2b, right panel). These results indicated that TCEP treatment was reducing not only the desired disulfide bond between glutathione and the protein but also the native disulfide bonds present in the protein.

More recently, an approach of cysteine bioconjugation known as the pi-clamp technology has been reported, wherein the free cysteine present in the 'FCPF' motif is specifically derivatized by thiol-reactive perfluorobiphenyl probes even in the presence of other competing free cysteines in the protein (Zhang et al., 2016a). In order to test the suitability of this approach, we generated a DkTx variant wherein the 'FCPF' sequence was inserted in the linker region replacing the wild-type linker and treated it with a surrogate non-fluorescent probe, *N*-acetyl-*S*-(perfluoro-[1,1'-biphenyl]-4-yl)cysteine, which was synthesized by Rahul Nisal in Dr. Jeet Kalia's laboratory (Figure 4.3, top panel). Purification of this reaction mixture gave two broad peaks suggestive of mixed species, which on MALDI characterization yielded results similar to those obtained with our cysteine variants discussed above—the glutathione adduct of the protein was obtained as the major product and although a small peak approximately corresponding to the mass of the desired conjugate was seen (Figure 4.3, bottom panel), it could not be purified.

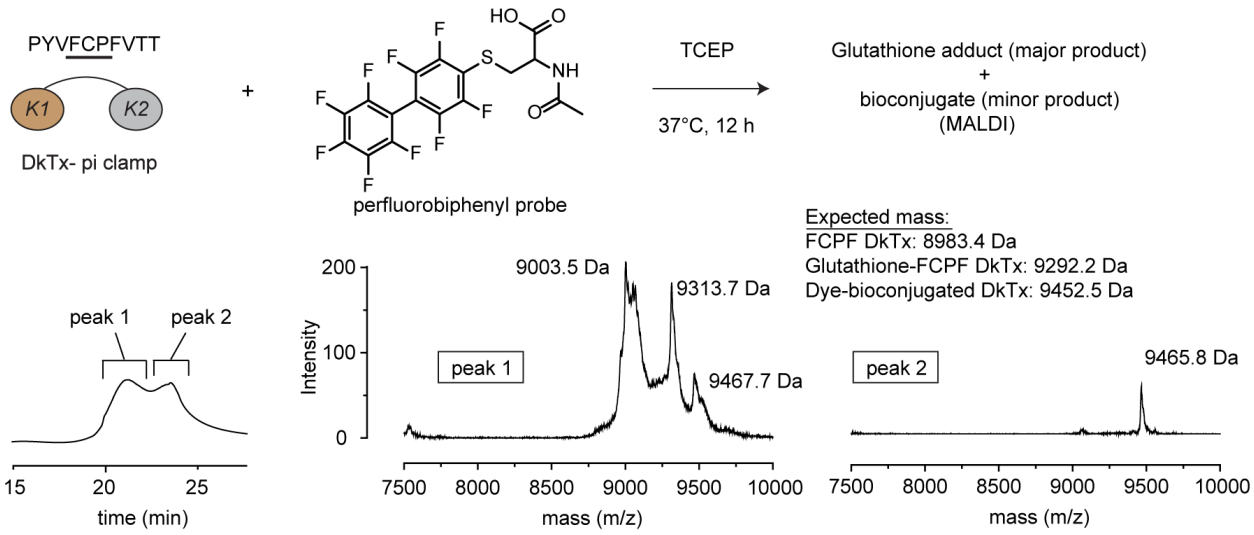

Figure 4.3. Pi-clamp based site-specific cysteine bioconjugation reaction scheme (top panel). Altered linker sequence comprising the FCPF pi-clamp motif was incubated with *N*-acetyl-*S*-(perfluoro-[1,1'-biphenyl]-4-yl)cysteine in presence of TCEP to yield desired bioconjugate as minor product. Lower panel depicts the HPLC chromatogram of the pi-clamp based reaction mixture yielding two peaks and the MALDI analysis of both demarcated peaks demonstrating low intensity peaks of desired conjugate.

***N*-terminal bioconjugation is not suitable for producing active DkTx bioconjugate.** Our unsuccessful attempts on performing thiol bioconjugation described in the previous section convinced us that DkTx was not compatible with thiol bioconjugation and motivated us to try other approaches for labeling the toxin.

We next attempted an *N*-terminal bioconjugation approach (Witus and Francis, 2010) that utilizes pyridoxal-5'-phosphate (PLP) for transaminating the $-NH_2$ group of the *N*-terminal Gly residue of the DkTx protein into an aldehyde (–CHO) group which can then react with an aminoxy dye (structure of the dye given in Figure 4.4b) to form an oxime conjugate (Figure 4.4a). Upon subjecting this reaction mixture to HPLC, we obtained purified toxin conjugates that yielded the desired mass (expected mass = 9651.3 Da, observed mass = 9651.8 Da; Figure 4.4c, e) and SDS-PAGE analysis (Figure 4.4d) yielded a fluorescent protein conjugate at the expected

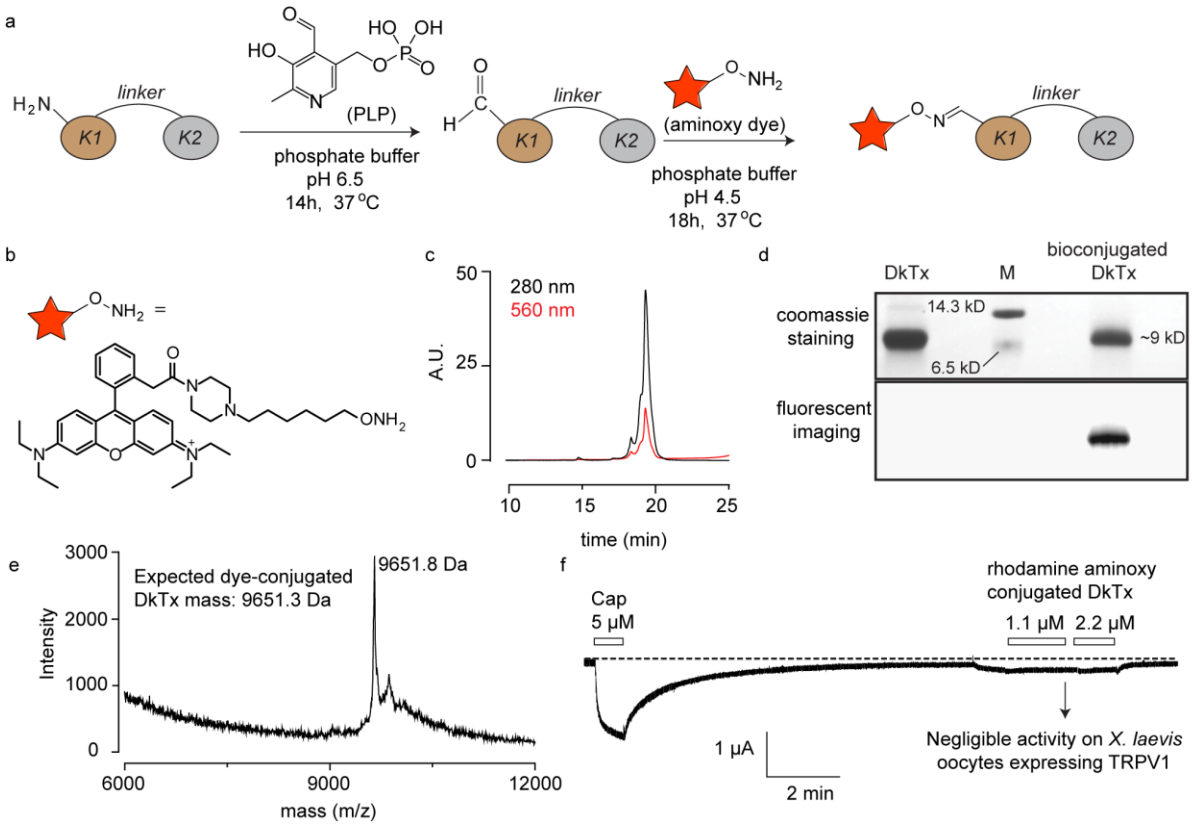

Figure 4.4. PLP mediated transamination followed by oxime formation. a) Scheme of the transamination reaction of DkTx with PLP followed by reaction of the *N*-terminal aldehyde DkTx with aminoxy dye to form the oxime conjugate. b) The structure of the rhodamine amioxy dye. c) HPLC chromatogram of the bioconjugate showing absorbance at 280 nm (black) and 560 nm (red). d) SDS-PAGE analysis of the bioconjugate formation by coomassie staining and fluorescence imaging. M: molecular weight marker. e) MALDI spectrum of the purified rhodamine aminoxy dye conjugated DkTx product (expected mass = 9651.3 Da, observed mass = 9651.8 Da). f) Representative electrophysiological trace of two-electrode voltage clamp recording with the rhodamine oxime-DkTx conjugate.

position with respect to molecular weight markers. After obtaining high-purity fluorescently labeled toxin, we evaluated its activity on TRPV1 channels expressed in *Xenopus laevis* oocytes. These experiments yielded negligible TRPV1 channel currents even at elevated toxin concentrations (3.3 µM) indicating that the conjugated toxin was functionally compromised (Figure 4.4f).

We attempted another approach for *N*-terminal bioconjugation using 2-pyridine carboxaldehyde (2-PCA) (MacDonald et al., 2015) in which 50 µM wild-type DkTx was reacted with 10 mM 2-PCA in 50 mM phosphate buffer (pH 7.5) at 37°C for 16 h (see section 4.4.5 of this chapter), followed by purification of the conjugate as per HPLC protocols described in the section 2.4.1 of Chapter 2. It was apparent from the HPLC chromatogram post incubation that the DkTx peak had split into two peaks appearing as a shoulder peak (Figure 4.5a). MALDI analysis revealed a product of 8782.7 Da mass as major product which corresponds to the addition of two molecules of 2-PCA to DkTx. The product that gave the mass of the desired monolabeled bioconjugate (8675.0 Da) was formed as a minor product (Figure 4.5b). Based on the collective failure of these two *N*-terminal bioconjugation approaches, we concluded that *N*-terminal labeling approaches were not suitable for the DkTx structure.

Successful DkTx labeling by sortase A mediated *C*-terminal bioconjugation. Sortase A is a bacterial enzyme isolated and cloned from *Staphylococcus aureus* species that recognizes the LPXTG motif in a protein resulting in the cleaving-off of the *C*-terminal glycine and the

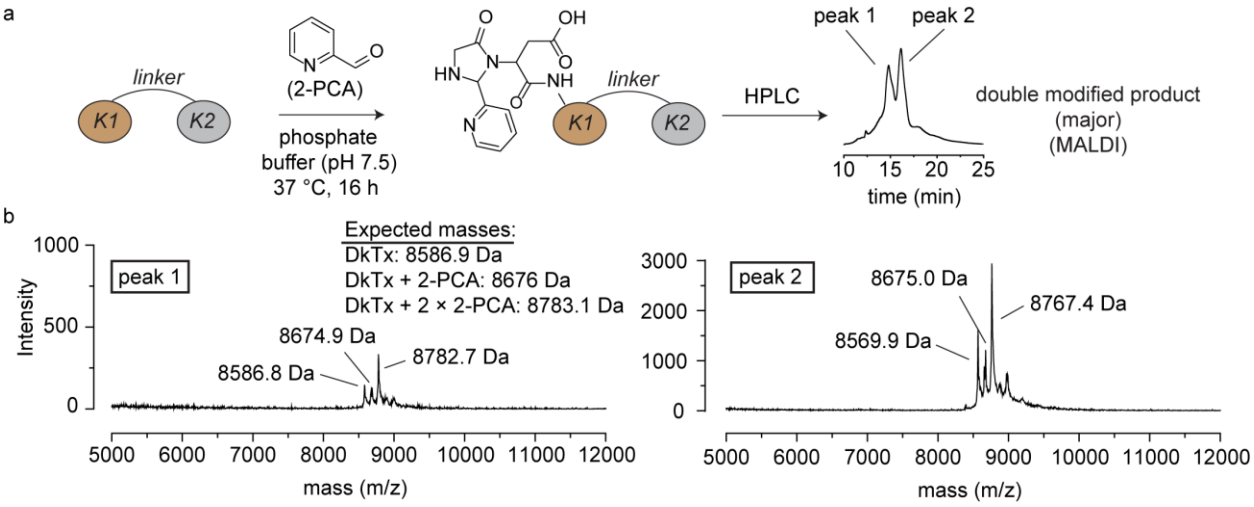

Figure 4.5. Scheme of reaction for *N*-terminal bioconjugation of wild-type DkTx with 2-PCA. HPLC profile on the right most panel of (a) depicts formation of two peak after bioconjugation. MALDI analysis of both peaks as shown in (b) represents formation of double-modified product as major product of the reaction, yielding trace amounts of single-modified product.

installation of a reactive thioester moiety on the threonine residue (Ton-That et al., 1999). Upon treatment with a probe containing an *N*-terminal glycine, the thioester undergoes a nucleophilic attack by the *N*-terminal amino group of the glycine residue to form a peptide bond between the *C*-terminal threonine and nucleophilic Gly of the probe (as depicted in Figure 4.6) (Dai et al., 2019; Guimaraes et al., 2013). As a prerequisite of sortase-based bioconjugation, we needed to express and purify the sortase A enzyme and generate a DkTx variant with a LPXTG motif that is required for this approach.

The *C*-terminal 6X-His tagged cDNA of the sortase A enzyme was generously gifted by Dr. Thomas J. Pucadyil's lab (IISER, Pune). I expressed this protein in in *E. coli* BL21 (DE3) cells and purified the enzyme by Ni-NTA affinity chromatography as described in the Materials and Methods section 4.4.6 (Figure 4.7). In parallel, a DkTx variant was generated by appending a GGGSLPETGGHHHHHH ($G_3SLPETG_2H_6$) sequence to the *C*-terminus of the wild-type DkTx following procedures described in section 2.4.1 of chapter 2. A triglycine conjugated fluoresceinamine dye was synthesized in Dr. Jeet Kalia's laboratory by Rohit Shrivas and was used as the nucleophile in the sortase reaction with the DkTx variant (Figure 4.8). The sortase-catalyzed bioconjugation reaction of the DkTx variant and the fluoresceinamine-GGG probe was

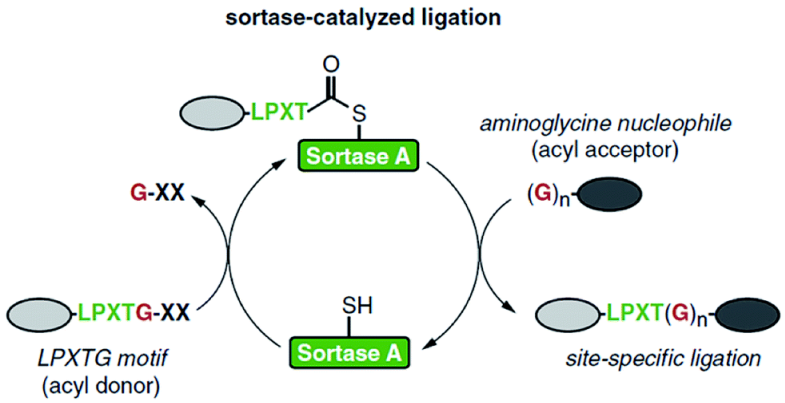

Figure 4.6. Mechanism of sortase-catalyzed *C*-terminal ligation. Figure reproduced from Dai et al., 2019 with permission from the Royal Society of Chemistry.

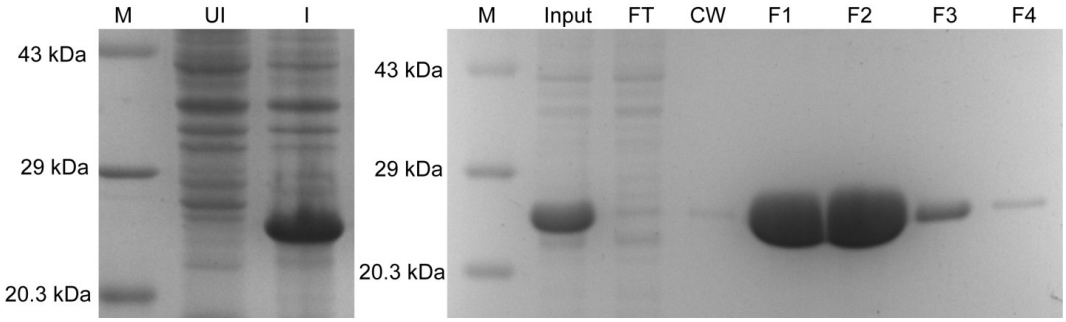

Figure 4.7. Sortase A production and purification. Left panel represents sortase induction gel depicting overexpressed sortase A protein in the induced (I) lane at ~25 kDa. The symbols M and UI stands for molecular weight marker and uninduced lane respectively. The right panel displays the sortase A purification gel. FT and CW stands for flow through (simultaneous with sample loading) and column wash (post sample loading) respectively. F1 though F4 depicts the fractions collected in elution buffer.

carried out for 16 h at RT and the reaction mixture was then subjected to HPLC, yielding the desired pure labeled toxin at 23.5 min (Figure 4.9a). SDS-PAGE analysis of the purified toxin yielded a fluorescent band at the expected molecular weight range (Figure 4.9c) and MALDI analysis confirmed the identity of the conjugate (Figure 4.9b, observed mass = 9789.8 Da; expected mass = 9784.9 Da). We performed two-electrode voltage clamp recordings on TRPV1 channel-expressing oocytes to examine the potency of the conjugate and it was found to be similar to the wild-type toxin with respect to its potency and wash-off kinetics (Figure 4.9d).

With the fluorescent DkTx in hand, the stage is set for using it for performing binding and imaging experiments. These experiments will be taken up in earnest by Dr. Jeet Kalia's laboratory in the future.

4.3. Discussion.

We initiated our efforts on fluorescently labeling DkTx in order to develop a fluorescence-based assay for quantitatively measuring the membrane- and channel-binding properties of the toxin

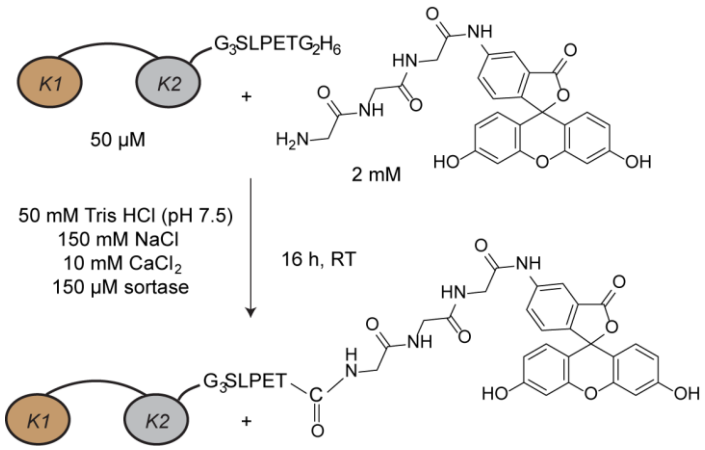

Figure 4.8. Scheme of sortase reaction between DkTx-$G_3SLPETG_2H_6$ and triglycine fluoresceinamine probe.

and its variants. To achieve this goal, we subjected DkTx to a panel of modern bioconjugation technologies and eventually succeeded in labeling the toxin by employing the sortase enzyme-based bioconjugation technology.

It is interesting that whereas thiol bioconjugation approaches have been successful on other ICK toxins (Hafidi et al., 2005; Pragl et al., 2002; Sinai et al., 2006; Tilley et al., 2014), this approach failed on DkTx (Figures 4.1, 4.2 and 4.3). This observation suggests that the structure of DkTx possesses some unique attributes that are not present in other ICK toxins. Most of our thiol bioconjugation attempts yielded misfolded toxins and on several occasions, we obtained glutathione-appended toxin adducts. Glutathione is an additive present in the redox buffer that is used for toxin refolding and it is surprising that the toxin-glutathione adduct is stable enough to persist through the refolding process. This observation suggests that probably the native cystine knots of DkTx are more prone to reduction as compared to those present in other ICK toxins.

Another intriguing result of my bioconjugation studies was that the poor activity of the *N*-terminally labeled toxin (Figure 4.4). This result suggests that the toxin's *N*-terminus plays an important role in its function. Interestingly, however, the D1A variant of the DkTx reported in Chapter 2 of this thesis did not disrupt the toxin's function significantly (Figure 2.5 of Chapter2). Even though the *N*-terminal Asp residue of the DkTx is not well resolved in the cryo-EM

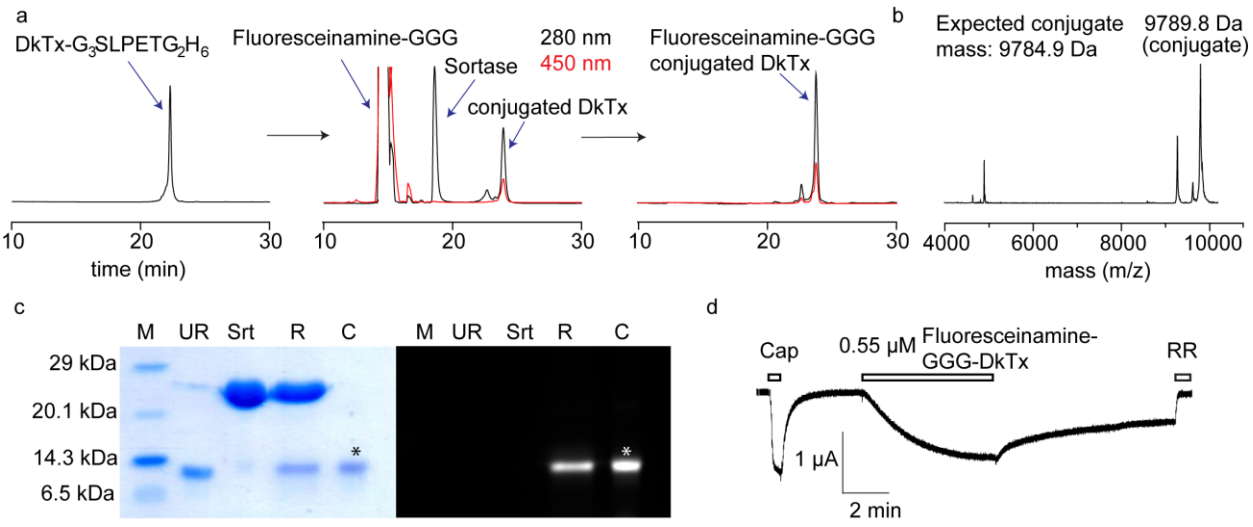

Figure 4.9. Fluorescent DkTx bioconjugate production by using the sortase reaction. a) HPLC trace of the pure DkTx-$G_3SLPETG_2H_6$ species (left panel), the reaction mixture post-incubation (middle panel), and the purified conjugate (right panel). b) MALDI analysis of the conjugate. c) SDS-PAGE analysis of the bioconjugation reaction with the coomassie-stained gel shown in the left and the image viewed through a fluorimager on the right. M: molecular weight marker; UR: unreacted DkTx, Srt: sortase enzyme; R: reaction mixture with conjugated DkTx and C: purified DkTx conjugate (marked with an *). d) Representative electrophysiological trace of TRPV1 ion channel activation by fluoresceinamine-GGG conjugated DkTx. Capsaicin (caps), Fluoresceinamine-GGG conjugated DkTx and ruthenium red (RR) were applied at 5 µM, 0.55 µM, and 7 µM concentrations respectively.

structure of the TRPV1-DkTx complex (PDB: 5irx) (Gao et al., 2016), the backbone carbonyl group of D1 of DTx is situated 4.4 Å apart from the ε-NH_2 of the Lys535 of the TRPV1 channel S4 helix engendering the possibility of an H-bonding interaction. It is, however, unlikely that the disruption of this interaction could bring about such drastic effect on toxin's potency. It is possible that the bulky fluorophore molecule appended onto the toxin disrupts functionally critical toxin-membrane interactions leading to loss of the toxin's function.

The successful development of protocols for sortase mediated bioconjugation on DkTx reported in this chapter sets the stage for not just labelling the toxin with fluorophores for imaging but also for installing affinity tags such as biotin for pull-down experiments and probes

for spectroscopy that may be used for studying the conformational dynamics of membrane partitioning of the toxin. Efforts are underway in Dr. Jeet Kalia's laboratory to use this technology for generating a panel of labelled DkTx conjugates for these applications.

4.4. Materials and Methods.

4.4.1. Production of DkTx variants for cysteine or sortase mediated bioconjugation.

Production of DkTx and its variants for all bioconjugation attempts utilized the same methodological workflow as described in Chapter 2, section 2.4.1. The refolding buffer employed for the refolding of all cysteine variants of DkTx discussed in this chapter was purged with nitrogen gas for 2 h before addition of the linear peptide solution made in degassed 50% acetonitrile containing 0.1% TFA. Progression of refolding was examined by RP-HPLC runs as described earlier.

4.4.2. Cysteine bioconjugation protocol.

The DkTx variants with free cysteine-appended in the linker region of DkTx-HYR (i.e., the 'CHYR' and 'HYRC' variants) formed a mixture of misfolded species which precluded purification of pure refolded forms of these toxins. Hence, no bioconjugation reactions were performed on these constructs.

The DkTx variants with free cysteine-appended on the *N*-terminal helical rigid spacer variant were incubated at 50 μM concentration with 150 μM TCEP solution (from a stock of 1.5 mM made in 10 mM phosphate buffer pH 7.4) in 10 mM sodium phosphate buffer (pH 7.4) for 20 min at room temperature. Alexa 594 C5 maleimide dye solution made in dimethyl sulfoxide was added to the TCEP-treated protein solution at a final concentration of 250 μM and incubated overnight at RT. Subsequently, the reaction mixture was purified by RP-HPLC using a linear acetonitrile-water (0.1% TFA) gradient (25-53% over 21 min) in an Agilent 300SB-C18 RP-HPLC column and analyzed for bioconjugate formation by ABSciex MALDI-TOF mass analyzer.

4.4.3. Site-specific cysteine bioconjugation protocol using pi-clamp technology.

The pi-clamp technology for thiol bioconjugation was attempted both in the folded and linear versions of the 'PYVFCPFVTT' linker construct of DkTx. The peptide (25 μM) was incubated with the perfluoroaromatic probe *N*-acetyl-*S*-(perfluoro-[1,1'-biphenyl]-4-yl)cysteine (final concentration = 500 μM, stock made at 2.5 mM in acetonitrile) in presence of TCEP (final concentration = 125 μM, stock made at 8.34 mM in ddH_2O) in 250 mM sodium phosphate buffer at pH 8, at 37°C for 12 h. The reaction mixture was subsequently injected into an Agilent 300SB-C18 RP-HPLC column for purification using a water-acetonitrile gradient described in section 2.4.1 of the Chapter 2. Purified HPLC eluates were subjected to MALDI characterization in an ABSciex MALDI-TOF mass analyzer.

4.4.4. PLP mediated transamination followed by *N*-terminal bioconjugation with rhodamine aminoxy dye.

To perform the transamination reaction to install the –CHO group on the *N*-terminus of the toxin, wild-type DkTx (50 μM in 50 mM phosphate buffer at pH 6.5) was incubated with pyridoxal-5'-phosphate (PLP) at a final concentration of 20 mM (added as 8.5 mg solid powder in a 1.5 mL DkTx solution in buffer) for 18 h at 37°C. The reaction mixture was then dialyzed against 200 mM phosphate buffer of pH 4.5 at 4°C and the *N*-terminal–CHO derivatized DkTx thus produced (37 μM in 200 mM phosphate buffer at pH 4.5) was then treated with the rhodamine-aminoxy dye (2.2 mM, stock made at 10 mM stock in acetonitrile) in presence of excess 2-amino-5-methoxy benzoic acid catalyst (1.7 mM, stock made at 53.8 mM in 200 mM phosphate buffer, pH 4.5) for 18 h. The conjugated toxin was purified by HPLC. Mass of the conjugate was confirmed by MALDI-TOF analysis Two-electrode voltage clamp recordings were performed for the fluorescently labeled DkTx variant following the same protocol mentioned in section 2.4.2 of Chapter 2.

4.4.5. Conjugation of 2-PCA with wild-type DkTx

Wild-type DkTx (50 μM in 50 mM phosphate buffer at 7.5 pH) was treated with 2-PCA (used at 10 mM final concentration, from a 100 mM stock solution made in 50 mM phosphate buffer of pH 7.5) at 37°C for 16 h and the resulting mixture was subjected to HPLC to purify the resulting conjugate.

4.4.6. Sortase mediated *C*-terminal bioconjugation.

Production and purification of sortase A (wild-type) enzyme: A plasmid containing the gene for sortase A (Δ59) in a pET28a vector was transformed into *E. coli* BL21(DE3) cells. LB broth cultures (1 L) containing ampicillin (100 µg/mL) were inoculated with transformed E. coli BL21(DE3) cells and induced with IPTG (0.5 mM) on reaching an O.D. (600 nm) of 0.4-0.6 at 37°C. The induced culture was pelleted after 16 h of growth at 25°C and lysed by sonication in ice cold lysis buffer (50 mM Tris-HCl (pH 7.5), 150 mM NaCl, 5 mM $MgCl_2$, 10 mM imidazole and 10% (*v/v*) glycerol). The lysate was subjected to centrifugation at 15000 × g and the supernatant fraction was then subjected to Ni-NTA affinity column purification as described previously (Guimaraes et al., 2013). The purified protein was quantified and stored at -20°C as a 20% glycerol solution of the sortase A enzyme.

Procedure for sortase mediated DkTx bioconjugation with GGG-Fluoresceinamine: DkTx-G_3SLPETG$_2H_6$ (50 µM in 1X sortase reaction buffer: 50 mM Tris HCl, 150 mM NaCl and 10 mM $CaCl_2$ at pH 7.5) was incubated with the sortase A enzyme (final concentration = 150 µM, stock made at 1.31 mM in a pH 7.5 buffer containing 50 mM Tris HCl, 150 mM NaCl, 5 mM $MgCl_2$ and 10% (*v/v*) glycerol) and triglycine fluoresceinamine dye (2 mM, stock made at 12.3 mM in ddH_2O). The reaction mixture was incubated for 16 h at room temperature and the desired bioconjugate was purified by HPLC was purified by RP-HPLC as described in section 2.4.1 of Chapter 2. The bioconjugate was characterized by MALDI analysis performed on an ABSciex MALDI-TOF mass analyzer. SDS-PAGE analysis was performed on a 15% polyacrylamide gel.

Functional characterization of the triglycine fluoresceinamine labeled DkTx: Two-electrode voltage clamp recordings were performed with the fluorescently labeled DkTx variant following protocol mentioned in section 2.4.2 of Chapter 2.

4.5. References.

Acs, G., Palkovits, M., and Blumberg, P.M. (1994). [3H]Resiniferatoxin binding by the human vanilloid (capsaicin) receptor. Molecular Brain Research *23*, 185-190.

Anderson, M.J., and Cohen, M.W. (1974). Fluorescent staining of Acetylcholine receptors in vertebrate skeletal muscle. J Physiol *237*, 385-400.

Angelides, K.J. and Nutter, T.J. (1983). Preparation and characterization of fluorescent scorpion toxins from Leiurus quinquestriatus quinquestriatus as probe of soudium channel of excitable cells. J Bio Chem *258*, 11948-11957.

Angelides, K.J. (1986). Fluorescently labelled Na^+ channels are localized and immobilized to synapses of innervated muscle fubres. Nature *321*, 63-66.

Angelides, K.J. (1989). Fluorescent Analogs of Toxins. Methods Cell Biol *29*, 29-58.

Bae, C., Kalia, J., Song, I., Yu, J., Kim, H.H., Swartz, K.J., and Kim, J.I. (2012). High yield production and refolding of the double-knot toxin, an activator of TRPV1 channels. PLoS One *7*, e51516.

Beeton, C., Wulff, H., Singh, S., Botsko, S., Crossley, G., Gutman, G.A., Cahalan, M.D., Pennington, M., and Chandy, K.G. (2003). A novel fluorescent toxin to detect and investigate Kv1.3 channel up-regulation in chronically activated T lymphocytes. J Biol Chem *278*, 9928-9937.

Bhandari, D.G., Levine, B.A., Trayer, I.P., and Yeadon, M.E. (1986). 1H-NMR study of mobility and conformational constraints within the proline-rich N-terminal of the LC1 alkali light chain of skeletal myosin. Correlation with similar segments in other protein systems. Eur J Biochem *160*, 349-356.

Bingham, J.P., Bian, S., Tan, Z.Y., Takacs, Z., and Moczydlowski, E. (2006). Synthesis of a biotin derivative of iberiotoxin: binding interactions with streptavidin and the BK Ca2+-activated K+ channel expressed in a human cell line. Bioconjug Chem *17*, 689-699.

Bogin, O. (2005). Venom Peptides and their Mimetics as Potential Drugs. In Modulator Issue (www.alomone.com), pp. 14-20.

Boutureira, O., and Bernardes, G.J. (2015). Advances in chemical protein modification. Chem Rev *115*, 2174-2195.

Chang, C.C., and Lee, C.Y. (1963). Isolation of neurotoxins from the venom of Bungarus multicinctus and their modes of neuromuscular blocking action. Archs int Pharmacodyn Ther *184*, 241-257.

Chen, X., Zaro, J.L., and Shen, W.C. (2013). Fusion protein linkers: property, design and functionality. Adv Drug Deliv Rev *65*, 1357-1369.

Crivat, G., and Taraska, J.W. (2012). Imaging proteins inside cells with fluorescent tags. Trends Biotechnol *30*, 8-16.

Cruz, L.J., Johnson, D.S., and Olivera, B.M. (1987). Characterization of the omega-conotoxin target. Evidence for tissue-specific heterogeneity in calcium channel types. Biochemistry *26*, 820-824.

Cruz, L.J., and Olivera, B.M. (1986). Calcium Channel Antaginists: ω-conotoxin defines a new high affinity site. The journal of biological chemistry *261*, 6230-6233.

Dai, X., Böker, A., and Glebe, U. (2019). Broadening the scope of sortagging. RSC Advances *9*, 4700-4721.

Fambrough, D.M. (1979). Control of acetylcholine receptors in skeletal muscle. Physiol Rev *59*, 165-227.

Fertuck, H.C., and Salpeter, M.M. (1974). Localization of acetylcholine receptor by 125I-labeled α-bungarotoxin binding at mouse motor endplates. Proceedings of the National Academy of Sciences *71*, 1376-1378.

Gao, Y., Cao, E., Julius, D., and Cheng, Y. (2016). TRPV1 structures in nanodiscs reveal mechanisms of ligand and lipid action. Nature *534*, 347-351.

Guimaraes, C.P., Witte, M.D., Theile, C.S., Bozkurt, G., Kundrat, L., Blom, A.E., and Ploegh, H.L. (2013). Site-specific C-terminal and internal loop labeling of proteins using sortase-mediated reactions. Nat Protoc *8*, 1787-1799.

Hafidi, A., Beurg, M., and Dulon, D. (2005). Localization and developmental expression of BK channels in mammalian cochlear hair cells. Neuroscience *130*, 475-484.

Jones, O.T., Kunze, D.L., and Angelides, K.J. (1989). Localization and mobility of omega-conotoxin-sensitive Ca2+ channels in hippocampal CA1 neurons. Science *244*, 1189-1193.

Kalia, J., and Raines, R. (2010). Advances in Bioconjugation. Current Organic Chemistry *14*, 138-147.

Kuzmenkov, A.I., Nekrasova, O.V., Kudryashova, K.S., Peigneur, S., Tytgat, J., Stepanov, A.V., Kirpichnikov, M.P., Grishin, E.V., Feofanov, A.V., and Vassilevski, A.A. (2016). Fluorescent protein-scorpion toxin chimera is a convenient molecular tool for studies of potassium channels. Sci Rep *6*, 33314.

Lukas, R.J., Morimoto, H., Hanley, M.R., and Bennett, E.L. (1981). Radiolabeled alpha-bungarotoxin derivatives: kinetic interaction with nicotinic acetylcholine receptors. Biochemistry *20*, 7373-7378.

MacDonald, J.I., Munch, H.K., Moore, T., and Francis, M.B. (2015). One-step site-specific modification of native proteins with 2-pyridinecarboxyaldehydes. Nat Chem Biol *11*, 326-331.

Marqueze, B., Martin-Moutot, N., Leveque, C., and Couraud, F. (1988). Characterization of the omega-conotoxin-binding molecule in rat brain synaptosomes and cultured neurons. Mol Pharmacol *34*, 87-90.

Massensini, A.R., Suckling, J., Brammer, M.J., Moraes-Santos, T., Gomez, M.V., and Romano-Silva, M.A. (2002). Tracking sodium channels in live cells: confocal imaging using fluorescently labeled toxins. J Neurosci Methods *116*, 189-196.

Pi, C., Liu, J., Wang, L., Jiang, X., Liu, Y., Peng, C., Chen, S., and Xu, A. (2007). Soluble expression, purification and functional identification of a disulfide-rich conotoxin derived from Conus litteratus. J Biotechnol *128*, 184-193.

Porter, C.W., Chiu, T.H., Wieckowski, J., and Barnard, E.A. (1973). Types and locations of cholinergic receptor-like molecules in muscle fibres. Nat New Biol *241*, 3-7.

Pragl, B., Koschak, A., Trieb, M., Obermair, G., Kaufmann, W.A., Gerster, U., Blanc, E., Hahn, C., Prinz, H., Schütz, G.*, et al.* (2002). Synthesis, Characterization, and Application of Cy-Dye- and Alexa-Dye-Labeled Hongotoxin1Analogues. The First High Affinity Fluorescence Probes for Voltage-Gated K+Channels. Bioconjugate Chemistry *13*, 416-425.

Rajamani, R., Wu, S., Rodrigo, I., Gao, M., Low, S., Megson, L., Wensel, D., Pieschl, R.L., Post-Munson, D.J., Watson, J.*, et al.* (2017). A Functional NaV1.7-NaVAb Chimera with a Reconstituted High-Affinity ProTx-II Binding Site. Mol Pharmacol *92*, 310-317.

Rudolph, R., and Lilie, H. (1996). In vitro folding of inclusion body proteins. FASEB J *10*, 49-56.

Schmalhofer, W.A., Calhoun, J., Burrows, R., Bailey, T., Kohler, M.G., Weinglass, A.B., Kaczorowski, G.J., Garcia, M.L., Koltzenburg, M., and Priest, B.T. (2008). ProTx-II, a selective inhibitor of NaV1.7 sodium channels, blocks action potential propagation in nociceptors. Mol Pharmacol *74*, 1476-1484.

Sinai, N., Meir, A., and Bogin, O. (2006). Fluorescently-labeled Toxins: Novel tools for Working with Live Cells. In Modulator Issue (www.alomone.com), pp. 22-24.

Szallasi, A., and Blumberg, P.M. (1993). [3H]resiniferatoxin binding by the vanilloid receptor: species-related differences, effects of temperature and sulfhydryl reagents. Naunyn Schmiedebergs Arch Pharmacol *347*, 84-91.

Tilley, D.C., Eum, K.S., Fletcher-Taylor, S., Austin, D.C., Dupre, C., Patron, L.A., Garcia, R.L., Lam, K., Yarov-Yarovoy, V., Cohen, B.E.*, et al.* (2014). Chemoselective tarantula toxins report voltage activation of wild-type ion channels in live cells. Proc Natl Acad Sci U S A *111*, E4789-4796.

Ton-That, H., Liu, G., Mazmanian, S.K., Faull, K.F., and Schneewind, O. (1999). Purification and characterization of sortase, the transpeptidase that cleaves surface proteins of Staphylococcus aureus at the LPXTG motif. Proc Natl Acad Sci U S A *96*, 12424-12429.

Toseland, C.P. (2013). Fluorescent labeling and modification of proteins. J Chem Biol *6*, 85-95.

Usup, G., Leaw, C.P., Cheah, M.Y., Ahmad, A., and Ng, B.K. (2004). Analysis of paralytic shellfish poisoning toxin congeners by a sodium channel receptor binding assay. Toxicon *44*, 37-43.

Witus, L.S., and Francis, M. (2010). Site-Specific Protein Bioconjugation via a Pyridoxal 5'-Phosphate-Mediated N-Terminal Transamination Reaction. Curr Protoc Chem Biol *2*, 125-134.

Zhang, C., Welborn, M., Zhu, T., Yang, N.J., Santos, M.S., Van Voorhis, T., and Pentelute, B.L. (2016a). Pi-Clamp-mediated cysteine conjugation. Nat Chem *8*, 120-128.

Zhang, F., Hanson, S.M., Jara-Oseguera, A., Krepkiy, D., Bae, C., Pearce, L.V., Blumberg, P.M., Newstead, S., and Swartz, K.J. (2016b). Engineering vanilloid-sensitivity into the rat TRPV2 channel. Elife *5*.

Zhang, H., Yuan, Q., Zhu, Y., and Ma, R. (2005). Expression and preparation of recombinant hepcidin in Escherichia coli. Protein Expr Purif *41*, 409-416.

Zhang, S.P., Kauffman, J., Yagel, S.K., and Codd, E.E. (2006). High-throughput screening for N-type calcium channel blockers using a scintillation proximity assay. J Biomol Screen *11*, 672-677.